DEPARTMENT OF CIVIL ENGINEERING

UNIVERSITY OF SOUTHERN CALIFORNIA

PRELIMINARY EMPIRICAL MODEL FOR SCALING FOURIER AMPLITUDE SPECTRA OF STRONG GROUND ACCELERATION IN TERMS OF EARTHQUAKE MAGNITUDE SOURCE TO STATION DISTANCE, SITE INTENSITY AND RECORDING SITE CONDITIONS

by

M. D. Trifunac and V. W. Lee

Report No. CE 85-03

Los Angeles, California

October, 1985

ABSTRACT

In this paper, we present the current improvements in empirical scaling of Fourier spectrum amplitudes of strong earthquake accelerations by introducing the frequency dependent attenuation function which has been developed (Trifunac and Lee, 1985) from the same data base. This function replaces the Richter's empirical attenuation function which we previously used together with a linear term in R, the epicentral distance. By using the new attenuation function, the scaling model has the additional flexibility for estimating the Fourier spectral amplitudes from earthquakes of given source dimensions and focal depths.

INTRODUCTION

The idea to scale Fourier amplitude spectra of strong earthquake ground motion directly in terms of earthquake magnitude or Modified Mercalli Intensity at a site is not new and has been considered by a number of investigators during the past ten years. In fact, the basic ideas and equations employed here are essentially the same as those we presented in 1976 (Trifunac, 1976b). With recent significant increase in the number of uniformly processes strong motion accelerograms however, it has been possible to detect frequency and source size dependent trends in the spectrum amplitude attenuation with distance. Because such refinement of attenuation laws should lead to smaller scatter of observed Fourier spectrum amplitudes about the empirical scaling models and thus to more reliable estimates of the amplitudes of future strong ground motion, the aim of this paper is to present the second generation of "preliminary empirical scaling models..." (Trifunac, 1976b) by including this new description of amplitude attenuation with distance.

In some respects the analyses such as this one will continue to be of preliminary nature so long as the new data will contribute new and significant changes in the functional forms of the regression equations. With the overall empirical scaling models slowly "converging" towards an accurate and complete representation, it is hoped that the present effort will contribute one such improvement.

In this analysis we continue to employ the "published" magnitude scale to describe the size of earthquakes in our data base (Trifunac and Lee 1985). With increasing number of well studied earthquakes for which strong motion data are available, it should be possible, in the near future, to develop similar empirical scaling relations, but in terms of more "physical" earthquake source parameters, for example, seismic moment and stress drop. Such scaling parameters are expected to decrease the overall fluctuations of the recorded amplitudes about the average empirical estimates. However, one of the principal uses of the scaling models presented here will continue to be for the calculation of Uniform Risk Spectra (Anderson and Trifunac, 1978). Such probabilistic estimates of strong ground motion are still, in many parts of the world, based on old seismicity records where in some cases even the estimates of earthquake magnitude have to be derived from old and often incomplete data on reported intensities of shaking. While the empirical relations between the seismic moment, magnitude and the reported intensities are available, it is not clear, at present, how much could be gained by converting all scaling relationships from magnitude to seismic moment, for example.

In defining the "distance" between the earthquake source and the recording stations, in this work we consider approximately the effects of source depth and source size, but we continue to employ the epicentral distance to define the principal horizontal distance component. One could consider, instead the closest distance to a fault or distance perpendicular to the fault projection on ground surface. Such distance definitions would imply that some information on the distribution of energy release along the fault is available. Since this is available only for a small subset of earthquakes contributing to the data base considered here, we chose to continue with the simplified distance definition in terms of the epicentral distance.

PART I: SCALING OF FOURIER SPECTRA IN TERMS OF M, R, H, S, h and v

I.1 PREVIOUS ANALYSIS

During the regression analyses of earthquake strong-motion parameters in the 1970's Trifunac (1976b) suggested that the Fourier amplitude spectra (FS) of strong motion acceleration at a selected set of discrete periods, T, can be scaled in terms of the definition of the earthquake magnitude scale and a "correction" function in the following form:

$$\log_{10}[FS(T)_{,p}] = M + \log_{10}A_o(R) - \log_{10}\{FS_o(T,M,p,s,v,R)\}, \quad (I.1.1)$$

where M is the local earthquake magnitude, M_L; $\log_{10}A_o(R)$ represents the amplitude attenuation function (Richter, 1958) versus distance (Table I.1.1). The term $\log_{10}\{FS_o(T,M,p,s,v,R)\}$ represents a "correction" function which incorporates the effects of: (1) distribution of observations with respect to the assumed empirical model, as represented by the confidence level p selected for the approximate bound of spectral amplitudes $FS(T)_{,p}$, (2) geologic site conditions, s, (s=0 for alluvium, s=2 for basement rock, s=1 for intermediate sites), (3) horizontal versus vertical ground motion differences, (v=0 for horizontal and v=1 for vertical), and (4) the frequency dependent attenuation effects of amplitudes versus distances, R. The term $\log_{10}A_o(R)$ was empirically determined for Southern California (Richter, 1958) and is representative of wave frequencies centered near the middle of the frequency band for the data obtained from digitization and data processing of strong motion accelerograms (0.1 Hz to 25 Hz). The term $\log_{10}\{FS_o(T,M,p,s,v,R)\}$ was then determined by regression analysis. The same empirical model was also used for scaling of pseudo relative velocity spectra, PSV (Trifunac and Anderson, 1978a) and relative velocity spectra, SV (Trifunac and Anderson, 1978b).

Table I.1.1 $\log_{10}A_o(R)$ vs epicentral distance R

R(km)	$-\log_{10}A_o(R)$	R(km)	$-\log_{10}A_o(R)$	R(km)	$-\log_{10}A_o(R)$
1	1.400	140	3.230	370	4.336
5	1.500	150	3.279	380	4.376
10	1.605	160	3.328	390	4.414
15	1.716	170	3.378	400	4.451
20	1.833	180	3.429	410	4.485
25	1.955	190	3.480	420	4.518
30	2.078	200	3.530	430	4.549
35	2.199	210	3.581	440	4.579
40	2.314	220	3.631	450	4.607
45	2.421	230	3.680	460	4.634
50	2.517	240	3.729	470	4.660
55	2.603	250	3.779	480	4.685
60	2.679	260	3.827	490	4.709
65	2.746	270	3.877	500	4.732
70	2.805	280	3.926	510	4.755
80	2.920	290	3.975	520	4.776
85	2.958	300	4.024	530	4.797
90	2.989	310	4.072	540	4.817
95	3.020	320	4.119	550	4.835
100	3.044	330	4.164	560	4.853
110	3.089	340	4.209	570	4.869
120	3.135	350	4.253	580	4.885
130	3.182	360	4.295	590	4.900

Trifunac and Lee (1978) refined the above analyses by introducing a measure of the depth of sedimentary deposits beneath the recording station, h, as a site characteristic to replace the scaling parameter s mentioned above. The new scaling equation then became (equation (1) of Trifunac and Lee (1978)):

$$\log_{10}[FS(T)] = M + \log_{10}A_o(R) - b(T)M - c(T) - d(T)h - e(T)v - f(T)M^2 - g(T)R , \qquad (I.1.2)$$

with all the parameters defined as above. The functions b(T), c(T), ... , and g(T) are estimated by regression analysis at 91 periods T between 0.04 sec and 15 sec.

Note that in the regression equation (I.1.2) the second and higher order terms of h, R, and the third and higher order terms of M are neglected. It was pointed out then that there is really no physical basis to assume that $\log_{10}FS(T)$ should be just a linear function of the depth of sediments. Before choosing the final form for equation (I.1.2) then, studies were carried out to find whether there is any significant dependence of spectral amplitudes on h^2, h^3, ... etc. It was found that with the database available then, the least-squares coefficients associated with these higher order terms of h are indistinguishable from zero at the 95% confidence level. It should be noted, also, that there is no physical justification for the chosen parabolic dependence on M. This choice is motivated by the simplicity of its mathematical form and the apparent trend of data indicated in earlier analyses (Trifunac and Brady, 1975).

Note that if the $\log_{10}A_o(R)$ in (I.1.2) were to represent the geometric spreading, the term g(T)R would model the equivalent anelastic attenuation. However, $\log_{10}A_o(R)$ was derived empirically from data on actual peak amplitudes in Southern California, and thus represents an average combination of geometric spreading and anelastic attenuation. The term g(T)R then only represents a correction to the average attenuation given by $\log_{10}A_o(R)$.

I.2 THE NEW DATABASE

The above regression analysis was carried out for 186 free-field records corresponding to a total of 558 components of data from 57 earthquakes starting with the Long Beach earthquake in 1933 and ending with the San Fernando earthquake in 1971. Through the years new earthquake acceleration data have been added to the original database. The list of 57 earthquakes has now grown to 104, most of which occurred in the regions of northern and southern California. Table I.2.1 is the list of earthquakes now used in our database. Each line contains information on the date and time of the earthquake, latitude and longitude of the epicenter, focal depth, local earthquake magnitude and maximum intensity, if available, and the name of the earthquake.

The original list of 186 free-field records corresponding to 57 earthquakes has now grown to 438 free-field records from these 104 earthquakes. With 3 components available for each record, this amounts to a total of 1314 acceleration components, of which there are 876 horizontal and 438 vertical components.

TABLE I.2.1

EQ #	MON	DAY	YR	TIME CODE	LATITUDE DEG	MIN	SEC	LONGTITUDE DEG	MIN	SEC	(KM) DEPTH	MAG	MAX MMI	NAME
1	3	10	1933	1754PST	33	37	00	-117	58	00	16.0	6.3	9	LONG BEACH, CALIF
2	10	2	1933	0110PST	33	47	00	-118	08	00	16.0	5.4	6	SOUTHERN CALIF
3	7	6	1934	1449PST	41	42	00	-124	36	00			5	EUREKA, CALIF
4	12	30	1934	0552PST	32	15	00	-115	30	00	16.0	6.5	9	LOWER CALIF
5	10	31	1935	1138MST	46	37	00	-111	58	00		6.0	8	HELENA, MT
6	10	31	1935	1218MST	46	37	00	-111	58	00			3	HELENA, MT
7	11	21	1935	2058MST	46	36	00	-112	00	00			6	HELENA, MT
8	11	28	1935	0742MST	46	37	00	-111	58	00			6	HELENA, MT
9	2	6	1937	2042PST	40	30	00	-125	15	00			5	HUMBOLDT BAY, CAL
10	4	12	1938	0825PST	32	53	00	-115	35	00	16.0	3.0		IMPERIAL VALLEY, CA
11	6	5	1938	1842PST	32	54	00	-115	13	00	16.0	5.0		IMPERIAL VALLEY, CA
12	6	6	1938	0435PST	32	15	00	-115	10	00	16.0	4.0		IMPERIAL VALLEY, CA
13	9	11	1938	2210PST	40	18	00	-124	48	00		5.5	6	NW CALIF
14	5	18	1940	2037PST	32	44	00	-115	30	00	16.0	6.7	10	IMPERIAL VALLEY, CA
15	2	9	1941	0145PST	40	42	00	-125	24	00		6.4		NW CALIF
16	6	30	1941	2351PST	34	22	00	-119	35	00	16.0	5.9	8	SANTA BARBARA, CAL
17	10	3	1941	0813PST	40	36	00	-124	36	00		6.4	7	NORTHERN CALIF
18	11	14	1941	0042PST	33	47	00	-118	15	00	16.0	5.4	8	TORRANCE-GARDENA CA
19	10	21	1942	0822PST	32	58	00	-116	00	00	16.0	6.5	7	BORREGO VALLEY, CAL
20	3	9	1949	0429PST	37	06	00	-121	18	00		5.3	7	NORTHERN CALIF
21	4	13	1949	1156PST	47	06	00	-122	42	00		7.1	8	WESTERN WASH
22	1	23	1951	2317PST	32	59	00	-115	44	00	16.0	5.6	7	IMPERIAL VALLEY, CA
23	10	7	1951	2011PST	40	17	00	-124	48	00		5.8	7	NW CALIF
24	7	21	1952	0453PDT	35	00	00	-119	01	00	16.0	7.7	11	KERN COUNTY, CALIF
25	7	23	1952		35	17	00	-118	39	00				KERN CNTY, CAL
26	9	22	1952	0441PDT	40	12	00	-124	25	00		5.5	7	NORTHERN CALIF
27	11	21	1952	2346PST	35	50	00	-121	10	00		6.0	7	SOUTHERN CALIF
28	6	13	1953	2017PST	32	57	00	-115	43	00	16.0	5.5	7	IMPERIAL VALLEY, CA
29	1	12	1954	1534PST	35	00	00	-119	01	00	16.0	5.9	8	WHEELER RIDGE, CALI
30	4	25	1954	1233PST	36	48	00	-121	48	00		5.3	7	CENTRAL CALIF
31	11	12	1954	0427PST	31	30	00	-116	00	00	16.0	6.3	5	LOWER CALIF
32	12	21	1954	1156PST	40	47	00	-123	52	00		6.5	7	EUREKA, CALIF
33	9	4	1955	1801PST	37	22	00	-121	47	00		5.8	7	SAN JOSE, CALIF
34	12	16	1955	2117PST	33	00	00	-115	30	00	16.0	4.3		IMPERIAL COUNTY, CA
35	12	16	1955	2142PST	33	00	00	-115	30	00	16.0	3.9		IMPERIAL COUNTY, CA
36	12	16	1955	2207PST	33	00	00	-115	30	00	16.0	5.4	7	IMPERIAL COUNTY
37	2	9	1956	0633PST	31	42	00	-115	54	00	16.0	6.8		EL ALAMO, BAJA CAL
38	2	9	1956	0725PST	31	42	00	-115	54	00		6.4		EL ALAMO, BAJA CAL
39	3	18	1957	1056PST	34	07	06	-119	13	12	13.8	4.7	6	SOUTHERN CALIF
40	3	22	1957	1048PST	37	40	00	-122	28	00		3.8	5	SAN FRANCISCO CA
41	3	22	1957	1144PST	37	40	00	-122	29	00		5.3	7	SAN FRANCISCO, CAL
42	3	22	1957	1515PST	37	39	00	-122	27	00		4.4	5	SAN FRANCISCO CA
43	3	22	1957	1627PST	37	39	00	-122	29	00		4.0	5	SAN FRANCISCO CA
44	1	19	1960	1926PST	36	47	00	-121	26	00		5.0	6	CENTRAL CALIF
45	6	5	1960	1718PST	40	49	00	-124	53	00		5.7	6	NORTHERN CALIF
46	4	8	1961	2323PST	36	30	00	-121	18	00	11.0	5.7	7	HOLLISTER, CALIF
47	9	4	1962	0917PST	40	58	00	-124	12	00		5.0	6	NORTHERN CALIF
48	4	29	1965	0729PST	47	24	00	-122	18	00		6.5	8	PUGET SOUND, WASH
49	7	15	1965	2346PST	34	29	06	-118	31	18	15.1	4.0	6	SOUTHERN CALIF
50	6	27	1966	2026PST	35	57	18	-120	29	54	6.0	5.6	7	PARKFIELD, CALIF
51	8	7	1966	0936PST	31	48	00	-114	30	00	16.0	6.3	6	GULF OF CALIF
52	9	12	1966	0841PST	39	24	00	-120	06	00		6.3	7	NORTHERN CALIF
53	12	10	1967	0407PST	40	30	00	-124	36	00		5.8	6	NORTHERN CALIF

54	12	18	1967	0925PST	37	00	36	-121	47	18		5.2	6	NORTHERN CALIF
55	4	8	1968	1830PST	33	11	24	-116	07	42	11.1	6.4	7	BORREGO MTN, CALIF
56	9	12	1970	0630PST	34	16	12	-117	32	24	8.0	5.4	7	LYTLE CREEK, CALIF
57	2	9	1971	0600PST	34	24	42	-118	24	00	13.0	6.4	11	SAN FERNANDO, CALIF
58	10	15	1979	1417PST	32	37	59	-115	19	59	12.0	6.6		IMPERIAL VALLEY, CA
59	8	6	1979	0805PST	37	06	43	-121	31	59	9.6	5.9		COYOTE LAKE, CALIF
60	8	13	1978	2254GMT	34	21	04	-119	42	00	12.5	5.5		SANTA BARBARA, CAL
61	1	24	1980	1100PST	37	49	37	-121	47	13	5.9	5.9		MT. DIABLO, LIVERMO
62	1	26	1980	1833PST	37	45	00	-121	42	47	7.3	5.2		MT. DIABLO, LIVERMO
63	08	02	1975	2022GMT	39	26	58	-121	28	25	4.1	5.2		OROVILLE AFTERSHOCK
64	08	02	1975	2059GMT	39	26	00	-121	28	31	5.1	5.2		OROVILLE AFTERSHOCK
65	08	03	1975	0103GMT	39	29	19	-121	30	59	8.8	4.6		OROVILLE AFTERSHOCK
66	08	03	1975	0247GMT	39	28	52	-121	30	21	7.4	4.1		OROVILLE AFTERSHOCK
67	08	05	1975	0228GMT	39	24	18	-121	29	43	6.2	3.2		OROVILLE AFTERSHOCK
68	08	06	1975	0350GMT	39	29	46	-121	31	49	9.2	4.7		OROVILLE AFTERSHOCK
69	08	06	1975	1641GMT	39	29	31	-121	31	45	9.7	3.9		OROVILLE AFTERSHOCK
70	08	08	1975	0700GMT	39	29	50	-121	30	41	7.7	4.8		OROVILLE AFTERSHOCK
71	08	11	1975	0611GMT	39	27	29	-121	28	59	3.1	4.4		OROVILLE AFTERSHOCK
72	08	11	1975	1559GMT	39	30	20	-121	31	35	9.8	3.8		OROVILLE AFTERSHOCK
73	08	16	1975	0548GMT	39	28	12	-121	31	42	8.5	4.1		OROVILLE AFTERSHOCK
74	08	16	1975	1223GMT	39	29	52	-121	30	16	7.1	3.1		OROVILLE AFTERSHOCK
75	09	27	1975	2234GMT	39	31	12	-121	31	56	10.4	4.6		OROVILLE AFTERSHOCK
76	11	28	1974	2301GMT	36	54	0	-121	30	0	9.0	0.	6	HOLLISTER, CAL
77	1	11	1975	1737PST	40	13	12	-124	15	36	2.0	4.7	6	NORTHERN CAL
78	5	6	1975	1835PST	40	16	48	-124	40	12	0.	4.0		NORTHERN CAL
79	6	7	1975	0846GMT	40	34	12	-124	08	24	21.0	5.7	7	NORTHERN CAL
80	3	8	1971	1508PST	35	40	0	-118	24	12	6.0	4.7	5	CENTRAL CAL
81	5	2	1971	0608GMT	51	24	0	-177	12	0	43.0	7.1	6	ANDREANOF, ALASKA
82	9	12	1971	1132PST	41	17	54	-123	40	24	20.0	4.6	5	NORTHERN CAL
83	7	30	1972	2145GMT	56	49	12	-135	40	48	25.0	7.1	7	SOUTHEAST ALASKA
84	9	4	1972	1804GMT	36	38	13	-121	17	13	2.0	4.8	6	CENTRAL CAL
85	5	26	1980	1857GMT	37	32	37	-118	51	41	2.8	4.9		MAMMOTH AFTERSHOCK
86	5	27	1980	1450GMT	37	27	49	-118	49	24	2.4	6.3		MAMMOTH AFTERSHOCK
87	5	27	1980	1901GMT	37	36	15	-118	46	11	3.8	5.0		MAMMOTH AFTERSHOCK
88	5	28	1980	0516GMT	37	34	49	-118	53	09	3.3	4.8		MAMMOTH AFTERSHOCK
89	5	31	1980	1516GMT	37	32	22	-118	54	22	8.2	5.1		MAMMOTH AFTERSHOCK
90	6	11	1980	0441GMT	37	30	24	-119	02	34	14.1	5.0		MAMMOTH AFTERSHOCK
91	6	28	1980	0058GMT	37	33	23	-118	51	45	5.1	4.1		MAMMOTH AFTERSHOCK
92	10	16	1979	1616PDT	33	4	29	-115	33	16	5.0	4.9		IMPERIAL VALLEY AFT
93	10	16	1979	1445PDT	33	2	44	-115	29	24	3.9	4.6		IMPERIAL VALLEY AFT
94	10	16	1979	1114PDT	32	58	19	-115	36	22	4.7	4.2		IMPERIAL VALLEY AFT
95	10	15	1979	2319GMT	32	46	0	-115	26	29	9.5	5.0		IMPERIAL VALLEY AFT
96	4	26	1981	1209GMT	33	7	48	-115	39	0	8.0	5.6		WESTMORELAND, CAL
97	1	24	1980	1900GMT	37	50	24	-121	48	0	5.9	5.9		LIVERMORE, CAL
98	1	26	1980	0233GMT	37	45	36	-121	42	0	7.3	5.2		LIVERMORE, CAL
99	5	25	1980	0934PDT	37	36	32	-118	50	49	9.0	6.1		MAMMOTH AFTERSHOCK
100	5	25	1980	0949PDT	37	37	41	-118	55	37	14.	6.0		MAMMOTH AFTERSHOCK
101	5	25	1980	1245PDT	37	33	40	-118	49	52	16.	6.1		MAMMOTH AFTERSHOCK
102	5	25	1980	1336PDT	37	37	30	-118	51	32	2.	5.7		MAMMOTH AFTERSHOCK
103	5	26	1980	1158PDT	37	32	35	-118	53	17	5.	5.7		MAMMOTH AFTERSHOCK
104	5	27	1980	0751PDT	37	30	22	-118	49	34	14.	6.2		MAMMOTH AFTERSHOCK

I.3 THE NEW ATTENUATION FUNCTION

The advantage in using the attenuation function, $\log_{10}A_o(R)$ (Richter, 1958), in the previous regression analyses has been that it contains information on the average properties of wave propagation through the crust in southern California, where virtually all strong motion data have been recorded up to and during the 70's. The disadvantages and limitations have been that its shape does not depend on the magnitude, source dimension and focal depth of an earthquake, on the geological environment of the recording station, or on the amplitudes of the recorded motions. That $\log_{10}A_o(R)$ or its analog should depend on the geometric size of the fault has been discussed in some detail previously (Trifunac, 1976b). Up to the 1970's only a few of the 186 records had epicentral distances less than 10 km and the empirical derivation of different shapes of $\log_{10}A_o(R)$, or its equivalent, to reflect different magnitudes or source dimensions then was not feasible.

With the new database now available, Trifunac and Lee (1985) have developed an iteration procedure for determining a new frequency dependent attenuation function, a complete description of which is given in the above reference. A brief summary and description of this new attenuation function is given here.

To take into account that the attenuation function should depend on the epicentral distance, R, on the focal depth, H, of the earthquake, and the "size" of the fault, S, a parameter, denoted by Δ, is introduced to replace the epicentral distance, R, and is defined as follows:

$$\Delta = S \Big/ \left(\ln \left(\frac{S^2+R^2+H^2}{S_o^2+R^2+H^2} \right) \right)^{\frac{1}{2}} \qquad (I.3.1)$$

Δ can be thought of as a "representative distance" from the earthquake source of size S, at depth H and at distance R from the recording site. S_0 is the coherence radius of the source. The definition of Δ used here in equation I.3.1 is identical to that used in Model III (equation 4.8) presented in Trifunac and Lee (1985). It has been proposed by Gusev (1983) in his descriptive statistical model of earthquake source radiation for the description of short-period strong ground motion. The coherence radius S_0 is taken to be a half of the wavelength, λ, for radiation of frequency f (or period T), namely, coherence radius, $S_0 = \lambda/2 = C_s/2f = C_sT/2$, where C_s is the velocity of the radiation (in this work C_s is taken to be 1 km/sec). Since the fault size, S, of the earthquake is not available for most of the earthquakes used in the data base, an empirical formula for the size, as a function of magnitude, epicentral distance R and period of the spectral amplitudes has been introduced as follows,

$$S = S(M,T) \qquad (I.3.2)$$

where S(M,T) is the size of the fault "felt" at the period T, and is assumed to be a linear function of magnitude, M, so that for

$$\begin{array}{ll} M = 3 & S(M,T) = 0.2 \text{ km} \\ M = 6.5 & S(M,T) = S_{6.5}(T) \text{ km} \end{array} \qquad (I.3.3)$$

and $S_{6.5}(T)$ is an empirically determined function. From (I.3.3), S(M,T) takes the form

$$S(M,T) = 0.2 + \frac{(M-3)}{3.5}\,(S_{6.5}(T) - .2) \qquad (I.3.4)$$

This definition of fault size "felt or "experienced" at the site is independent of how close the site is to the epicenter of the earthquake.

The new frequency dependent attenuation function then takes the form (Trifunac and Lee, 1985):

$$\mathscr{A}tt(\Delta,M,T) = \begin{cases} \mathscr{A}_0(T)\log_{10}\Delta & R \le R_0 \\ \mathscr{A}_0(T)\log_{10}\Delta_0 - (R-R_0)/200, & R > R_0 \end{cases}$$

with

$$\Delta = S\left(\ln \frac{R^2 + H^2 + S^2}{R^2 + H^2 + S_0^2}\right)^{-\frac{1}{2}}$$

and

$$\Delta_0 = S\left(\ln \frac{R_0^2 + H^2 + S^2}{R_0^2 + H^2 + S_0^2}\right)^{-\frac{1}{2}} \quad , \qquad \text{(I.3.5)}$$

where $\mathscr{A}_0(T)$ is an empirically determined parabolic function of T. It is used to calculate the attenuation function at distances R less than R_0. For distances $R > R_0$, the attenuation function is a linear function of distance with slope -1/200. The transition distance R_0 is given by (Model III; Trifunac and Lee, 1985):

$$R_0 = \frac{1}{2}\left(\frac{-200\mathscr{A}_0(T)(1-S_0^2/S^2)}{\ln 10} + \sqrt{\left(\frac{200\mathscr{A}_0(T)(1-S_0^2/S^2)}{\ln 10}\right)^2 - 4H^2}\right), \qquad \text{(I.3.6)}$$

which is a function of H,S (hence M,R,T), S_0 and $\mathscr{A}_0(T)$. Detailed description and plots of $S_{6.5}(T)$, $\mathscr{A}_0(T)$ and R_0 and of the attenuation function $\mathscr{A}tt(\Delta,M,T)$ are all given in Trifunac and Lee (1985).

I.4 THE NEW SCALING RELATION

With the new attenuation function defined, the regression equation of Fourier amplitudes to be used now takes the form:

$$\log_{10}FS(T) = M + \mathcal{A}tt(\Delta,M,T) + b_1(T)M$$
$$+ b_2(T)h + b_3(T)v + b_4(T)\Delta/100 + b_5(T) + b_6(T)M^2. \quad (I.4.1)$$

Equation (I.4.1) is of the same form as equation (I.1.2), the old scaling equation, with the old attenuation function $\log_{10}A_0(T)$ replaced by new attenuation function $\mathcal{A}tt(\Delta,M,T)$. The regression analysis is performed on the new database of 1314 components of Fourier amplitude data FS(T), at 91 discrete periods T ranging from 0.04 to 15.0 sec. This is in fact Step 2 of the iteration procedure described in Trifunac and Lee (1985) for the determination of the new attenuation function $\mathcal{A}tt(\Delta,M,T)$, and is identical to the regression analysis procedure used with the old database (Trifunac, 1976a,b; Trifunac and Lee, 1978). For completeness, the details of this step are repeated here.

The data are screened to minimize possible bias in the model that could result from possible uneven distribution of data among the different magnitudes and from excessive contribution to the database from several abundantly recorded earthquakes. To carry out this screening the data are partitioned into six groups corresponding to magnitude ranges: 2.0-2.9, 3.0-3.9, 4.0-4.9, 5.0-5.9, 6.0-6.9 and 7.0-7.9. The data in each of these magnitude ranges are next subdivided according to the site classifications s = 0,1 and 2. The data within each of these subgroups were then divided into 2 sets corresponding to horizontal (v=0) and vertical (v=1) components. The resulting data in each of the groups correspond to the Fourier spectral amplitudes from a specified earthquake magnitude range for a specified site classification and with specified component orientation. To properly balance the effects of attenuation at small and large distances, the data in each of the subgroups are subdivided further into 2 sets: one for epicentral distances $\leq$ 100 km and the other for distances > 100 km. The data in each of these two final subsets are then arranged in increasing order in terms of their amplitudes. If the number of data points in the first set ($R \leq 100$ km) is less than 19, all the data points are taken. If there are more than 19 points in this first set, at most 19 points are selected from among the ordered set of data so that they correspond uniformly, as close as possible, to the 5%, 10%, ..., 90% and 95% percentiles at distances $R \leq 100$ km. Similarly, at most 5 points are selected from the second set ($R > 100$ km) of data so that they correspond uniformly to around 16 2/3%, 33 1/3%, 50%, 66 2/3 and 83 1/3% percentiles at distances $R > 100$ km. This approximate scheme has the effect of reducing the biases described above. Note that this selection process is repeated for each of the 91 periods in the range .04 sec. to 15 sec. At the long period end, the Fourier data whose amplitudes are below that of the average digitization noise i.e., those with signal-to-noise ratio less than one, are automatically eliminated before the above selection process. This will be the case for many of the data from earthquakes of smaller magnitudes and/or recorded at sites of larger epicentral distances. The number of data points used in the regression analysis at the long period end are thus comparatively smaller than those at the rest of the period ranges. The resulting fitted coefficients at each period T resulting from linear regression will be denoted by $\hat{b}_1(T)$, $\hat{b}_2(T)$, $\hat{b}_3(T)$, $\hat{b}_4(T)$, $\hat{b}_5(T)$ and $\hat{b}_6(T)$, (equation (I.4.1)) respectively.

I.5 THE NEW REGRESSION COEFFICIENTS

During the regression analysis, it was found that the linear term in Δ in (I.4.1), $b_4(T)$, is insignificant for most of the periods. Subsequently, this term has been deleted from the regression analysis and the empirical scaling equation, (I.4.1), becomes

$$\log_{10} FS(T) = M + \mathcal{A}tt(\Delta,M,T) + b_1(T)M + b_2(T)h + b_3(T)v + b_5(T) + b_6(T)M^2 \qquad (I.5.1)$$

Figure I.5.1 shows $\hat{b}_1(T)$, $\hat{b}_2(T)$, $\hat{b}_3(T)$, $\hat{b}_5(T)$ and $\hat{b}_6(T)$ (solid lines) and the estimates of their 80%, 90% and 95% confidence intervals (Westermo and Trifunac, 1978), represented by the corresponding dashed lines.

Substituting these coefficients in equation (I.5.1) gives $\hat{FS}(T)$, where:

$$\log_{10} \hat{FS}(T) = M + \mathcal{A}tt(\Delta,M,T) + \hat{b}_1(T)M + \hat{b}_2(T)h + \hat{b}_3(T)v + \hat{b}_5(T) + \hat{b}_6(T)M^2, \qquad (I.5.2)$$

$\hat{FS}(T)$ then represents the least squares estimate of the Fourier amplitude spectrum at period T.

For given values of T, h, v and Δ, $\log_{10} FS(T)$ represents a parabola when plotted versus M. Following the previous work, it is also assumed in the present analysis that equation (I.5.2) applies only in the range $M_{min} \leq M \leq M_{max}$, where $M_{min} = -b_1(T)/(2b_6(T))$ and $M_{max} = -(1+b_1(T))/(2b_6(T))$. Equation (I.5.2) is then modified to:

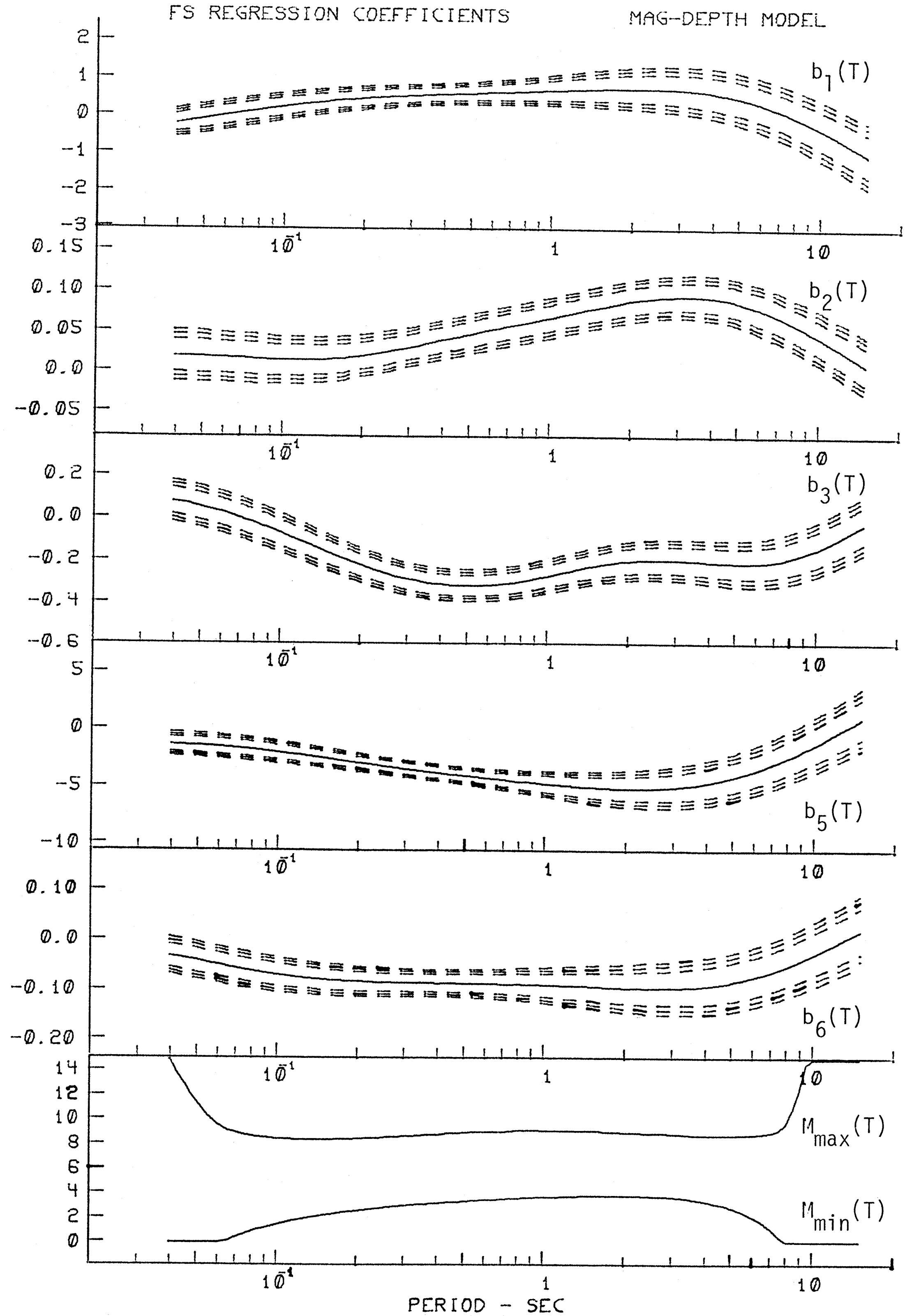

FS REGRESSION COEFFICIENTS
MAG-DEPTH MODEL
b1(T)
b2(T)
b3(T)
b5(T)
b6(T)
Mmax(T)
Mmin(T)
PERIOD - SEC

Figure I.5.1

$$\log_{10}\hat{FS}(T) = \mathscr{A}tt(\Delta,M,T) + \begin{cases} M + \hat{b}_1(T)M_{min} + \hat{b}_2(T)h + \hat{b}_3(T)v + \hat{b}_5(T) + \hat{b}_6(T)M_{min}^2 , & M \le M_{min} \\ M + \hat{b}_1(T)M \quad + \hat{b}_2(T)h + \hat{b}_3(T)v + \hat{b}_5(T) + \hat{b}_6(T)M^2 , & M_{min} \le M \le M_{max} \\ M_{max} + \hat{b}_1(T)M_{max} + \hat{b}_2(T)h + \hat{b}_3(T)v + \hat{b}_5(T) + \hat{b}_6(T)M_{max}^2 , & M_{max} \le M \end{cases} \tag{I.5.3}$$

In other words, for $M \le M_{min}$, M_{min} is used in the terms following M in (I.5.3), i.e. M_{min} is used with $b_1(T)$ and $b_6(T)$. For $M \ge M_{max}$, M_{max} is used in all the terms. This will result in linear growth of $\log_{10}FS(T)$ with M for $M \le M_{min}$, in parabolic growth for $M_{min} \le M \le M_{max}$ and in constant FS(T) corresponding to M_{max} for all $M \ge M_{max}$. The bottom curves of Figure I.5.1 show M_{min} and M_{max} plotted versus T.

With FS(T) representing the Fourier amplitude spectra computed from recorded accelerograms, the residues were calculated as in the previous analysis (Trifunac and Lee, 1978), where the residue given by $\varepsilon(T) = \log_{10}[FS(T)] - \log_{10}[\hat{FS}(T)]$, describes the distribution of the observed FS(T) about the estimated $\hat{FS}(T)$. As in the previous work, it is assumed that $\varepsilon(T)$ can be described by a normal distribution function with mean $\mu(T)$ and standard deviation $\sigma(T)$ as follows:

$$p(\varepsilon,T) = \frac{1}{\sigma(T)\sqrt{2\pi}} \int_{-\infty}^{\varepsilon(T)} \exp\left[-\frac{1}{2}\left(\frac{x-\mu(T)}{\sigma(T)}\right)^2\right] dx , \tag{I.5.4}$$

where $p(\varepsilon,T)$ represents the probability that $\log_{10}[FS(T)] - \log_{10}[\hat{FS}(T)] \le \varepsilon(T)$.

For a given residual value $\varepsilon(T)$ at a particular period T, the actual probability $P^*(\varepsilon,T)$ that $\varepsilon(T)$ will not be exceeded can be evaluated by finding the fraction of residues $\varepsilon(T)$ (computed from the database at that particualr period) which are smaller than a given value.

For $p^*(\varepsilon,T)$ calculated at 91 periods, $\varepsilon(T)$ corresponding to $p^* =$ 0.1, 0.2,...,0.8 and 0.9 are plotted in Figure I.5.2. The nine sets of curves, plotted versus period, T, from bottom to top correspond to one at each of the probability levels, 0.1 through 0.9. At each of the nine probability levels, the rough solid curve represents the actual calculated residuals at that particular level. The smooth solid curves are obtained by smoothing the rough solid curves along the T-axis. The smooth surface $p^*(\varepsilon,T)$, from the nine smooth solid curves thus represents the distribution of data ($FS(T)$ computed from recorded accelerograms) about the estimate $\widehat{FS}(T)$ in (I.5.1). By fitting $p(\varepsilon,T)$ in (I.5.4) to $p^*(\varepsilon,T)$ at 91 periods, the mean and standard deviation of the assumed normal distribution function, respectively $\hat{\mu}(T)$ and $\hat{\sigma}(T)$, can thus be evaluated. Substituting these values into (I.5.4) with $p(\varepsilon,T)$ equal to 0.1 through 0.9 will result in $\hat{\varepsilon}(T)$ for the nine probability levels to be calculated. These are the nine dashed lines in Figure I.5.3. The surface $p^*(\varepsilon,T)$ that resulted from the new model in the present analysis (Figure I.5.2) is narrower in ε range when compared to the corresponding surface in our previous analysis (Figure 2 of Trifunac and Lee, 1978).

To test the quality of fit of $\hat{p}(\varepsilon,T)$ to $p^*(\varepsilon,T)$ as in the previous analysis, two statistical tests for goodness of fit, namely the Kolmogorov-Smirnov (K-S) and the X^2 tests of the hypothesis that $p^*(\varepsilon,T)$ can be approximated by a normal distribution $p(\varepsilon,T)$ (equation (I.5.4)) have been performed. The Kolmogorov-Smirnov statistic calculates, for each period T, the maximum allowed difference between the estimated and the calculated probability levels:

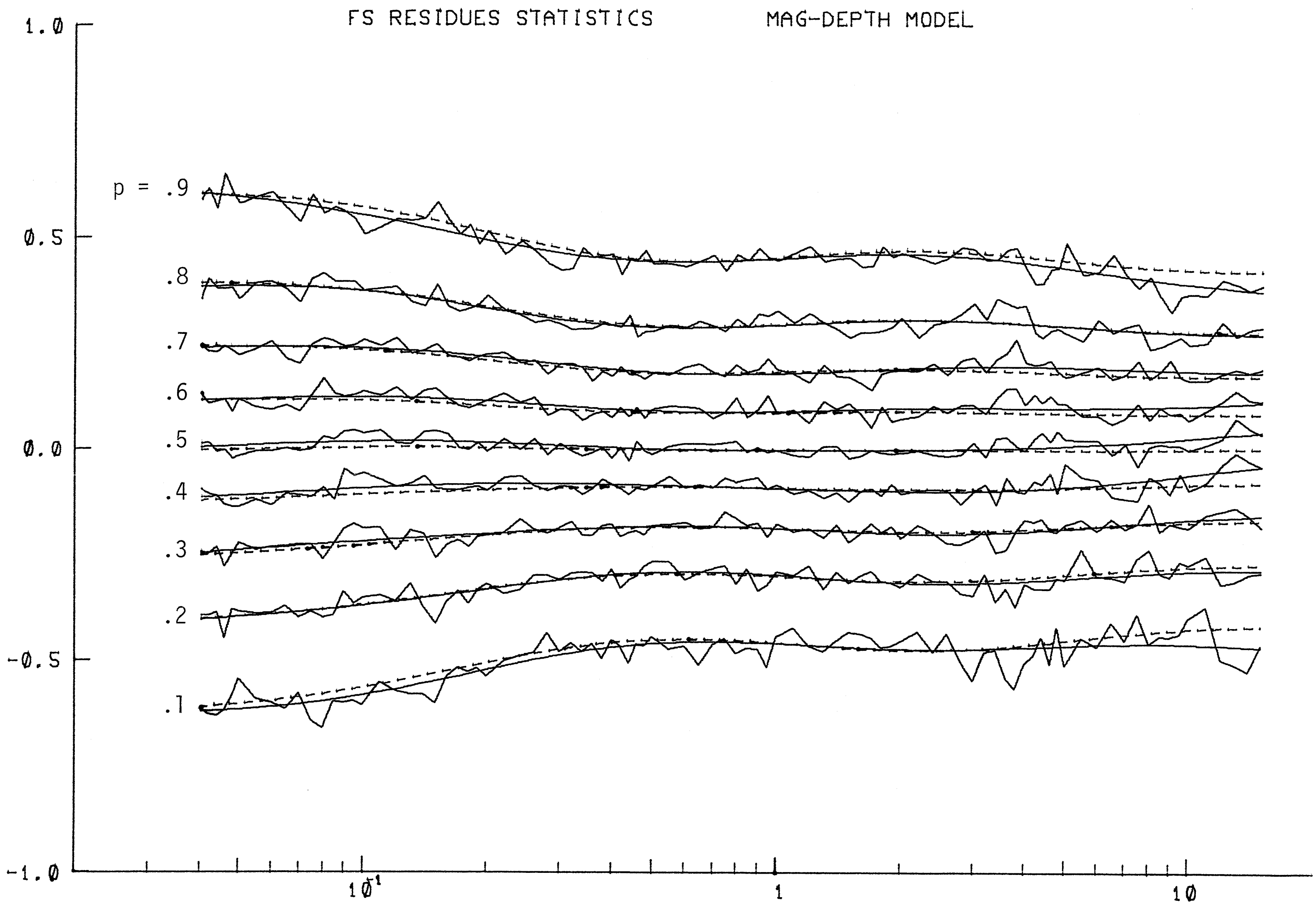
FS RESIDUES STATISTICS
MAG-DEPTH MODEL
1.0
0.5
0.0
-0.5
-1.0
p = .9
.8
.7
.6
.5
.4
.3
.2
.1
10^{-1}
1
10

Figure I.5.2

$$KS(T) = \max_{\varepsilon} | p(\hat{\varepsilon},T) - p^*(\varepsilon,T) | \ . \qquad (I.5.5)$$

To calculate the X^2 statistic, a standard procedure was adopted, which is different from that of the previous analysis, so that the number of intervals used is the same for all periods, T:

Step 1: The ε-axis of residues is subdivided into 10 intervals $I_0, I_1, \ldots, I_9$ such that $I_k = [\underline{\varepsilon}_k, \underline{\varepsilon}_{k+1}]$ for each i contains residues in the probability levels between p_k and p_{k+1}, where $p_k = 0.1k$. The residues are divided in intervals of 10% probability each: 0-10%, 10-20%, ... to 90-100%. Note that $\underline{\varepsilon}_o = -\infty$ and $\underline{\varepsilon}_{10} = +\infty$.

Step 2: For each $\underline{\varepsilon}_k$, the estimated probability level $\hat{p}_k = \hat{p}(\underline{\varepsilon}_k,T)$ is computed from (I.5.4) using the estimated coefficients $\hat{\mu}_k(T)$ and $\hat{\sigma}_k(T)$. Note that $\hat{p}_o = \hat{p}(\underline{\varepsilon}_o,T) = 0$ and $\hat{p}_{10} = \hat{p}(\underline{\varepsilon}_{10},T) = 1$. The estimated probability that the residue ε assumes any value in the interval $I_k[\underline{\varepsilon}_k,\underline{\varepsilon}_{k+1}]$, for k = 0 to 9, is then given by the difference $\hat{p}_{k+1} - \hat{p}_k$. The actual probability that the residue ε assumes value in any of the intervals is of course the chosen value of .1 (10%).

Step 3: In each interval I_k, k = 0 to 9, define

$$\hat{n}_k = (\hat{p}_{k+1} - \hat{p}_k)N, \text{ and}$$

$$n_k = 0.1\ N\ , \qquad (I.5.6)$$

where N is the total number of residues in all the intervals. $\hat{n}_k$ is the estimated number of residuals theoretically expected in the interval I_k and n_k is the actual number of residues in the same interval. The X^2 statistics are then calculated from the formula

$$X^2(T) = \sum_{k=1}^{9} \frac{(\hat{n}_k - n_k)^2}{\hat{n}_k} \quad . \tag{I.5.7}$$

Another convenient form of (I.5.7) for X^2 is

$$X^2(T) = N \sum_{k=0}^{9} \frac{(\hat{p}_{k+1} - \hat{p}_k - .1)^2}{(\hat{p}_{k+1} - \hat{p}_k)} \quad . \tag{I.5.8}$$

Note that this differs from the X^2 statistics used in the previous analysis by having the factor N. The above definition is adopted from Kreyszig (1972).

Having computed the values of KS(T) and $X^2(T)$ for each period T, those were compared with their corresponding cutoff values at 95% probability level. For the Kolmogorov-Smirnov statistic,

$$P(KS \leq C) = 95\% \quad \Rightarrow \quad C = 0.058. \tag{I.5.9}$$

Thus if $KS(T) < 0.058$, the hypothesis that the probability distribution is normal will not be rejected. Similarly, for the X^2-statistic, with $K = 10$ intervals, $r = 2$ the number of parameters used in estimating $\hat{n}_k$, the number of degrees of freedom is $K-r-1 = 7$, and

$$P(X^2 \leq C) = 95\% \quad \Rightarrow \quad C = 14.07. \tag{I.5.10}$$

Thus again if $X^2(T) < 14.07$, the hypothesis that the probability distribution is normal will not be rejected.

Figure I.5.3 shows a plot of the statistical parameters of the residuals. The smooth amplitudes of $\hat{\mu}(T)$ and $\hat{\sigma}(T)$ and their 95% confidence intervals are given in the top 2 plots of the figure respectively. The two full curves in the bottom of Figure I.5.3 show the smoothed amplitudes of the computed $X^2(T)$ and KS(T) respectively. The dashed

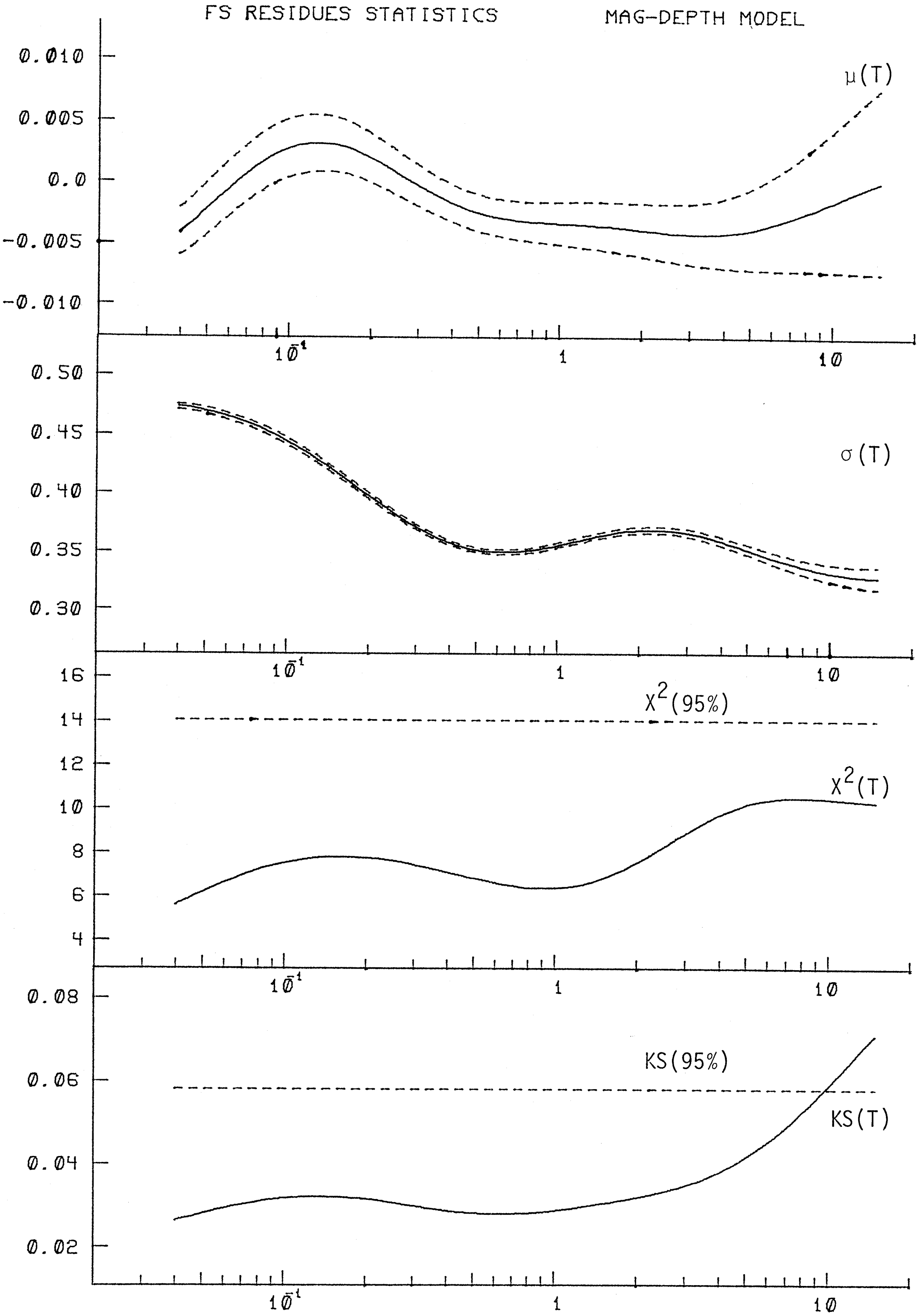
FS RESIDUES STATISTICS
MAG-DEPTH MODEL
0.010
0.005
0.0
-0.005
-0.010
μ(T)
10̄¹
1
10
0.50
0.45
0.40
0.35
0.30
σ(T)
16
14
12
10
8
6
4
X²(95%)
X²(T)
0.08
0.06
0.04
0.02
KS(95%)
KS(T)

Figure I.5.3

TABLE I.5.1

$$\log_{10} FS(T) = M + \mathcal{A}tt(\Delta,M,T) + b_1(T)M + b_2(T)h + b_3(T)v + b_5(T) + b_6(T)M^2$$

PERIOD, T(SEC)	.040	.065	.11	.19	.34	.50	.90	1.60	2.80	4.40	7.50	14.00
COEFFICIENTS:												
$b_1(T)$	-.228	.014	.251	.432	.545	.594	.668	.734	.718	.549	.048	-.933
$b_2(T)$	.018	.014	.012	.017	.033	.045	.063	.082	.093	.089	.063	.013
$b_3(T)$	.077	.007	-.098	-.219	-.308	-.325	-.287	-.219	-.196	-.214	-.196	-.050
$b_5(T)$	-1.401	-1.714	-2.241	-2.967	-3.724	-4.164	-4.766	-5.187	-5.141	-4.477	-2.698	.556
$b_6(T)$	-.034	-.056	-.076	-.086	-.089	-.090	-.092	-.096	-.098	-.090	-.058	.011
M_{min}	.000	.126	1.660	2.508	3.053	3.305	3.640	3.811	3.656	3.038	.416	.000
M_{max}	14.850	8.992	8.274	8.308	8.654	8.874	9.090	9.004	8.748	8.573	9.053	15.000
RESIDUES:												
p = .1	-.621	-.607	-.575	-.527	-.479	-.461	-.458	-.470	-.474	-.467	-.461	-.468
p = .2	-.404	-.389	-.366	-.336	-.305	-.293	-.296	-.313	-.318	-.310	-.296	-.287
p = .3	-.246	-.232	-.217	-.203	-.189	-.184	-.187	-.197	-.201	-.193	-.177	-.160
p = .4	-.115	-.105	-.092	-.084	-.084	-.087	-.093	-.099	-.101	-.095	-.076	-.045
p = .5	.004	.012	.018	.015	.006	-.000	-.004	-.003	-.001	.004	.016	.037
p = .6	.117	.120	.122	.114	.098	.090	.088	.094	.097	.097	.099	.109
p = .7	.241	.242	.237	.220	.195	.182	.178	.187	.195	.196	.189	.182
p = .8	.384	.384	.368	.335	.299	.288	.291	.303	.304	.294	.280	.271
p = .9	.604	.580	.543	.496	.455	.443	.447	.459	.455	.435	.404	.375
RESIDUE STATISTICS:												
$\mu(T)$	-.004	.000	.003	.002	-.001	-.003	-.003	-.004	-.004	-.004	-.003	-.000
$\sigma(T)$	.473	.462	.438	.401	.364	.351	.353	.366	.367	.356	.338	.328
$\chi^2(T)$	5.655	6.823	7.671	7.795	7.295	6.813	6.365	7.007	8.689	9.990	10.563	10.308
KS(T)	.027	.030	.032	.032	.029	.028	.029	.031	.034	.040	.051	.069

lines are their corresponding 95% cutoff levels. It is seen that with the minor exception in the long period end, both the X^2 and K-S tests fail to reject the hypothesis that the distribution is normal. The function $p(\varepsilon,T)$ in (I.5.4) thus represents an acceptable approximation to $p^*(\varepsilon,T)$.

Table I.5.1 presents, for 12 periods, between T = 0.04 sec and T = 14 sec, the amplitudes of the smoothed regression coefficients $\hat{b}_1(T)$, $\hat{b}_2(T)$, $\hat{b}_3(T)$, $\hat{b}_5(T)$, $\hat{b}_6(T)$ (note that $b_4(T)$ has been deleted), $\hat{M}_{min}(T)$, $\hat{M}_{max}(T)$, the nine smoothed calculated residue levels corresponding to $p^*(\varepsilon,T) = 0.1, 0.2, \ldots, 0.8$ and 0.9, the smoothed amplitudes $\hat{\mu}(T)$, $\hat{\sigma}(T)$ in equation (I.5.4), the X^2 and the Kolmogorov-Smirnov statistics. The 12 periods used appear to be sufficient for most practical computations since the smoothness of the coefficients is such that almost any interpolation scheme will yield adequate estimates of the FS(T) amplitudes at any period in the range between 0.04 sec and 15 sec.

I.6 EXAMPLES OF ESTIMATED FOURIER SPECTRA

Figures I.6.1 and I.6.2 present examples of FS(T) computed for M = 4.5, 5.5, 6.5, 7.5 at R = 0, H = 5 km, or then $\Delta \approx 5$ km, for $p(\varepsilon,T) = 0.5$, and the spectral amplitudes which have signal-to-noise ratio greater than one (Trifunac, 1976a). Figure I.6.1 is for horizontal motion while Figure I.6.2 is for vertical motion. The solid lines in both figures correspond to an alluvial depth of h = 0 km while the dashed lines correspond to h = 4 km.

The trends of computed FS(T) spectral amplitudes in the figures are in many ways similar to those discussed by Trifunac and Lee (1978). The rate of growth of amplitudes with earthquake magnitude, M clearly decreases as M approaches M = 7.5. The effect of the depth of sediments beneath the recording station is important only for intermediate to long periods and is small at short periods.

Comparison of the two figures shows that the vertical spectral amplitudes are smaller than the horizontal spectral amplitudes, except at short periods.

Figure I.6.3 illustrates the effects of epicentral distance R on the changes of spectral amplitudes for $p(\varepsilon,T) = 0.5$, magnitude M = 6.5, focal depth H = 5 km, sedimentary depth h = 2 km and for horizontal (solid lines) and vertical (dashed lines) components. Four sets of curves corresponding to R = 0, 25, 50 and 100 km are shown. As can be seen from equation (I.5.1), the only term governing these distance changes is the change in Δ, the representative distance, in the frequency dependent attenuation term $\mathcal{A}tt(\Delta,M,T)$. As already noted in Trifunac and Lee (1985), the attenuation of the high frequency waves is somewhat faster than that of the low-frequency waves.

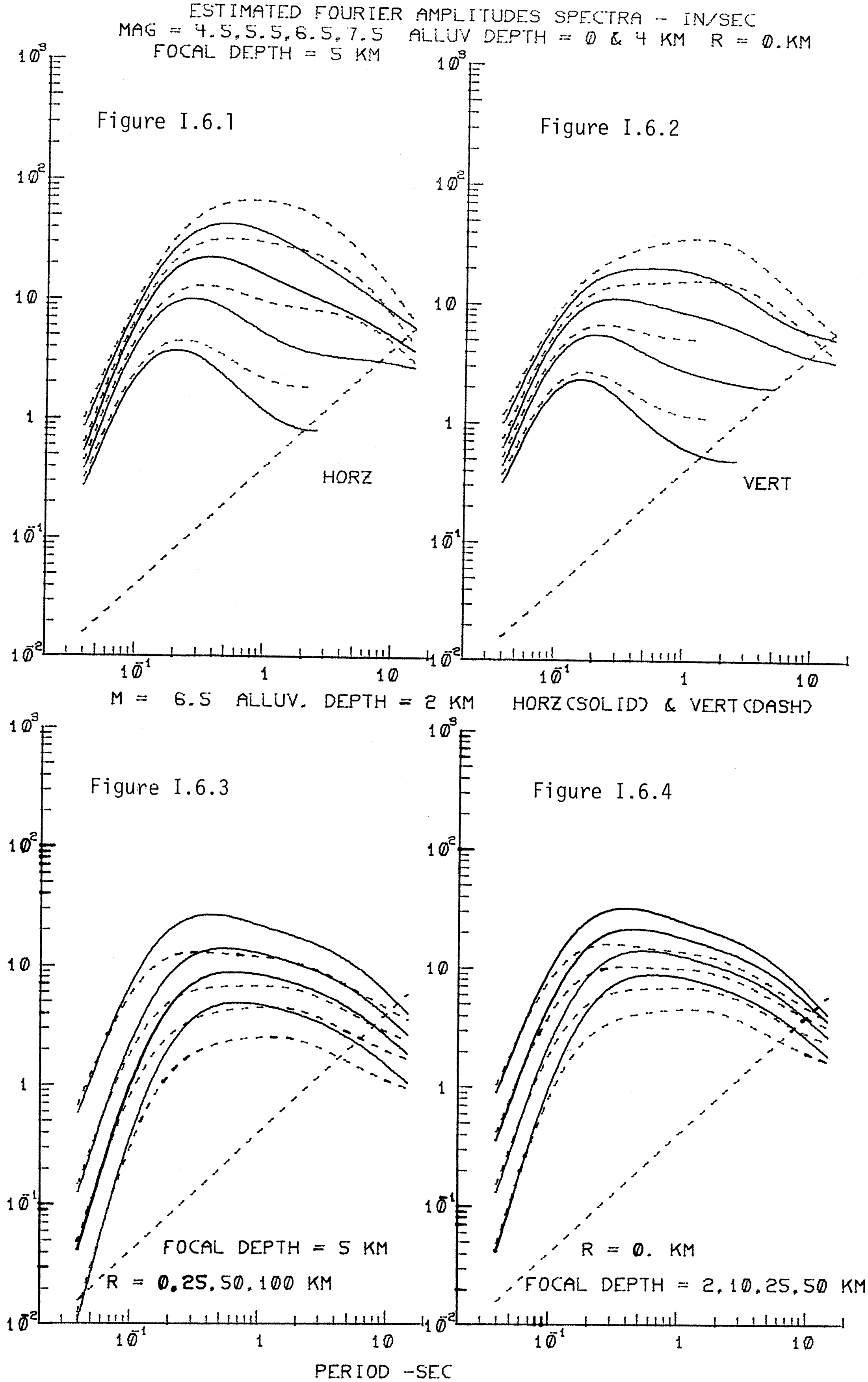
ESTIMATED FOURIER AMPLITUDES SPECTRA - IN/SEC
MAG = 4.5,5.5,6.5,7.5 ALLUV DEPTH = 0 & 4 KM R = 0.KM
FOCAL DEPTH = 5 KM
Figure I.6.1
HORZ
Figure I.6.2
VERT
M = 6.5 ALLUV. DEPTH = 2 KM HORZ (SOLID) & VERT (DASH)
Figure I.6.3
FOCAL DEPTH = 5 KM
R = 0,25,50,100 KM
Figure I.6.4
R = 0. KM
FOCAL DEPTH = 2,10,25,50 KM
PERIOD -SEC

Figure I.6.4 illustrates the effects of focal depth H on the changes of spectral amplitudes for $p(\varepsilon,T) = 0.5$, $M = 6.5$, $R = 0$ km, $h = 2$ km and for horizontal (solid lines) and vertical (dashed line) components. Four sets of curves corresponding to H = 2, 5, 25 and 50 km are presented. As in the case for distances R, the attenuation of the high frequency waves with focal depth is faster than that of the low frequency waves.

Figures I.6.5 and I.6.6 show an example of how horizontal and vertical Fourier spectra computed from equations (I.5.2) and (I.5.4) compare with the acceleration spectra for the three components of strong-motion recorded in El Centro during the Imperial Valley, California earthquake of 1940. During this earthquake, the fault rupture was initiated most probably at a distance of about 10 km, southeast of El Centro. With the introduction of fault size and focal depth now available in the new scaling model, a reduction in the observed differences between the computed and estimated Fourier spectra is to be expected. In these figures, as in the previous analysis, the $\log_{10}FS(T)$ spectra were computed for $p(\varepsilon,T) = 0.1$, 0.5 and 0.9. The interval between the spectra for $p = 0.1$ and 0.9 represents an estimate of the 80% confidence interval. The statistical parameters used are $M = 6.4$, $R = 9.3$ km, focal depth $H = 5$ km and alluvial depth $h = 15000$ ft. As may be concluded from these figures, the agreement between the recorded and empirically predicted spectra in this case is very satisfactory, as in the previous analysis. The only difference between the present and the previous analysis is that the 80% confidence interval is now narrower than before.

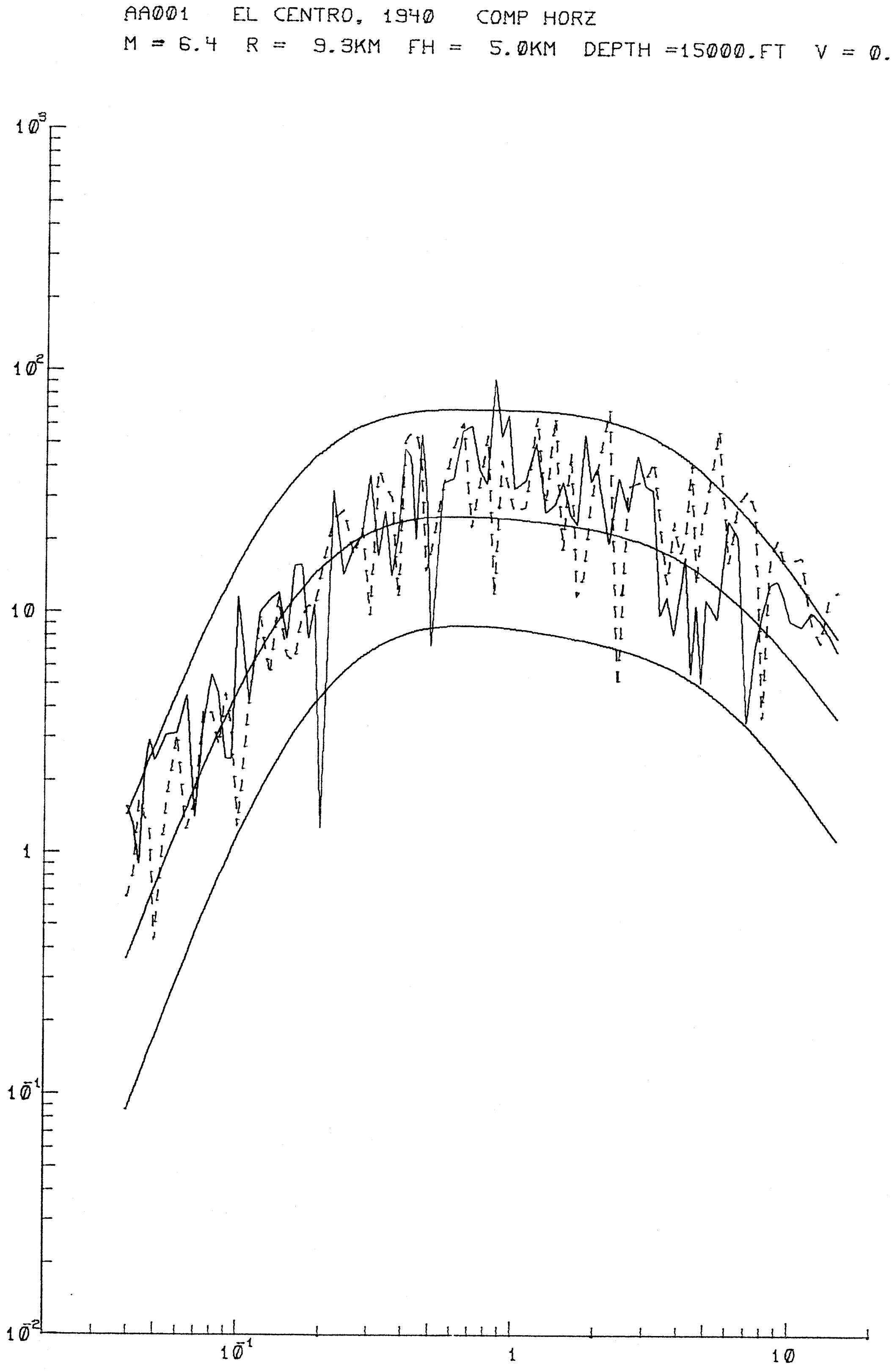
AA001 EL CENTRO, 1940 COMP HORZ
M = 6.4 R = 9.3KM FH = 5.0KM DEPTH =15000.FT V = 0.
10³
10²
10
1
10⁻¹
10⁻²
10⁻¹
1
10

Figure I.6.5

AA001 EL CENTRO, 1940 COMP VERT

M = 6.4 R = 9.3KM FH = 5.0KM DEPTH =15000.FT V = 1.

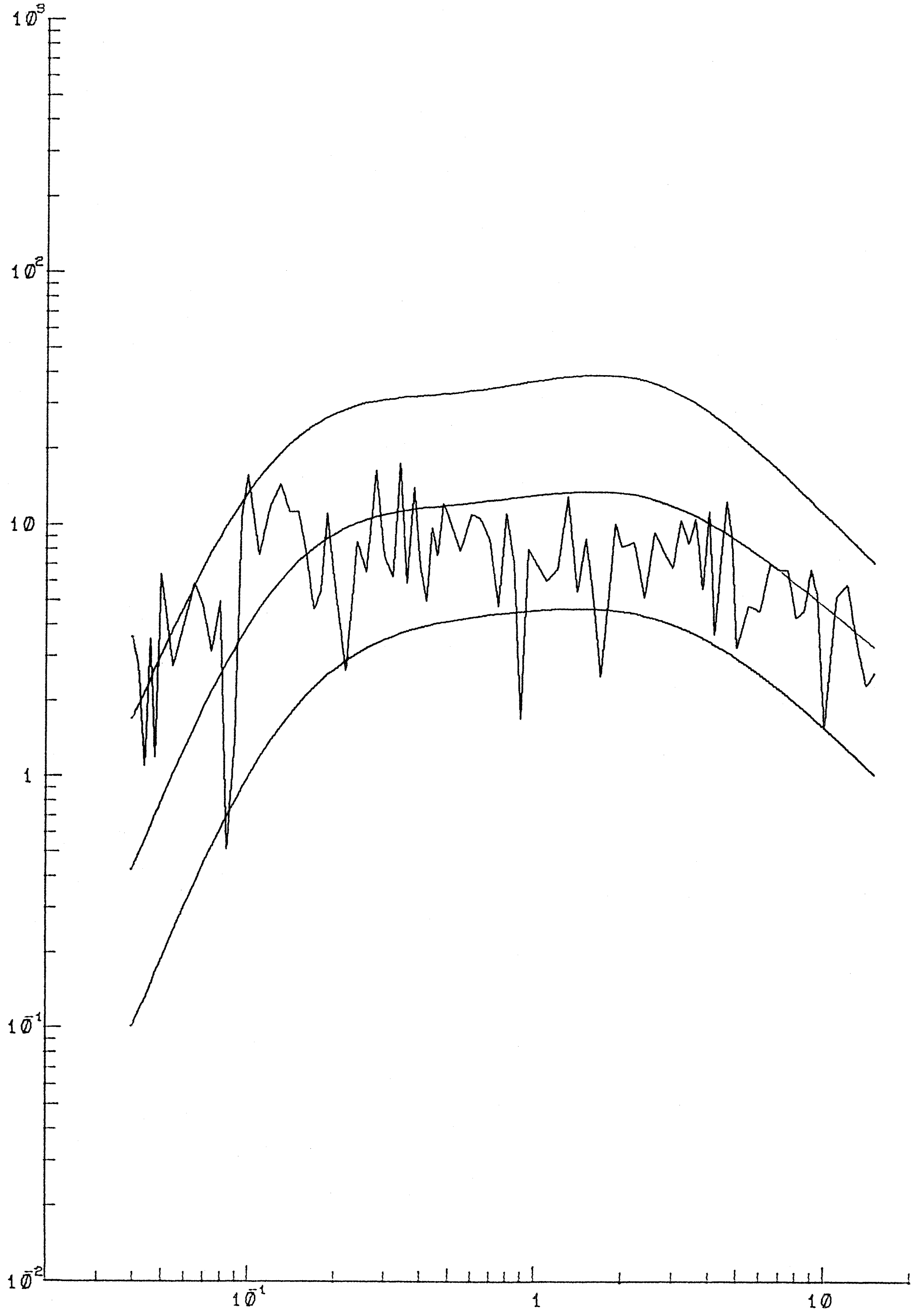

Figure I.6.6

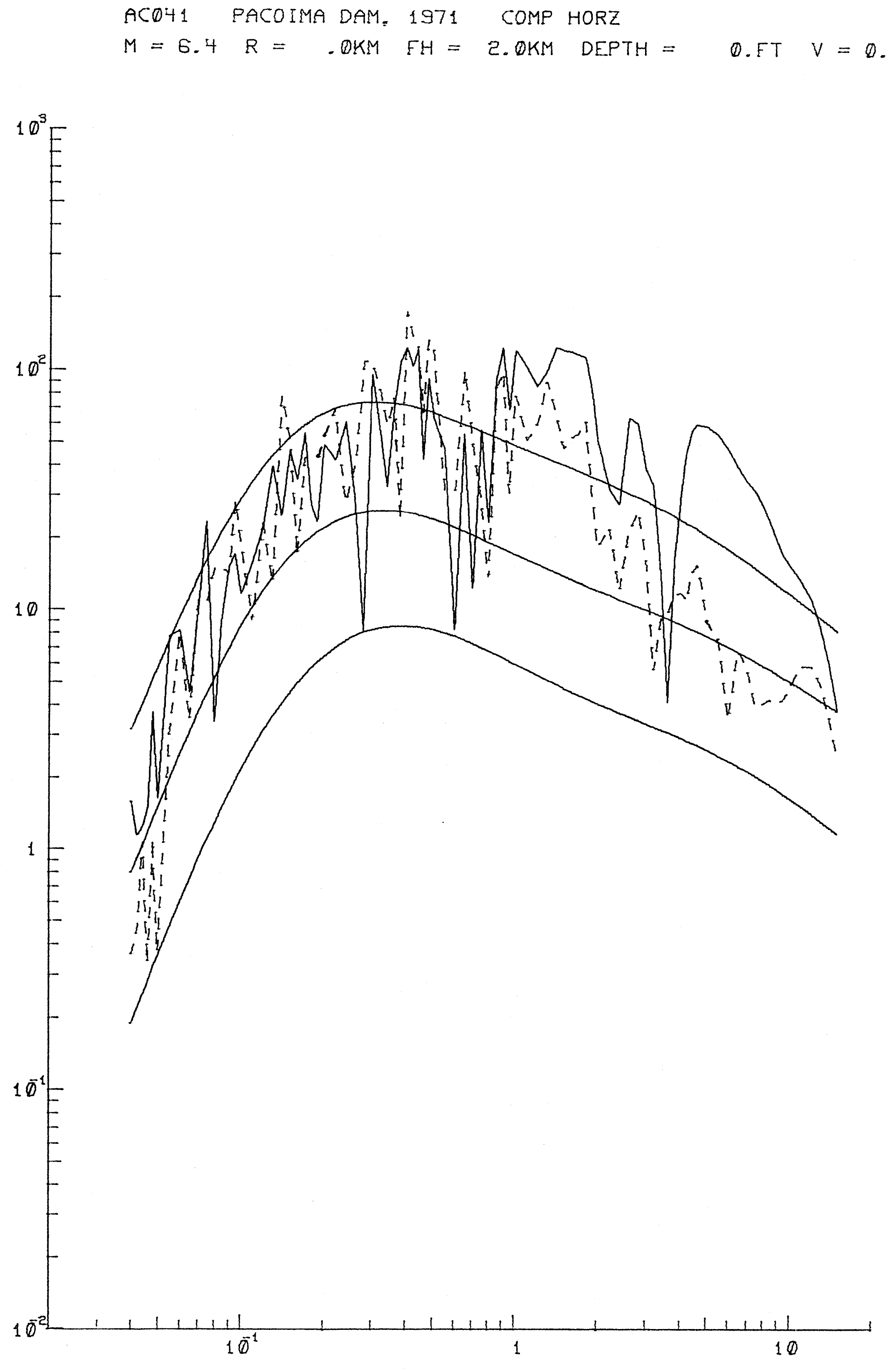
AC041 PACOIMA DAM, 1971 COMP HORZ
M = 6.4 R = .0KM FH = 2.0KM DEPTH = 0.FT V = 0.
10³
10²
10
1
10⁻¹
10⁻²
10⁻¹
1
10

Figure I.6.7

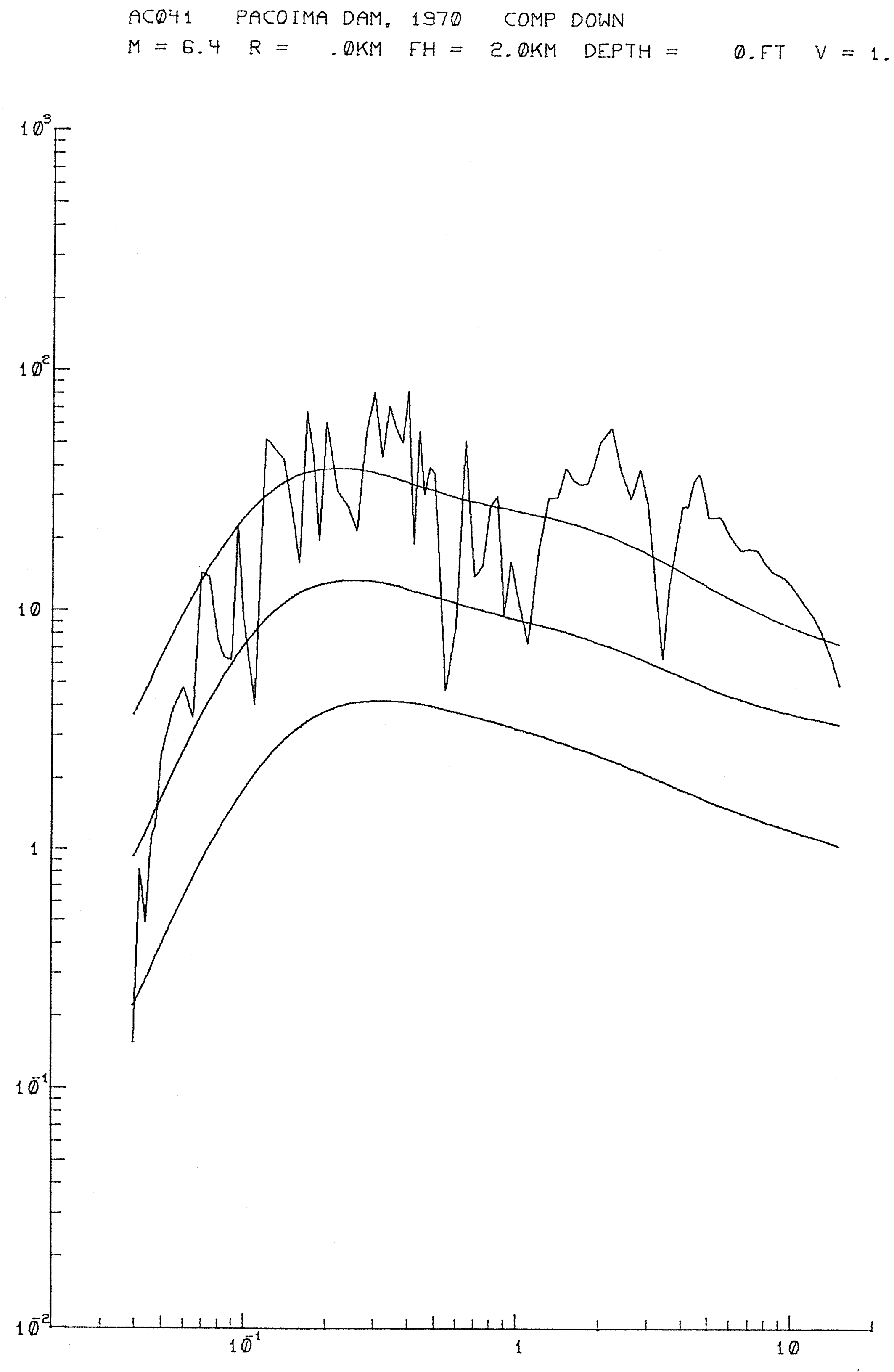

ACØ41 PACOIMA DAM, 1970 COMP DOWN
M = 6.4 R = .ØKM FH = 2.ØKM DEPTH = Ø.FT V = 1.
1Ø³
1Ø²
1Ø
1
1Ø⁻¹
1Ø⁻²
1Ø⁻¹
1
1Ø

Figure I.6.8

This type of agreement between empirically predicted and actually recorded spectra may be expected in many of the average or better than average cases. An example of a fit which is below average is illustrated in Figures I.6.7 and I.6.8 for the spectra of strong-motion accelerograms recorded at the Pacoima Dam site during the San Fernando, California earthquake of February 9, 1971. During this earthquake the fault rupture passed underneath the dam site (so $R = 0$ km) at a "focal depth" of $H \cong 2$ km. The other scaling parameters used are $M = 6.4$ and $h = 0$ ft. The average trend of the spectra of the recorded accelerograms is larger than that of the 50th percentile ($p = 0.5$) of the estimated spectra. Nevertheless, the estimated curves do follow the overall amplitude and shape trends quite well.

PART II: SCALING OF FOURIER SPECTRA IN TERMS OF M, R, S, s AND V

II.1 THE SCALING RELATION

Part II of this work continues the description of the preliminary empirical model for scaling Fourier amplitude spectra of strong ground motion in terms of earthquake magnitude, source-to-station "representative" distance and the local site geology. Part I characterizes the local geology by the approximate overall depth of sedimentary deposits beneath the recording station, h, in km. It has been pointed out previously, that while the depth of sediments at each recording station represents a preferable site characterization, in many instances, little may be known about the depth of alluvium and sedimentary layers at some sites so that the scaling of amplitudes at such sites using depth, h, is not possible. The site characterization in terms of s = 0, 1 and 2 (Trifunac and Brady, 1975), which can be determined from knowledge of surface geology only, thus remains a useful approach to the scaling of strong-motion amplitudes.

Ideally, a site should be classified either as an alluvium site (s = 0) or as a basement rock site (s = 2). The intermediate classification (s = 1) should be used only in complicated cases when it is not obvious how to select s = 0 or s = 2, typically corresponding to consolidated sedimentary rock or to a complex geologic environment (Trifunac and Brady, 1975), or when information on the site geology is not available. With this classification, of the 186 records of the original database, 87 records (63%) have been recorded on alluvium sites, 43 records (23%) come from "intermediate" sites and only 15 records (8%) were recorded on basement rock sites. With the new database of 438 records now available 313 records (71%) have been recorded on alluvium sites (s = 0), 76 records (17%) on "intermediate" sites (s = 1) and 47 records (11%) on basement rock sites (s = 2). The majority of records in the new database thus continue to come from alluvium sites.

Following Part I of this report, and adopting the form of the scaling relation in equation (I.5.1), the required scaling relation now takes the form

$$\log_{10} FS(T) = M + \mathcal{A}tt(\Delta,M,T) + b_1(T)M + b_2(T)s + b_3(T)v + b_5(T) + b_6(T)M^2 , \quad \text{(II.1.1)}$$

with all parameters defined as before. $b_2(T)$ is now the coefficient associated with the site condition s. Note that the term $b_4(T)\Delta/100$ is again deleted.

The scaling functions $b_1(t)$ through $b_6(T)$ are determined through the regression analysis of the new database of 1314 components of spectral amplitudes, FS(T) at 91 discrete periods T ranging from 0.04 sec to 15.0 sec. As in Part I of this report, the data are first screened for possible bias in the model. All procedures in data preparation and selection, and the form of the regression analysis employed here are identical to those in Part I of this report, and their description need not be repeated here.

The resulting fitted coefficients, at each period T, from linear regression are again denoted by $\hat{b}_1(T)$ through $\hat{b}_6(T)$, (as in equation (I.5.2)), respectively. Much of the format of the description in this and the sections to follow will almost be identical to that in Part I of this work.

Substituting the fitted coefficients in equation (II.1.1) gives $\hat{FS}(T)$, where

$$\log_{10}\hat{FS}(T) = M + \mathscr{A}tt(\Delta,M,T) + \hat{b}_1(T)M + \hat{b}_2(T)s + \hat{b}_3(T)v + \hat{b}_5(T) + \hat{b}_6(T)M^2 \qquad \text{(II.1.2)}$$

As before, equation (II.1.2) applies only in the range $M_{min} \le M \le M_{max}$, where

$$M_{min} = -\hat{b}_1(T)/(2\hat{b}_6(T)) \text{ and}$$

$$M_{max} = -(1 + \hat{b}_1(T))/(2\hat{b}_6(T)), \qquad \text{(II.1.3)}$$

and equation (II.1.2) is then modified to:

$$\log_{10}\hat{FS}(T) = \mathscr{A}tt(\Delta,M,T) + \begin{cases} M + b_1(T)M_{min} + \hat{b}_2(T)s + \hat{b}_3(T)v + \hat{b}_5(T) + \hat{b}_6(T)M^2_{min}, & M \le M_{min} \\ M + \hat{b}_1(T)M + \hat{b}_2(T)s + \hat{b}_3(T)v + \hat{b}_5(T) + \hat{b}_6(T)M^2, & M_{min} \le M \le M_{max} \\ M_{max} + \hat{b}_1(T)M_{max} + \hat{b}_2(T)s + \hat{b}_3(T)v + \hat{b}_5(T) + \hat{b}_2(T)M^2_{max}, & M_{max} \le M \end{cases}$$

The residues $\varepsilon(T) = \log_{10}[FS(T)] - \log_{10}[\hat{FS}(T)]$ describing the distribution of the observed FS(T) about the estimated $\hat{FS}(T)$ are next calculated. As in the previous part, $\varepsilon(T)$ is described by a normal distribution function with mean $\mu(T)$ and standard deviation $\sigma(T)$.

II.2 THE REGRESSION COEFFICIENTS

Figure II.2.1 shows the smoothed coefficients $\hat{b}_1(T)$, $\hat{b}_2(T)$, $\hat{b}_3(T)$, $\hat{b}_5(T)$ and $\hat{b}_6(T)$ (solid lines) together with the estimates of their 80%, 90% and 95% confidence intervals (dashed lines). Comparison of this figure with the corresponding Figure I.5.1 in the previous Part I of this work shows that the functions $\hat{b}_1(T)$, $\hat{b}_3(T)$, $\hat{b}_5(T)$ and $\hat{b}_6(T)$ as given respectively by the first, third, fourth and fifth graphs from the top are almost identical. The functions correspond to the same parameters, M, v, 1 and M^2, respectively, in the scaling relations and their similarity demonstrates the consistency of the two models of scaling. The functions $\hat{b}_2(T)$ as given by the second graph from the top in both figures are of opposite sign, which again is consistent with the models since s = 2 corresponds to h = 0 km (basement rock), while s = 0 corresponds to h >> 0 km (alluvium). The bottom graph of Figure II.2.1 shows M_{min} and M_{max} as given by equation (II.1.3).

Figure II.2.2 shows the plot of the residual levels corresponding to $p^* (\varepsilon,T) = 0.1, 0.2,\ldots,0.8$ and 0.9 for $\log_{10}FS(T)$. Refer to the same Figure I.5.2 in Part I of this work for a complete description of each of the nine sets of curves. It is of interest to compare these two figures, since those illustrate the spread of the observed data about their corresponding models, which differ only in the characterization of local site geology. The resemblance of the two figures demonstrates clearly that the uncertainties associated with the characterization of local geology in terms of site parameters s = 0, 1 and 2 are not much greater than those associated with site characterization in terms of alluvial depth, h.

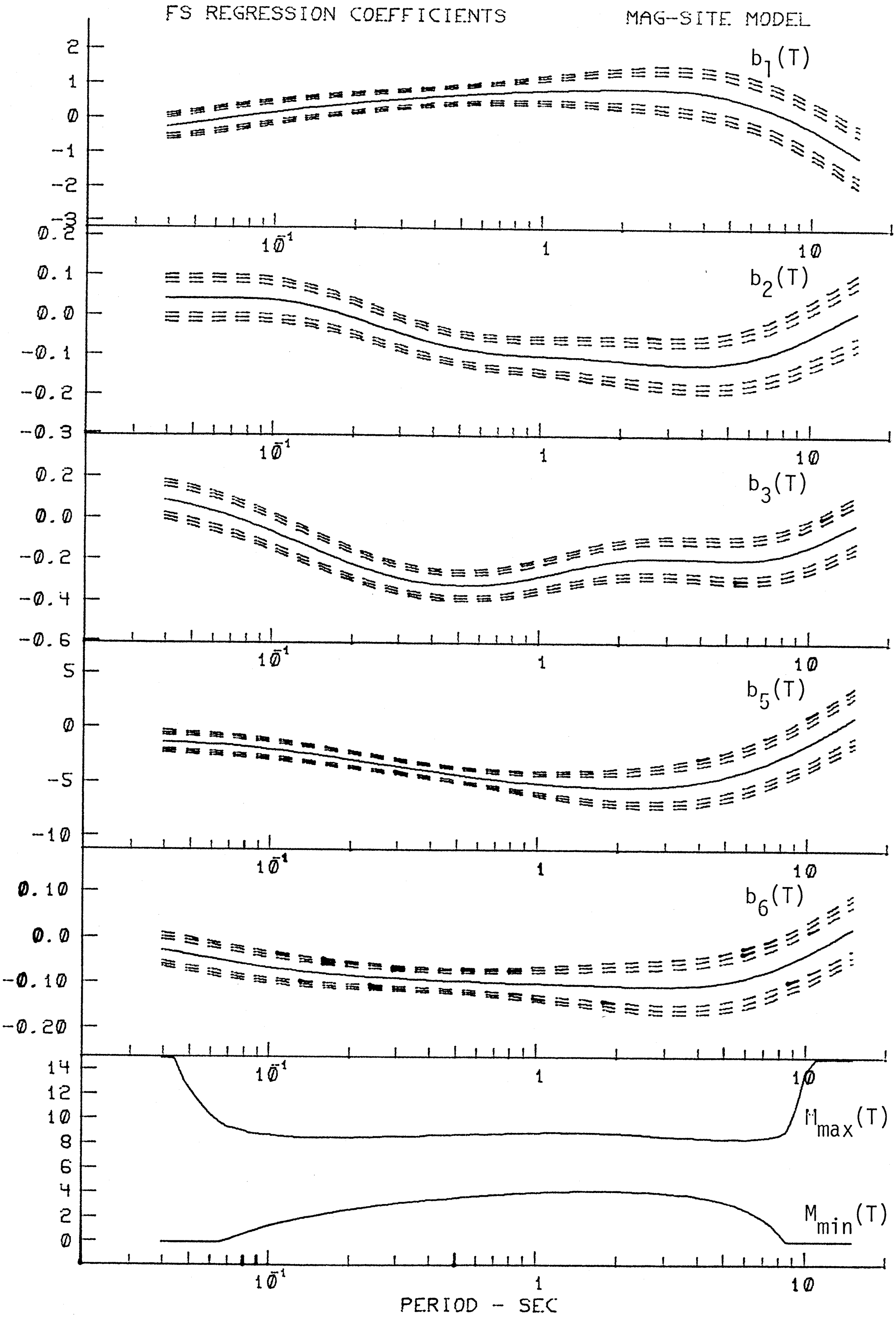
FS REGRESSION COEFFICIENTS
MAG-SITE MODEL
$b_1(T)$
$b_2(T)$
$b_3(T)$
$b_5(T)$
$b_6(T)$
$M_{max}(T)$
$M_{min}(T)$
2
1
Ø
-1
-2
-3
Ø.2
Ø.1
Ø.Ø
-Ø.1
-Ø.2
-Ø.3
Ø.2
Ø.Ø
-Ø.2
-Ø.4
-Ø.6
5
Ø
-5
-1Ø
Ø.1Ø
Ø.Ø
-Ø.1Ø
-Ø.2Ø
14
12
1Ø
8
6
4
2
Ø
1Ø⁻¹
1
1Ø
PERIOD - SEC

Figure II.2.1

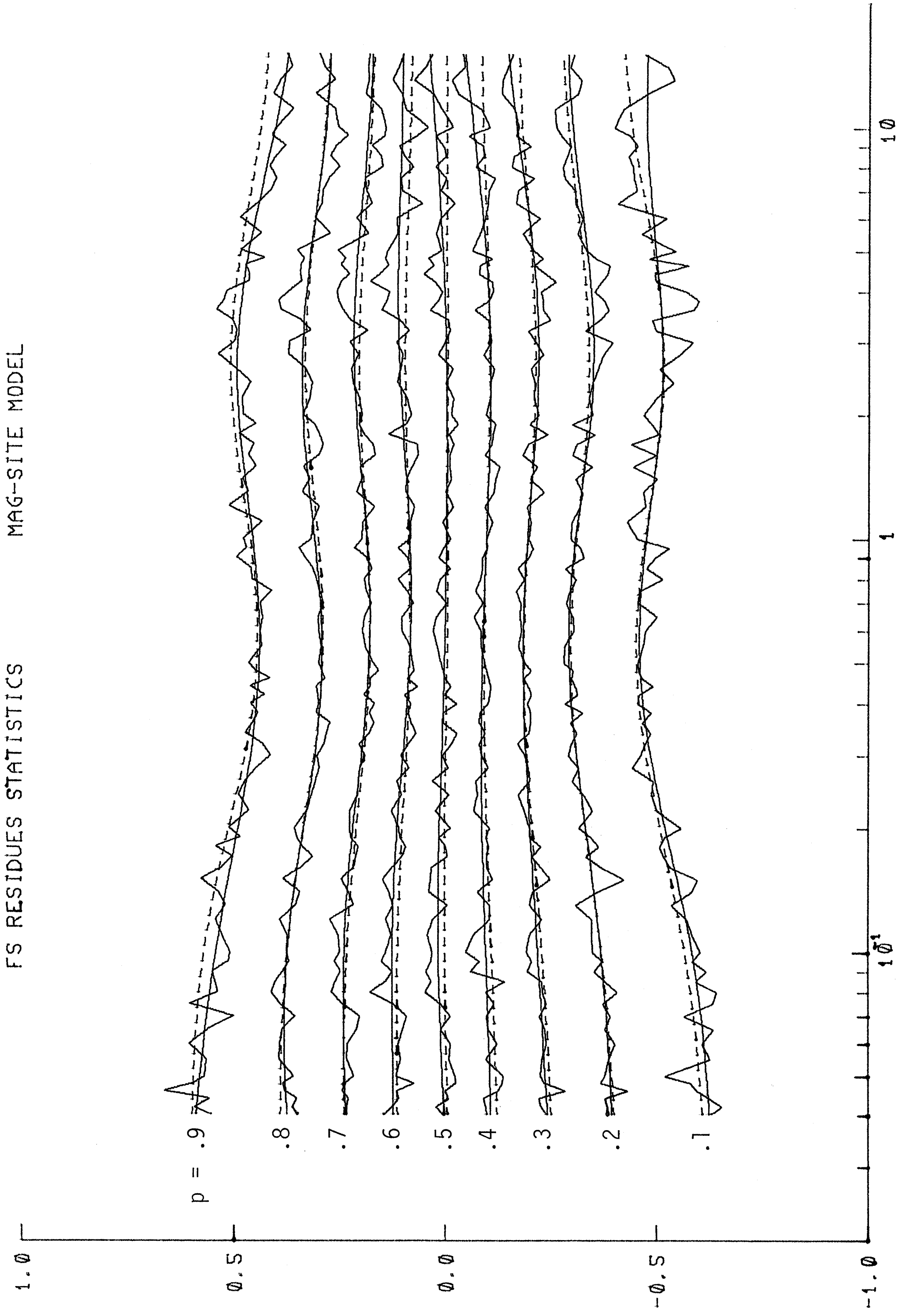
FS RESIDUES STATISTICS
MAG-SITE MODEL
p = .9
.8
.7
.6
.5
.4
.3
.2
.1
1.0
0.5
0.0
-0.5
-1.0
10⁻¹
1
10

Figure II.2.2

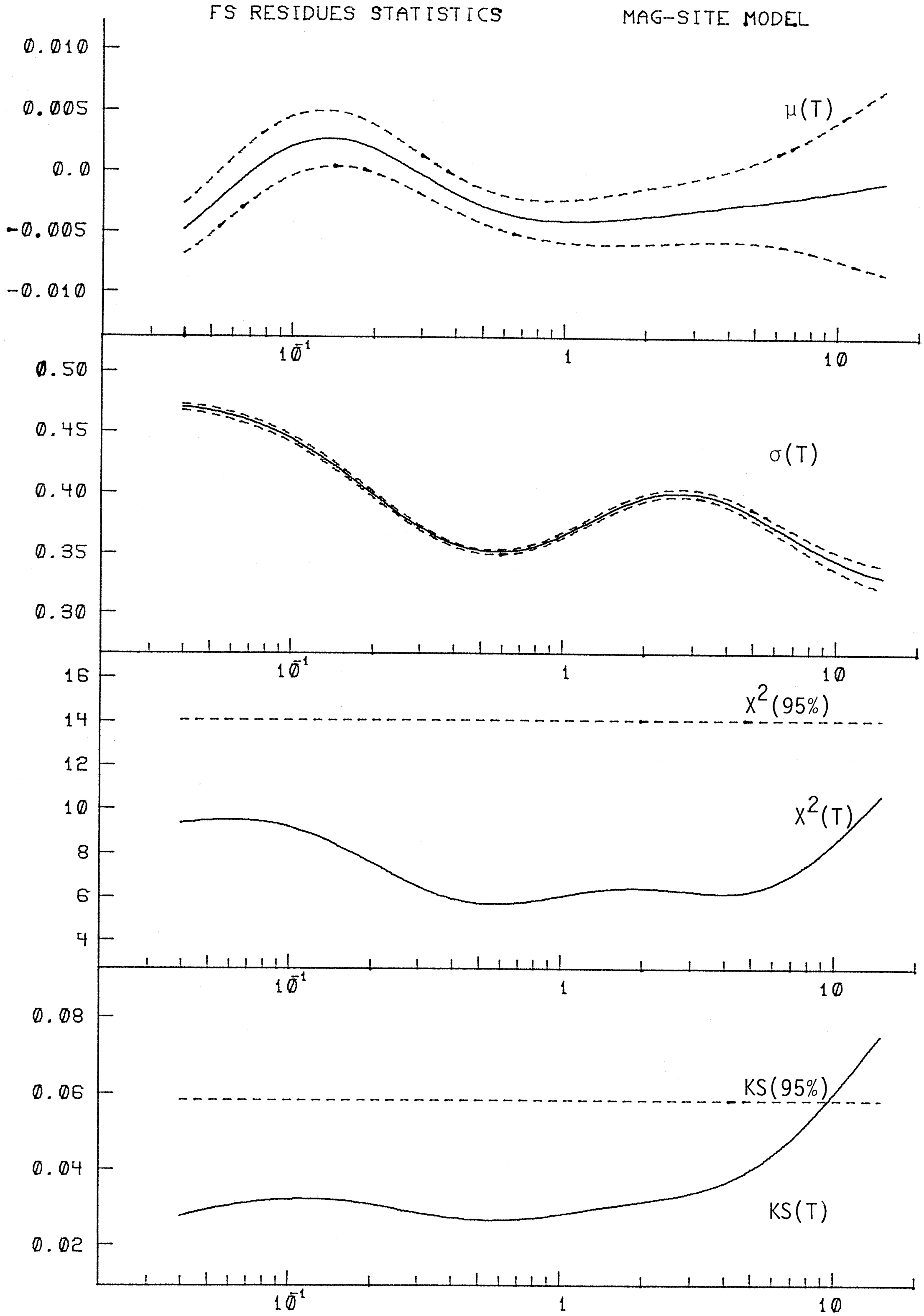
FS RESIDUES STATISTICS
MAG-SITE MODEL
0.010
0.005
0.0
-0.005
-0.010
μ(T)
10⁻¹
1
10
0.50
0.45
0.40
0.35
0.30
σ(T)
16
14
12
10
8
6
4
χ²(95%)
χ²(T)
0.08
0.06
0.04
0.02
KS(95%)
KS(T)

Figure II.2.3

TABLE II.2.1

$$\log_{10} FS(T) = M + \mathscr{A}tt(\Delta,M,T) + b_1(T)M + b_2(T)s + b_3(T)v + b_5(T) + b_6(T)M^2$$

PERIOD, T(SEC)	.040	.065	.11	.19	.34	.50	.90	1.60	2.80	4.40	7.50	14.00
COEFFICIENTS:												
$b_1(T)$	-.258	-.019	.222	.433	.610	.706	.820	.883	.869	.712	.184	-.933
$b_2(T)$	.041	.042	.033	-.003	-.057	-.084	-.102	-.110	-.122	-.121	-.086	.002
$b_3(T)$	.086	.015	-.092	-.216	-.309	-.329	-.294	-.223	-.191	-.201	-.183	-.044
$b_5(T)$	-1.373	-1.681	-2.207	-2.965	-3.844	-4.394	-5.100	-5.487	-5.395	-4.741	-2.924	.580
$b_6(T)$	-.030	-.052	-.072	-.086	-.094	-.098	-.103	-.107	-.109	-.102	-.069	.012
M_{min}	.000	.000	1.542	2.530	3.240	3.598	3.985	4.137	3.976	3.478	1.340	.000
M_{max}	16.756	9.599	8.476	8.374	8.550	8.692	8.845	8.823	8.551	8.361	8.608	15.000
RESIDUES:												
p = .1	-.624	-.609	-.576	-.526	-.476	-.460	-.469	-.500	-.513	-.502	-.481	-.475
p = .2	-.395	-.384	-.365	-.337	-.305	-.293	-.303	-.333	-.350	-.341	-.313	-.290
p = .3	-.243	-.231	-.217	-.202	-.188	-.184	-.191	-.209	-.219	-.211	-.184	-.150
p = .4	-.108	-.103	-.095	-.088	-.086	-.088	-.095	-.104	-.105	-.098	-.078	-.048
p = .5	.004	.012	.017	.014	.007	.003	-.001	-.003	-.001	.005	.019	.038
p = .6	.123	.125	.125	.115	.096	.086	.084	.097	.111	.114	.109	.104
p = .7	.237	.240	.237	.220	.194	.181	.184	.204	.218	.213	.193	.175
p = .8	.374	.380	.369	.337	.302	.292	.306	.332	.340	.326	.297	.275
p = .9	.589	.567	.535	.494	.454	.441	.452	.482	.494	.476	.431	.378
RESIDUE STATISTICS:												
$\mu(T)$	-.005	-.001	.002	.002	-.001	-.003	-.004	-.004	-.003	-.003	-.002	-.001
$\sigma(T)$	.471	.460	.438	.402	.363	.351	.361	.388	.400	.388	.358	.331
χ^2	9.379	9.498	9.017	7.698	6.169	5.687	5.950	6.418	6.270	6.194	7.257	10.267
KS(T)	.028	.031	.032	.031	.028	.027	.028	.030	.033	.038	.050	.073

Figure II.2.3 shows the plot of the statistical parameters in the description of the residues, namely, $\hat{\mu}(T)$, $\hat{\sigma}(T)$, $X^2(T)$ and KS(T) from top to bottom. Note that except for T beyond 10 sec, both the X^2 and KS tests again fail to reject the hypothesis that the distribution is normal.

Table II.2.1 gives, for 12 periods between T = 0.04 sec and and T = 14 sec, the five regression coefficients, $\hat{b}_1(T)$, $\hat{b}_2(T)$, $\hat{b}_3(T)$, $\hat{b}_5(T)$ and $\hat{b}_6(T)$, $\hat{M}_{min}(T)$, $\hat{M}_{max}(T)$, the nine residue levels corresponding to $p^*(\varepsilon,T) = 0.1$ through 0.9, the coefficients $\hat{\mu}(T)$, $\hat{\sigma}(T)$ of the normal distribution and finally the $X^2(T)$ and KS(T) statistics.

II.3 EXAMPLES OF ESTIMATED FOURIER SPECTRA

Figures II.3.1 and II.3.2 present examples of FS(T) computed for M = 4.5, 5.5, 6.5 and 7.5 at R = 0, H = 5 km for $p(\varepsilon, T) = 0.5$. Figure II.3.1 is for horizontal motion (v = 0) while Figure II.3.2 is for vertical motion (v = 1). The solid lines in the figures correspond to s = 2, while the dashed lines correspond to s = 0. The diagonal dashed lines again represent the empirical average Fourier amplitudes of digitization noise.

Comparison of these figures with the corresponding Figures I.6.1 and I.6.2 of Part I shows an interesting trend. It has been noted previously, that for the same magnitude, M, the spectral amplitudes are slightly higher for basement rock (s = 2) then for alluvial site (s = 0) for periods up to 0.2 seconds, beyond which the trend is reversed. This trend is observed here, but not for the model using depth of sediments as shown in Figures I.6.1 and I.6.2. There it is only observed that the effect of the depth of sediments is negligible at short periods, and for the same magnitude, M, and spectral amplitudes are higher for alluvial site ($h >> 0$) than for basement roch (h = 0) only for intermediate to long periods.

Figure II.3.3 illustrates the effects of epicentral distance R, and Figure II.3.4 shows the effects of focal depth H, on the changes of spectral amplitudes. Comparison of these figures with the corresponding Figures I.6.3 and I.6.4 in Part I of this work shows considerable degree of similarity.

Figures II.3.5 and II.3.6 compare the amplitudes computed from the accelerations recorded in 1940 in El Centro, with those calculated

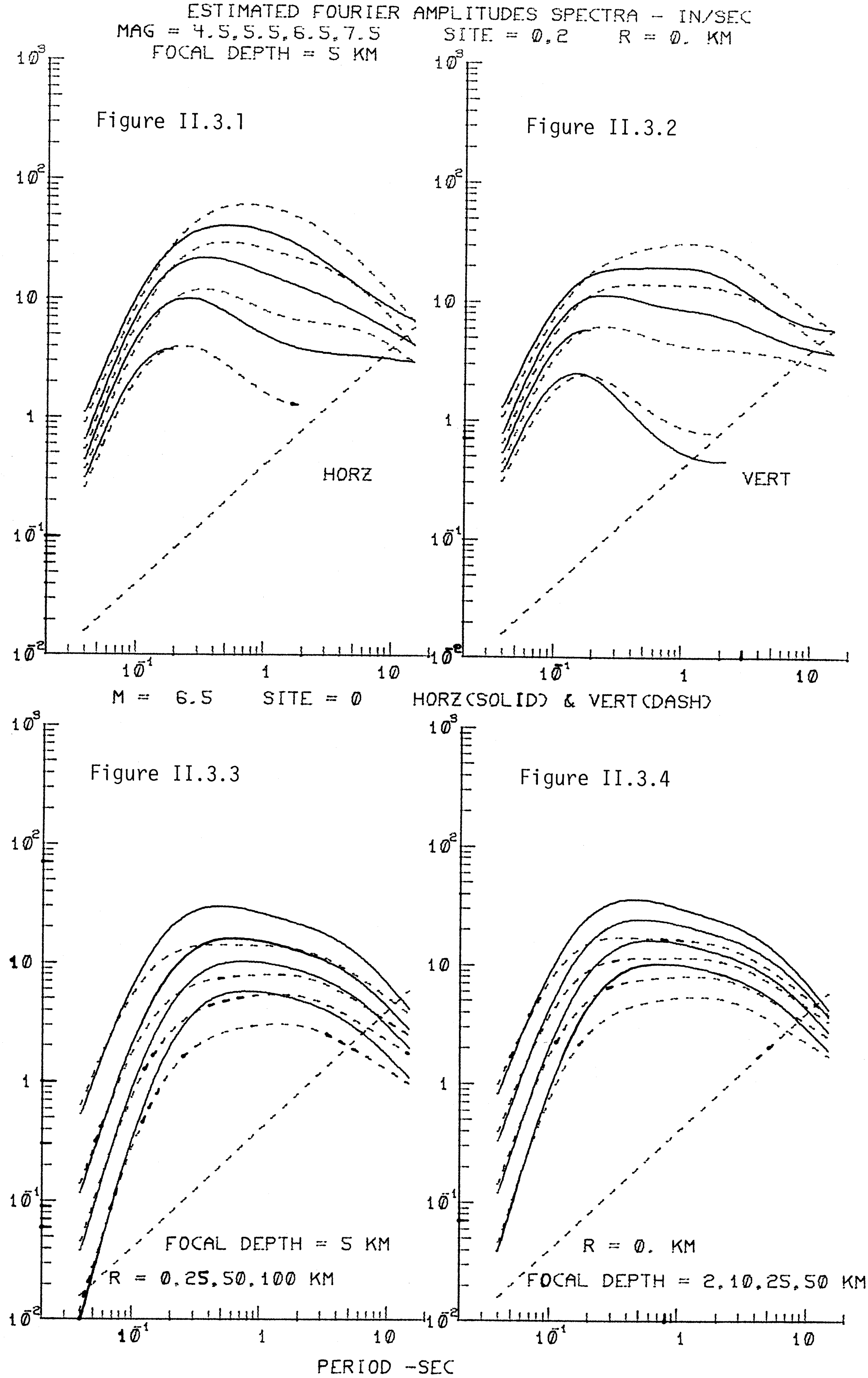
ESTIMATED FOURIER AMPLITUDES SPECTRA - IN/SEC
MAG = 4.5,5.5,6.5,7.5
SITE = 0,2
R = 0. KM
FOCAL DEPTH = 5 KM
Figure II.3.1
HORZ
Figure II.3.2
VERT
M = 6.5
SITE = 0
HORZ(SOLID) & VERT(DASH)
Figure II.3.3
FOCAL DEPTH = 5 KM
R = 0,25,50,100 KM
Figure II.3.4
R = 0. KM
FOCAL DEPTH = 2,10,25,50 KM
PERIOD -SEC

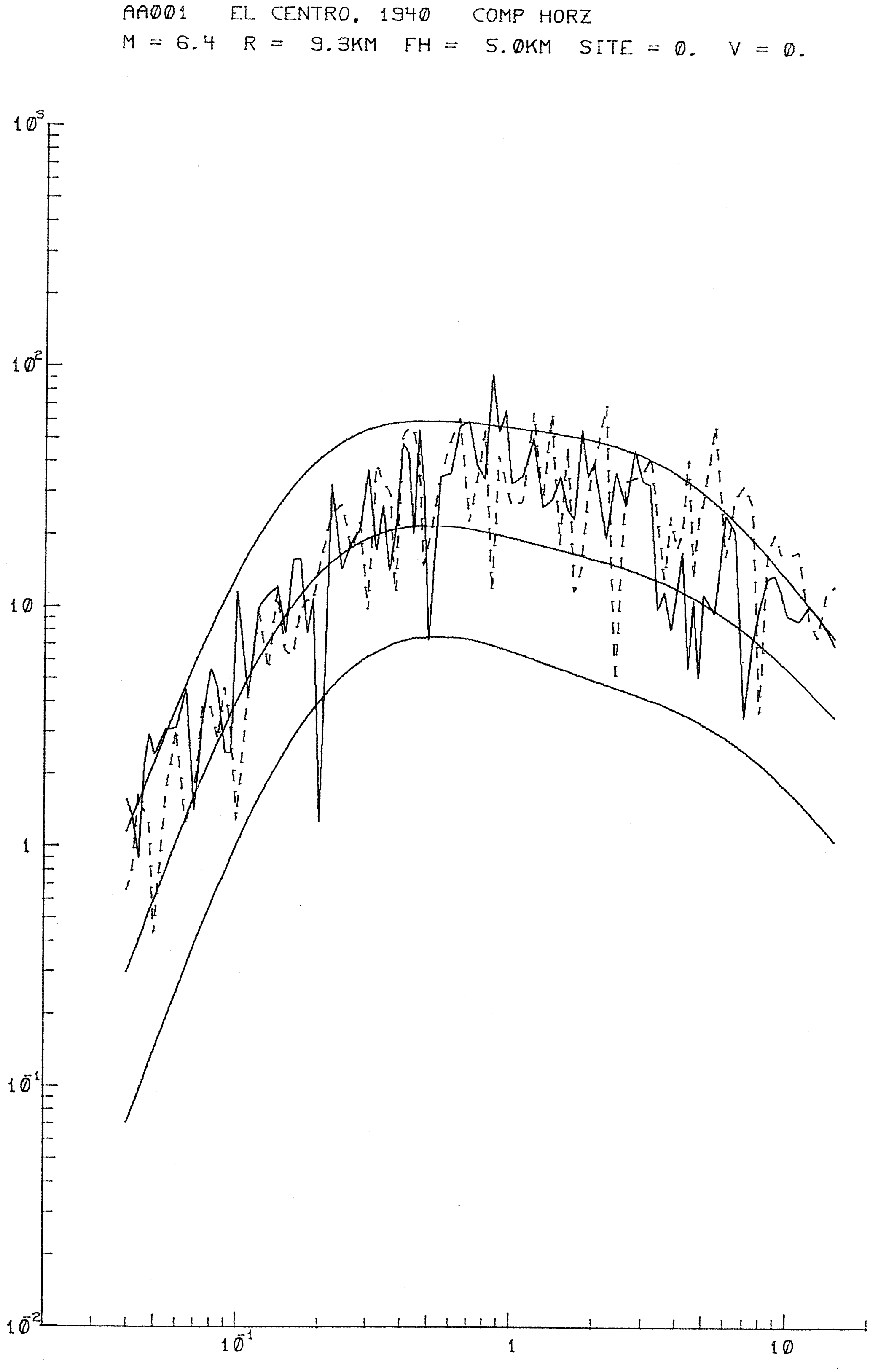
AA001 EL CENTRO, 1940 COMP HORZ
M = 6.4 R = 9.3KM FH = 5.0KM SITE = 0. V = 0.
10^3
10^2
10
1
10^{-1}
10^{-2}
10^{-1}
1
10

Figure II.3.5

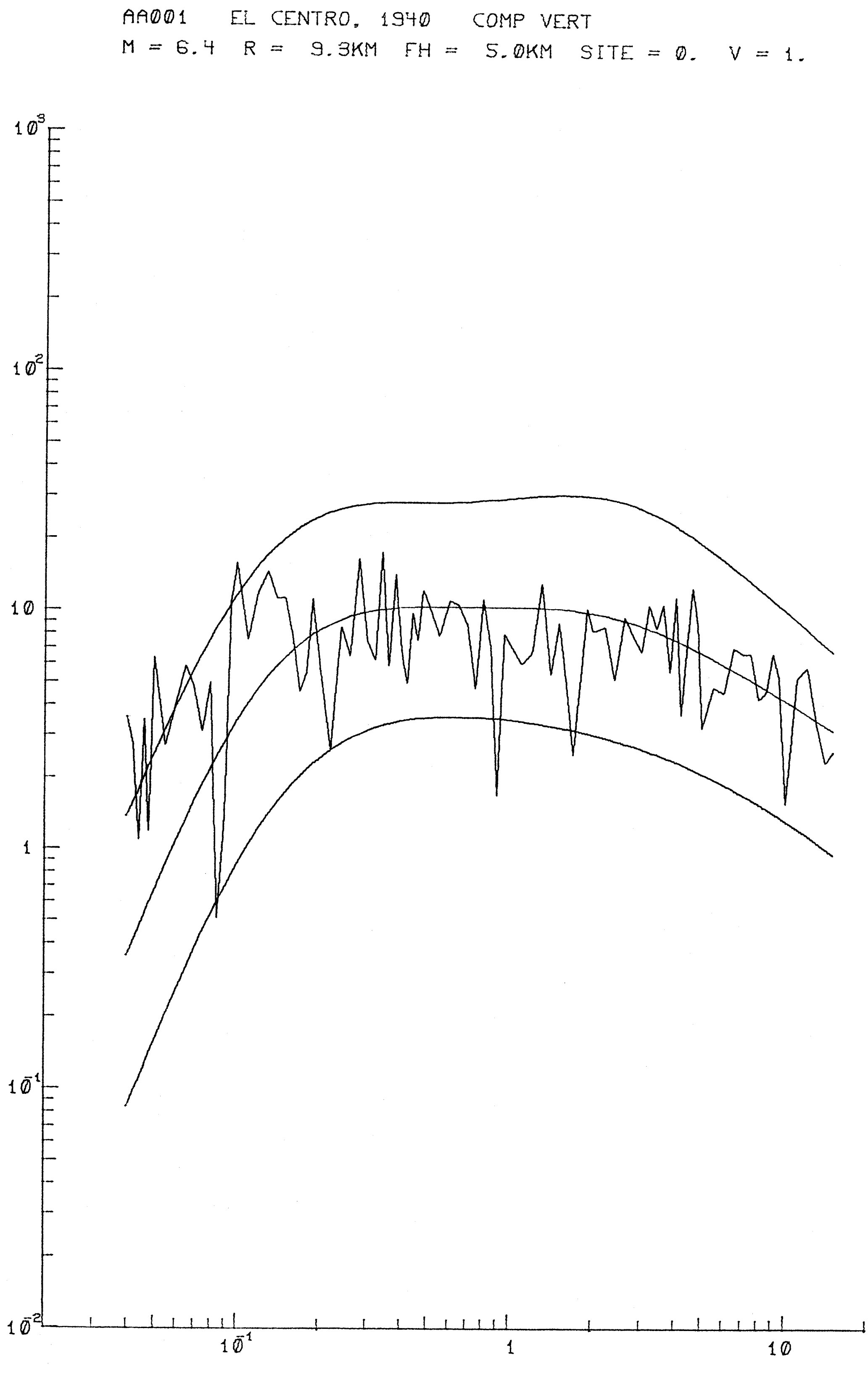
AA001 EL CENTRO, 1940 COMP VERT
M = 6.4 R = 9.3KM FH = 5.0KM SITE = 0. V = 1.
10³
10²
10
1
10⁻¹
10⁻²
10⁻¹
1
10

Figure II.3.6

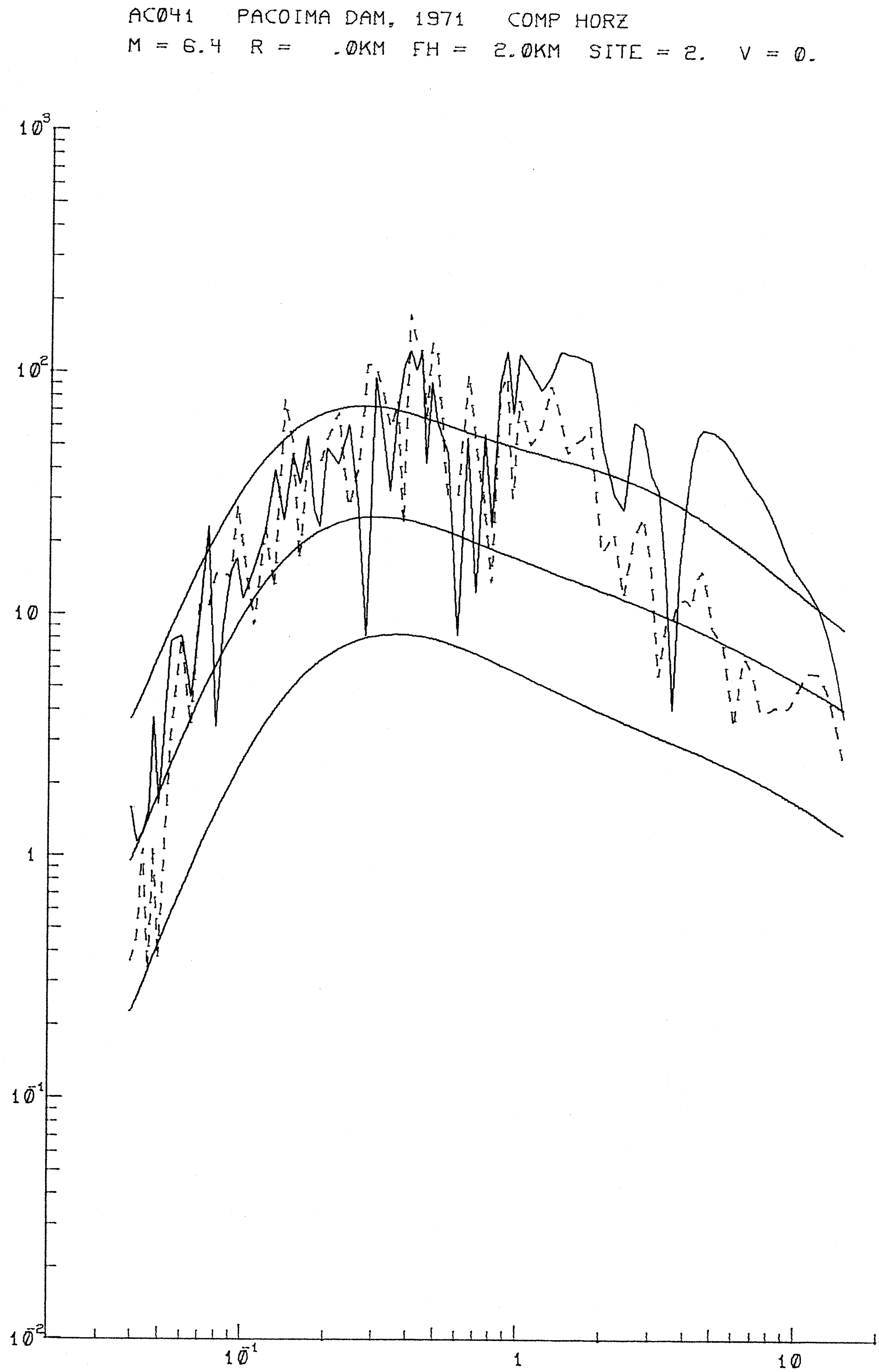
AC041 PACOIMA DAM, 1971 COMP HORZ
M = 6.4 R = .0KM FH = 2.0KM SITE = 2. V = 0.
10³
10²
10
1
10⁻¹
10⁻²
10⁻¹
1
10

Figure II.3.7

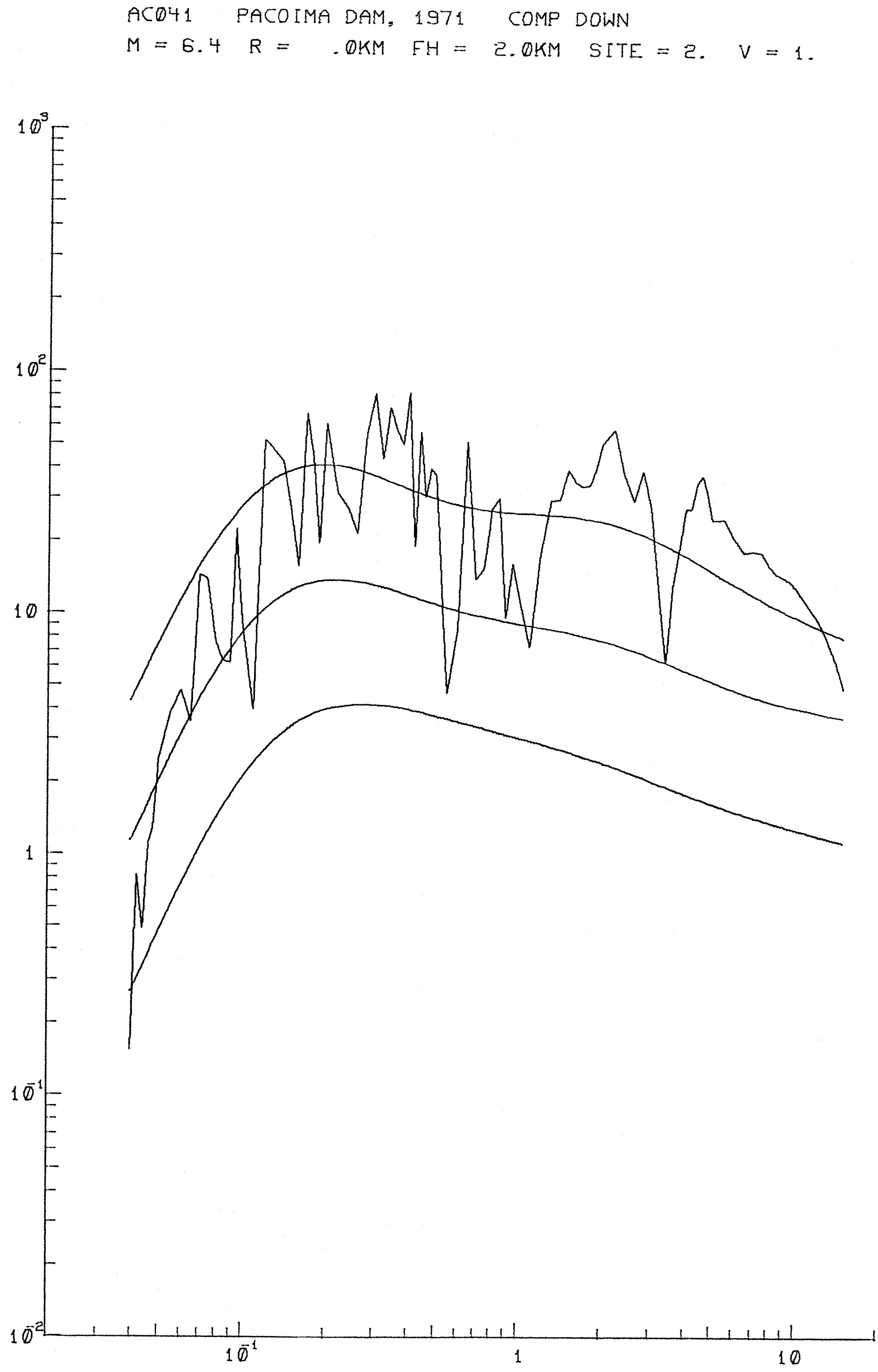
AC041 PACOIMA DAM, 1971 COMP DOWN
M = 6.4 R = .0KM FH = 2.0KM SITE = 2. V = 1.
10³
10²
10
1
10⁻¹
10⁻²
10⁻¹
1
10

Figure II.3.8

from M = 6.4, R = 9.3 km, H = 5 km and s = 0. The agreement is fair to good. Figures II.3.7 and II.3.8 compare the spectral amplitudes computed from the 1971 Pacoima Dam accelerations with the spectral estimates calculated for M = 6.4, R = 0 km, H = 2 km and s = 2. The fit is again of similar quality, as that in the case of the model in Part I (Figures I.6.7 and I.6.8).

This completes the presentation of Part II of the scaling of FS(T) in terms of M, R, H, s and v.

PART III: SCALING OF FOURIER SPECTRA IN TERMS OF MMI, h AND v

III.1 THE SCALING RELATION

Parts I and II of this work presented a description of the preliminary empirical model for scaling Fourier amplitude spectra of strong earthquake ground motion in terms of earthquake magnitude, souce-to-station distance and a characterization of local geology at the recording station. Parts III and IV of this work will extend this method to the scaling of Fourier amplitude spectra in terms of the Modified Mercalli Intensity (MMI) and a characterization of local geology at the recording site.

Such an analysis was initiated by Trifunac (1979) who pointed out that a description of the expected levels of ground shaking at a site in terms of earthquake intensity will likely remain a common engineering tool for many years to come. Although new instrumentation is now being deployed in many parts of the world, the long-term historical seismicity records are still available only in terms of the locally developed intensity scales. For this reason, it is worthwhile now to re-evaluate the nature of correlations that exist between earthquake intensity and the Fourier amplitudes of recorded ground motions, in spite of all the shortcomings associated with this qualitative and descriptive scaling of strong earthquake ground motion. Further it is worthwhile to re-examine the meaning of such scaling as it still represents an important basis for extrapolating the possible future earthquake risk in many seismic zones of the world.

Trifunac (1979) developed a direct correlation between the Fourier spectrum amplitudes and the reported MMI at the recording stations using the database of the same 57 earthquakes and the corresponding 186 records that were used earlier (Trifunac (1976b)) for scaling of spectra in terms of earthquake magnitudes. The distribution of these data with respect to the levels of Modified Mercalli Intensity reported at the recording sites is as follows: MMI = III, 1 record; MMI = IV, 3 records; MMI = V, 34 records: MMI = VI, 66 records; MMI = VII, 75 records; MMI = VIII, 6 records, and MMI = X, 1 record. The local geology was then characterized by the geologic site conditions, s, (see Part II of this report for discussion and references on parameters).

Trifunac and Lee (1978) extended this type of analysis by including the depth of sedimentary deposits beneath the recording station, h, as a site characteristic, in place of the site parameter s. The scaling equation then became (equation (5) of Trifunac and Lee (1978)):

$$\log_{10}[FS(T)] = b(T)I_{MM} + c(T) + d(T)h + e(T)v \ , \qquad \text{(III.1.1)}$$

with I_{MM} denoting the reported levels on the MMI scale, and with all other parameters defined as above. The form of equation (III.1.1) was chosen on the basis of several previous analyses (Trifunac (1976a,b); Trifunac and Anderson (1977)), suggesting that only the linear terms in the equations are statistically significant and that all higher order terms as well as the mixed terms may be omitted from the analysis.

The same analysis has been carried out now on the new database of 438 free-field records from 104 earthquakes. The new set of earthquakes that have been added to the catalogue through the years 1972 to 1981 have magnitudes typically below 6. For this reason the MMI levels for many of these earthquakes are not well documented or have not been reported. One possible approach then to estimating spectral amplitudes of strong shaking in terms of MMI at the recording site would be first to develop correlations between the MMI levels with the corresponding earthquake magnitude, representative source to station distance and local site geology. Lee and Trifunac (1985) used the original database of 57 earthquakes and 186 stations where the reported MMI levels are available and performed the above correlation with the following equation:

$$I_{MM} = 1.5M - A - B\ell n\Delta - C\Delta/100 - Ds \qquad \text{(III.1.2)}$$

where the parameters M, Δ and s are defined as before. The estimated MMI levels at the 186 stations were next compared with the corresponding reported MMI levels. The resulting coefficient of correlation was found to be around 0.8. The point by point comparisons also showed very good agreement between equation III.1.2 and observed intensities. Equation (III.1.2) was then used to calculate the estimated MMI levels at those free-field sites in the new database for which no reported site intensities were available.

For scaling the Fourier amplitude spectra the following equation was employed:

$$\log_{10}[FS(T)] = b_1(T)\hat{I}_{MM} + b_2(T)h + b_3(T)v + b_4(T) \;, \qquad \text{(III.1.3)}$$

which is the same as equation (III.1.1). Here $\hat{I}_{MM}$ is the estimated MMI level at the site computed from equation (III.1.2) or the reported MMI level if available.

The distribution of the new database with respect to the levels of Modified Mercalli Intensity estimated or reported at the recording sites now becomes: MMI = II, 1 record, MMI = III, 8 records, MMI = IV, 15 records; MMI = V, 99 records; MMI = VI, 161 records; MMI = VII, 117 records; MMI = VIII, 30 records, MMI = IX, 2 records; and MMI = X, 1 record.

The regression analysis was next performed on the new database with 1314 components of Fourier amplitudes FS(T), at 91 discrete periods T ranging from 0.04 to 15.0 sec. This procedure is identical to the procedure used with the old database (Trifunac, 1979; Trifunac and Lee, 1978). For completeness of this writing the details are repeated here briefly. As in the previous parts of the report, the data are first screened to minimize possible bias in the model. The data are partitioned into groups corresponding to MMI levels III, IV, V, VI, VII, VIII, IX and X. The data in each of these MMI levels are further subdivided according to the site classification parameter s = 0, 1 or 2. Depending on whether the recording component is horizontal or vertical, each of these subgroups is divided into 2 sets corresponding to horizontal (v = 0) and vertical (v = 1) components. The resulting data in each of the groups correspond to the Fourier spectral amplitudes from a specified MMI level for a specified site classification and with specified component orientation. The data points, $\log_{10}FS(T)$, within these groups are then arranged in increasing order according to their amplitudes. If the number of data points in a group is less than 19, all the data points are selected. If there are more than 19 points, at most 19 points are selected from among the ordered set of data so that they correspond uniformly, as close as possible, to the 5%, 10%,...,90% and 95% percentiles.

The resulting fitted coefficients at each period T resulting from linear regression have been denoted by $\hat{b}_1(T)$, $\hat{b}_2(T)$, $\hat{b}_3(T)$ and $\hat{b}_4(T)$, (equation (III.1.3) respectively.

III.2 THE REGRESSION COEFFICIENTS

Figure III.2.1 shows the smoothed coefficients $\hat{b}_1(T)$, $\hat{b}_2(T)$, $\hat{b}_3(T)$ and $\hat{b}_4(T)$ (solid lines) and the estimates of their 80%, 90% and 95% confidence intervals, represented by the corresponding dashed lines. Substituting these coefficients into equation (III.1.3) gives:

$$\log_{10}\hat{FS}(T) = \hat{b}_1(T)\hat{I}_{MM} + \hat{b}_2(T)h + \hat{b}_3(T)v + \hat{b}_4(T). \qquad (III.2.1)$$

$\hat{FS}(T)$ then represents the least squares estimate of the Fourier amplitude spectrum at period T for this model.

With FS(T) the corresponding Fourier amplitude spectrum computed from recorded accelerograms, the residuals, $\varepsilon(T)$, were calculated as in Parts I and II of this report, where

$$\varepsilon(T) = \log_{10}FS(T) - \log_{10}\hat{FS}(T) \; . \qquad (III.2.2)$$

As for Parts I and II, the assumption that $\varepsilon(T)$ can be described by a normal distribution function with mean $\mu(T)$ and standard deviation $\sigma(T)$ is employed here. The probability $p(\varepsilon,T)$ at period T that

$$\log_{10}FS(T) - \log_{10}\hat{FS}(T) \leq \varepsilon(T) \qquad (III.2.3)$$

is then given by (equation (I.5.4) of Part I):

$$p(\varepsilon,T) = \frac{1}{\sigma(T)\sqrt{2\pi}} \int_{-\infty}^{\varepsilon(T)} \exp\left[-\frac{1}{2}\left(\frac{x-\mu(T)}{\sigma(T)}\right)^2\right]dx \qquad (III.2.4)$$

For a given residue, $\varepsilon(T)$, at a particular period T, the actual probability $p^*(\varepsilon,T)$ that $\varepsilon(T)$ will not be exceeded can be evaluated by finding the fraction of residuals $\varepsilon(T)$ (computed from the database at that particular period) which are smaller than a given value. Using (III.2.4), the estimated probability $\hat{p}(\varepsilon,T)$ that $\varepsilon(T)$ will not be

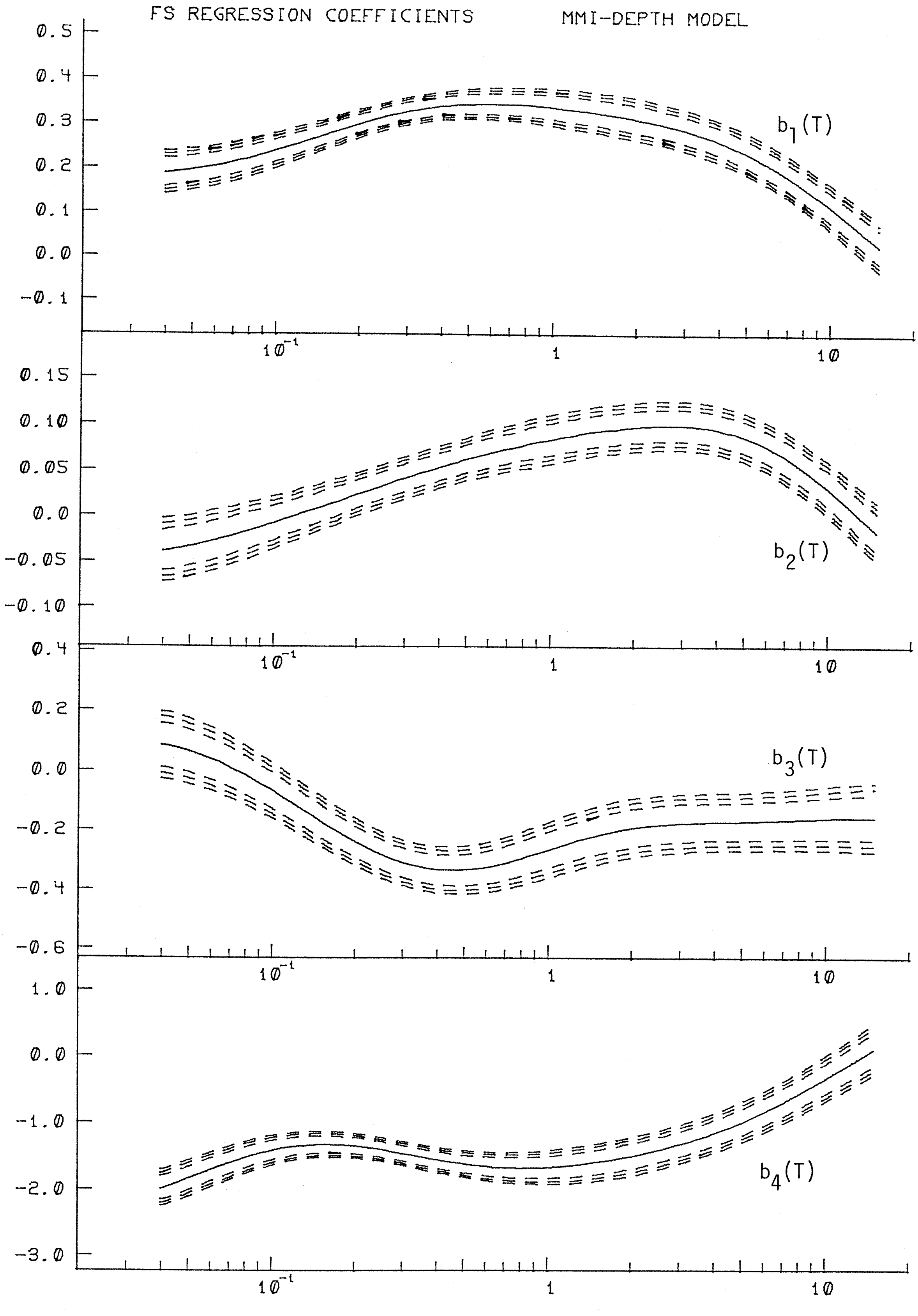

Figure III.2.1

exceeded can be compared with the above fractions. The Kolmogorov-Smirnov, KS(T), and the X^2 statistic, $X^2(T)$, can be computed to test the quality of fit of the normal distribution function in (III.2.4). A complete description of the steps involved in this and the formulae employed are given in Part I of this report and will not be repeated here.

Figure III.2.2 shows the plot of the amplitudes of the residuals corresponding to $p^*(\varepsilon,T) = 0.1, 0.2,\ldots,0.8$ and 0.9 for $\log_{10}FS(T)$. The nine sets of curves, plotted versus period T, from the bottom to the top of the plot correspond to the residual levels at each of the probability levels, 0.1 through 0.9. At each of the nine probability levels, the rough solid curve represents the actual calculated residuals at that particular level. The smoothed solid curve is obtained by smoothing the rough solid curve along the T-axis. The corresponding dashed curve is the estimated residual $\varepsilon(T)$ at the particular probability level using equation (III.2.4).

It is of interest to compare this figure with the corresponding figure (Fig. I.5.3) in Part I of this report dealing with the scaling of FS(T) in terms of earthquake magnitude M and representative source to station distance Δ. There both the calculated and estimated residue levels of $p^* = 0.1$ to $p^* = 0.9$ range from $\varepsilon = -0.6$ to $\varepsilon = +0.6$ at the short period end to about $\varepsilon = -0.5$ to $\varepsilon = +0.5$ in the long period end (Part I, Fig. I.5.2). Correspondingly, here, they range from $\varepsilon = -0.7$ to $\varepsilon = +0.7$ at the short period end, and from $\varepsilon = -0.5$ to $\varepsilon = +0.5$ in the long period end. Since the smooth surface $p^*(\varepsilon,T)$ from the nine smooth curves represents the spread of the observed data about the models given here (equation (III.1.3))

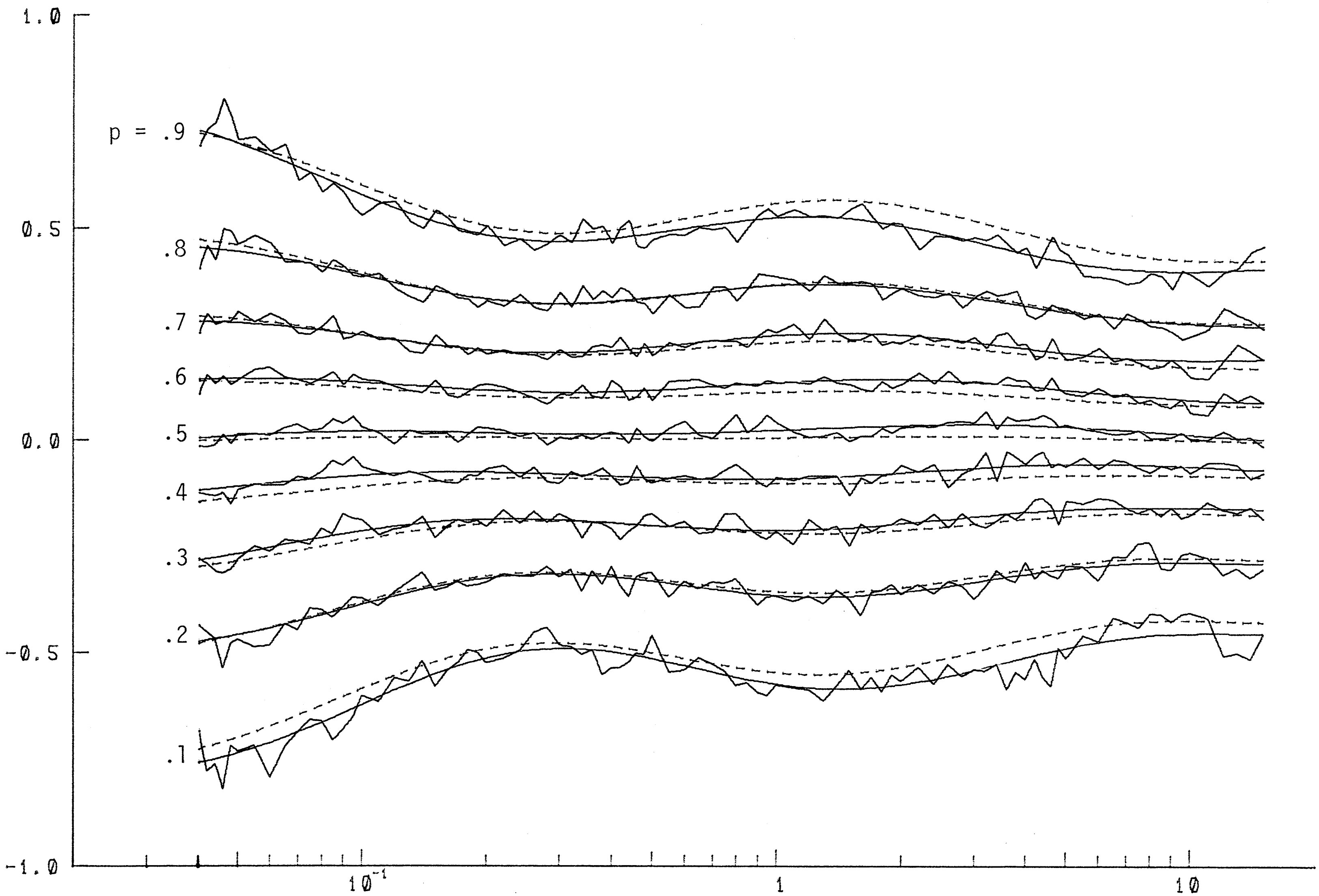

Figure III.2.2

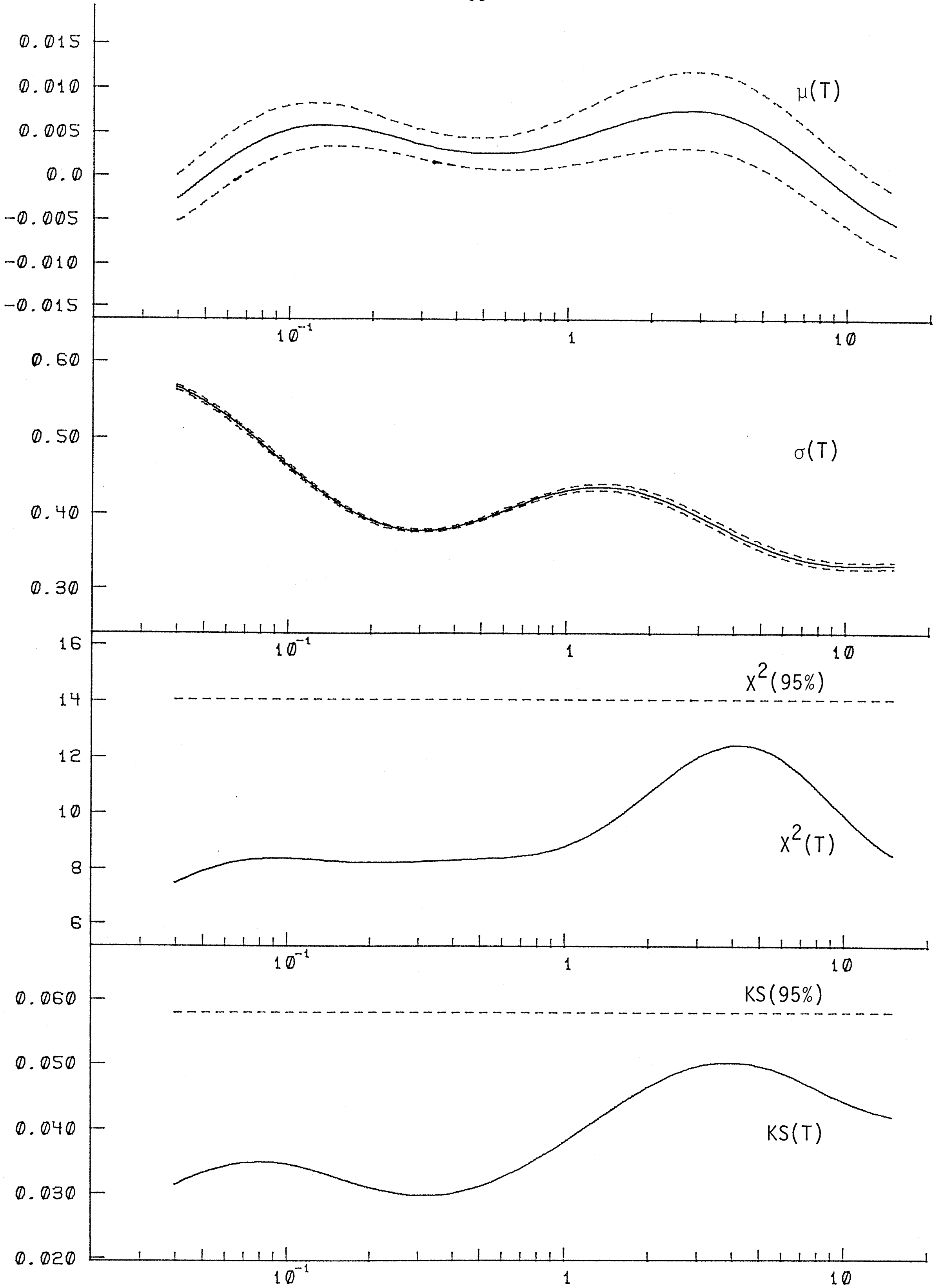

Figure III.2.3

TABLE III.2.1

$$\log_{10} FS(T) = b_1(T)I_{MM} + b_2(T)h + b_3(T)v + b_4(T)$$

PERIOD, T(SEC)	.040	.065	.11	.19	.34	.50	.90	1.60	2.80	4.40	7.50	14.00
COEFFICIENTS:												
$b_1(T)$	.189	.209	.247	.296	.334	.345	.339	.320	.290	.249	.170	.040
$b_2(T)$	-.038	-.024	-.003	.022	.047	.063	.081	.095	.099	.091	.058	-.009
$b_3(T)$	.084	.022	-.095	-.231	-.326	-.335	-.279	-.209	-.177	-.170	-.163	-.156
$b_4(T)$	-1.993	-1.657	-1.388	-1.352	-1.522	-1.637	-1.687	-1.579	-1.357	-1.081	-.626	.039
RESIDUES:												
p = .1	-.759	-.700	-.606	-.519	-.493	-.515	-.568	-.585	-.549	-.503	-.463	-.456
p = .2	-.474	-.435	-.378	-.329	-.319	-.334	-.363	-.368	-.340	-.312	-.292	-.292
p = .3	-.284	-.248	-.210	-.189	-.193	-.203	-.214	-.207	-.185	-.169	-.161	-.164
p = .4	-.118	-.098	-.082	-.077	-.084	-.090	-.093	-.084	-.068	-.059	-.059	-.070
p = .5	.005	.015	.020	.016	.012	.013	.020	.030	.036	.032	.019	.002
p = .6	.144	.143	.132	.117	.111	.116	.132	.142	.136	.121	.101	.088
p = .7	.281	.267	.240	.212	.206	.217	.242	.250	.233	.209	.190	.188
p = .8	.454	.425	.378	.334	.321	.334	.360	.364	.338	.308	.280	.266
p = .9	.728	.654	.558	.485	.467	.485	.518	.516	.472	.428	.398	.400
RESIDUE STATISTICS:												
$\mu(T)$	-.003	.003	.006	.005	.003	.003	.004	.006	.008	.006	.001	-.005
$\sigma(T)$	.566	.518	.450	.392	.378	.393	.427	.433	.401	.365	.336	.331
$\chi^2(T)$	7.490	8.241	8.336	8.191	8.278	8.363	8.669	9.970	11.855	12.426	11.101	8.650
KS(T)	.031	.034	.034	.031	.030	.031	.037	.044	.049	.050	.047	.042

and in Part I (equation I.5.1), this comparison shows that the uncertainties associated with the prediction of FS(T) in terms of MMI are very similar and certainly not much worse than those associated with the scaling of FS(T) in terms of M and Δ.

Figure III.2.3 shows a plot of the statistical parameters employed in the description of the residuals. The smooth amplitudes of $\hat{\mu}(T)$ and $\hat{\sigma}(T)$ of equation (III.2.4) and their 95% confidence intervals are shown in the top 2 plots of the figure, respectively. The two full curves in the bottom of the figure show the smoothed amplitudes of the computed X^2, $X^2(T)$ and Komolgorov-Smirnov, KS(T), statistics, respectively. The dashed lines are their corresponding 95% cutoff levels. It is seen that in the whole period range considered (0.04 sec to 15 sec), both the X^2 and K-S tests fail to reject the hypothesis that the distribution is normal.

Table III.2.1 gives, for 12 periods between T = 0.04 sec and T = 14 sec, the amplitudes of the smoothed regression coefficients: $\hat{b}_1(T)$, $\hat{b}_2(T)$, $\hat{b}_3(T)$, $\hat{b}_4(T)$, the nine smoothed calculated residue levels corresponding to $p^*(\varepsilon,T) = 0.1$ through 0.9, the smoothed coefficients $\hat{\mu}(T)$, $\hat{\sigma}(T)$ of the normal distribution function in (III.2.4), and finally, the X^2 and the Komolgorov-Smirnov statistics.

III.3 THE ESTIMATED FOURIER SPECTRA

Figures III.3.1 and III.3.2 present examples of the Fourier amplitude spectra, FS(T), computed from equation (III.1.3) for $p(\varepsilon,T) = 0.5$, for MMI levels IV, VI, VIII, X and XII. Figure III.3.1 is for horizontal motion ($v = 0$) while Figure III.3.2 is for vertical motion ($v = 1$). The solid lines in both figures correspond to the depth of sediments $h = 0$, while the dashed lines correspond to $h = 4$ km. The diagonal dashed lines at the bottom of each graph represent the average Fourier amplitudes of the digitization noise. The plot of each spectrum is presented only for those periods where the low signal-to-noise ratio in the data does not distort the estimates of small spectral amplitudes.

The overall trends of the computed FS(T) spectral amplitudes in these figures are in many ways similar to those of the same model in our previous analysis (Trifunac and Lee, 1978). The results can be considered representative of the observed shaking for MMI levels up to about VIII. The curves plotted for MMI = X and XII are presented here only for completeness, and represent an extrapolation based on the currently available data.

It has been noted in the previous analysis of the same model (Trifunac, 1979; Trifunac and Lee, 1978), that for the same MMI, spectral amplitudes tend to be slightly higher for $h = 0$ km than for say $h = 4$ km in the short period range (up to 0.2 sec), with this trend being reversed for long periods. Note that the same trend is observed here in Figures III.3.1 and III.3.2, but to a smaller extent. Here the amplitudes are slightly higher for $h = 0$ km than for $h = 4$ km, only in

ESTIMATED FOURIER AMPLITUDES SPECTRA - IN/SEC

H = Ø.4 KM M.M.I. = 4,6,8,1Ø,12

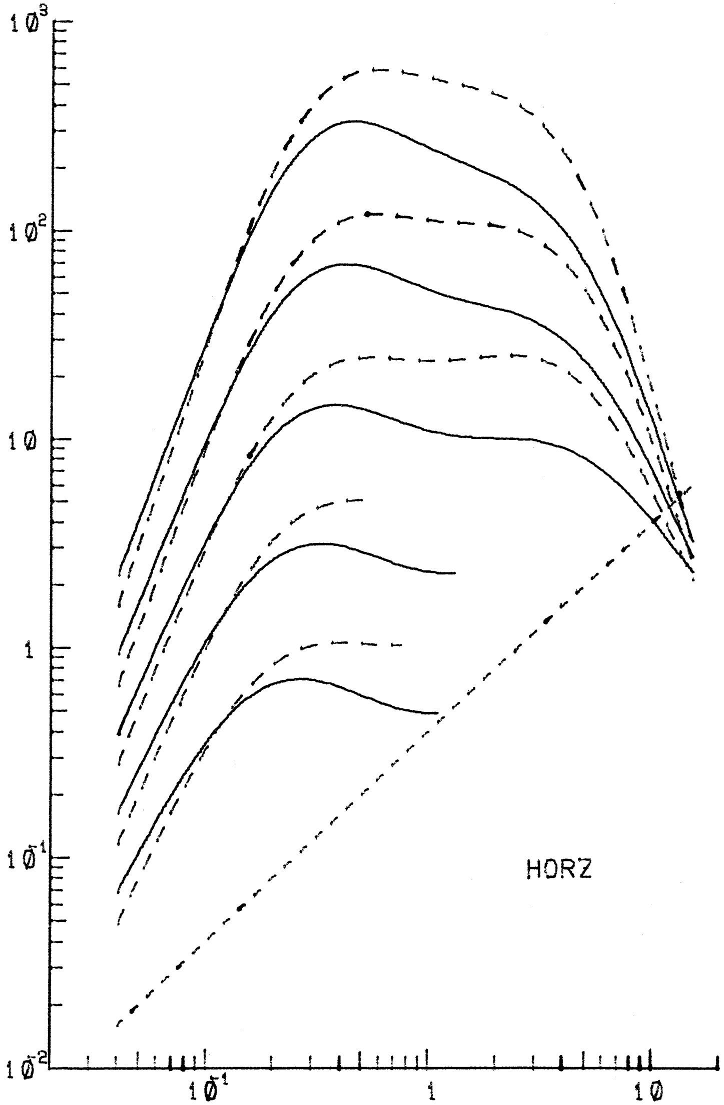

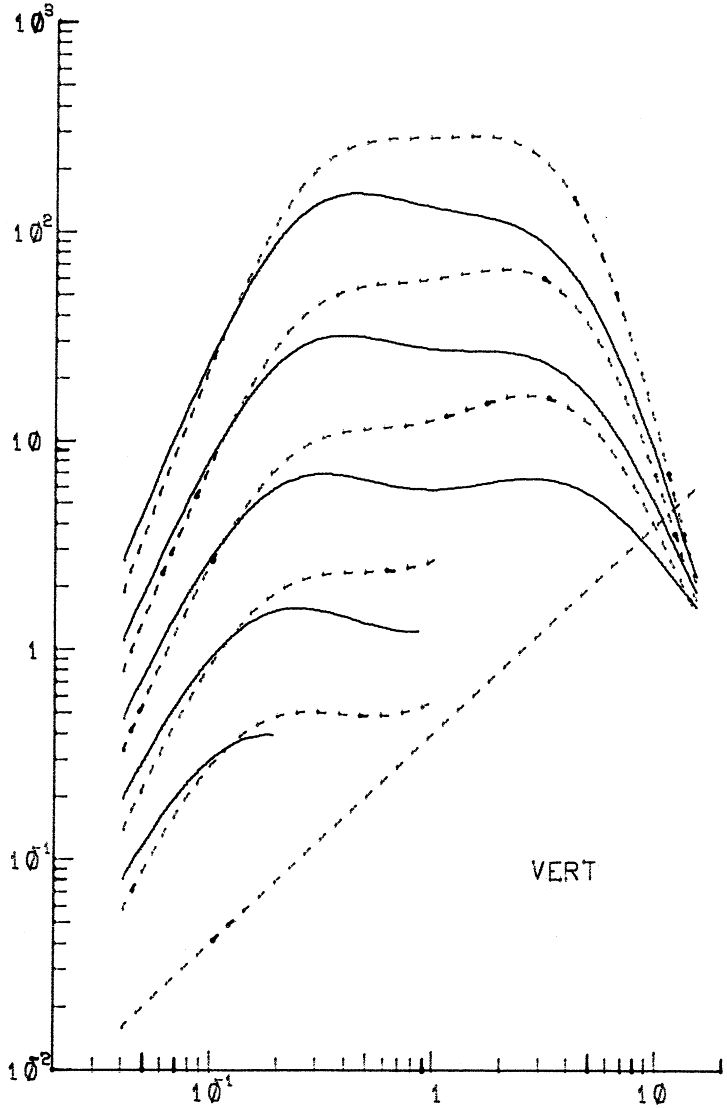

PERIOD - SEC

Figure III.3.1

Figure III.3.2

ACØ41 PACOIMA DAM, 1971 COMP HORZ
MMI = 1Ø. DEPTH = Ø.FT V = Ø.

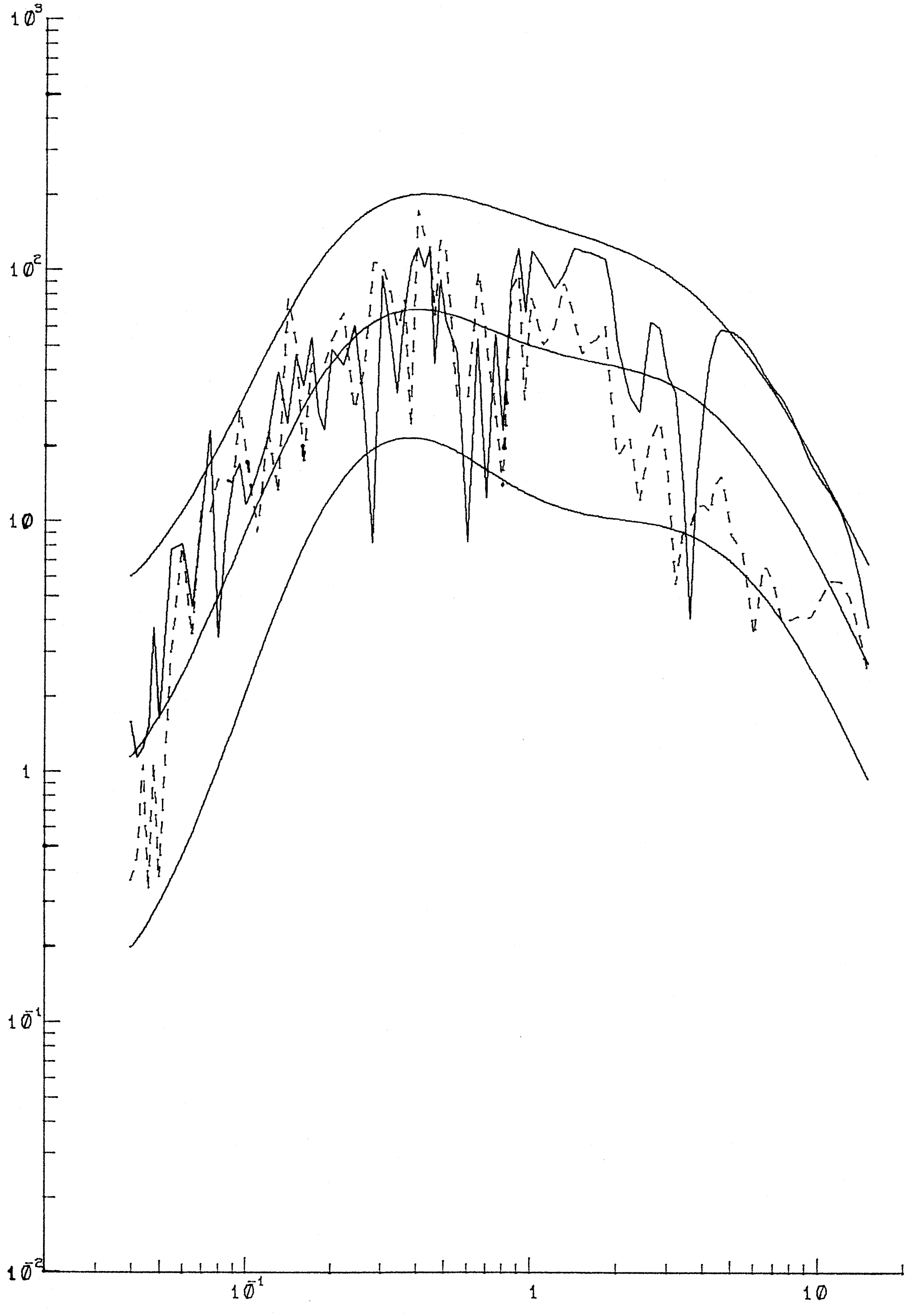

Figure III.3.3

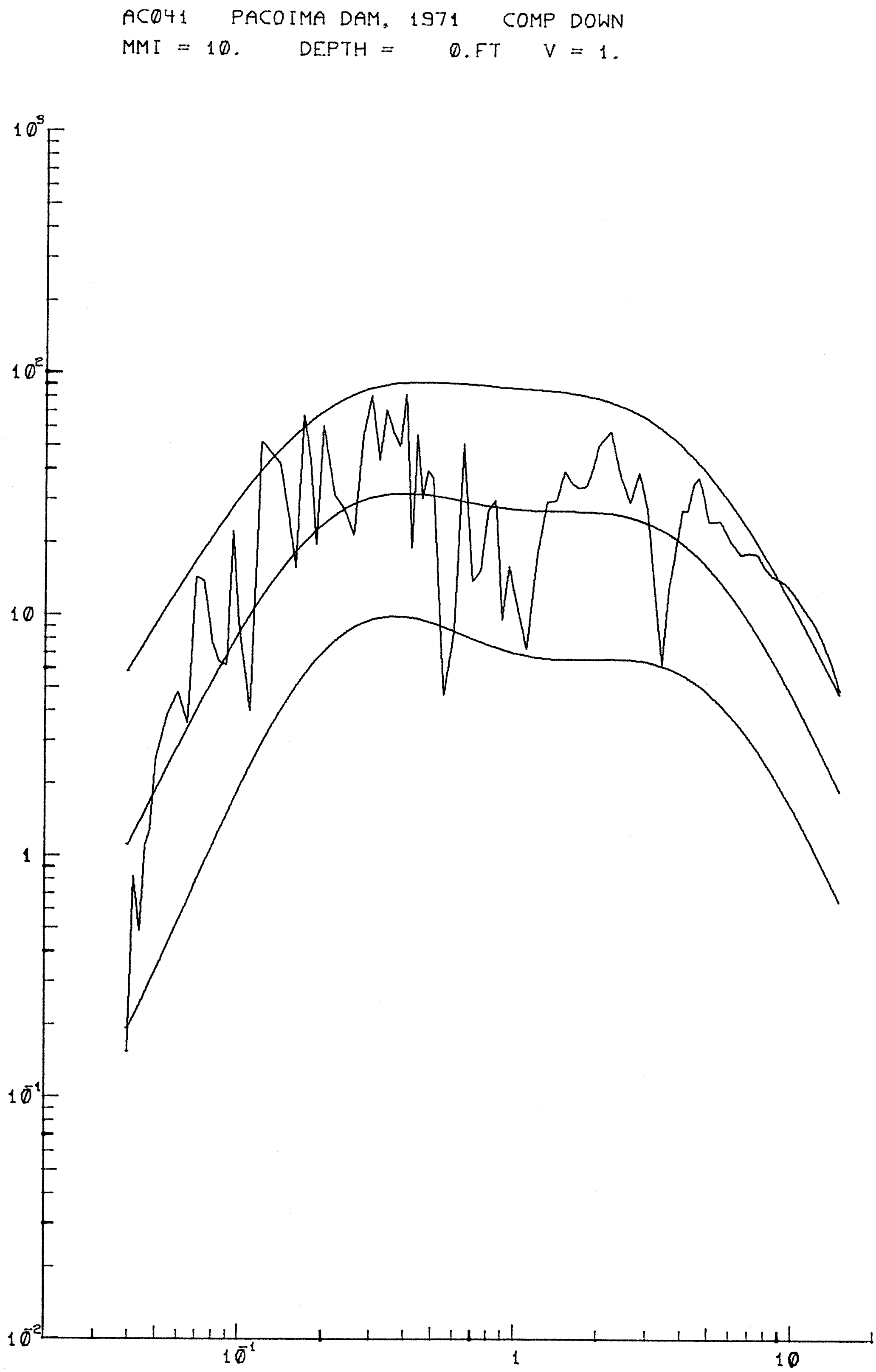

Figure III.3.4

AAØØ1 EL CENTRO, 1940 COMP HORZ
MMI = 8. DEPTH =15000.FT V = Ø.

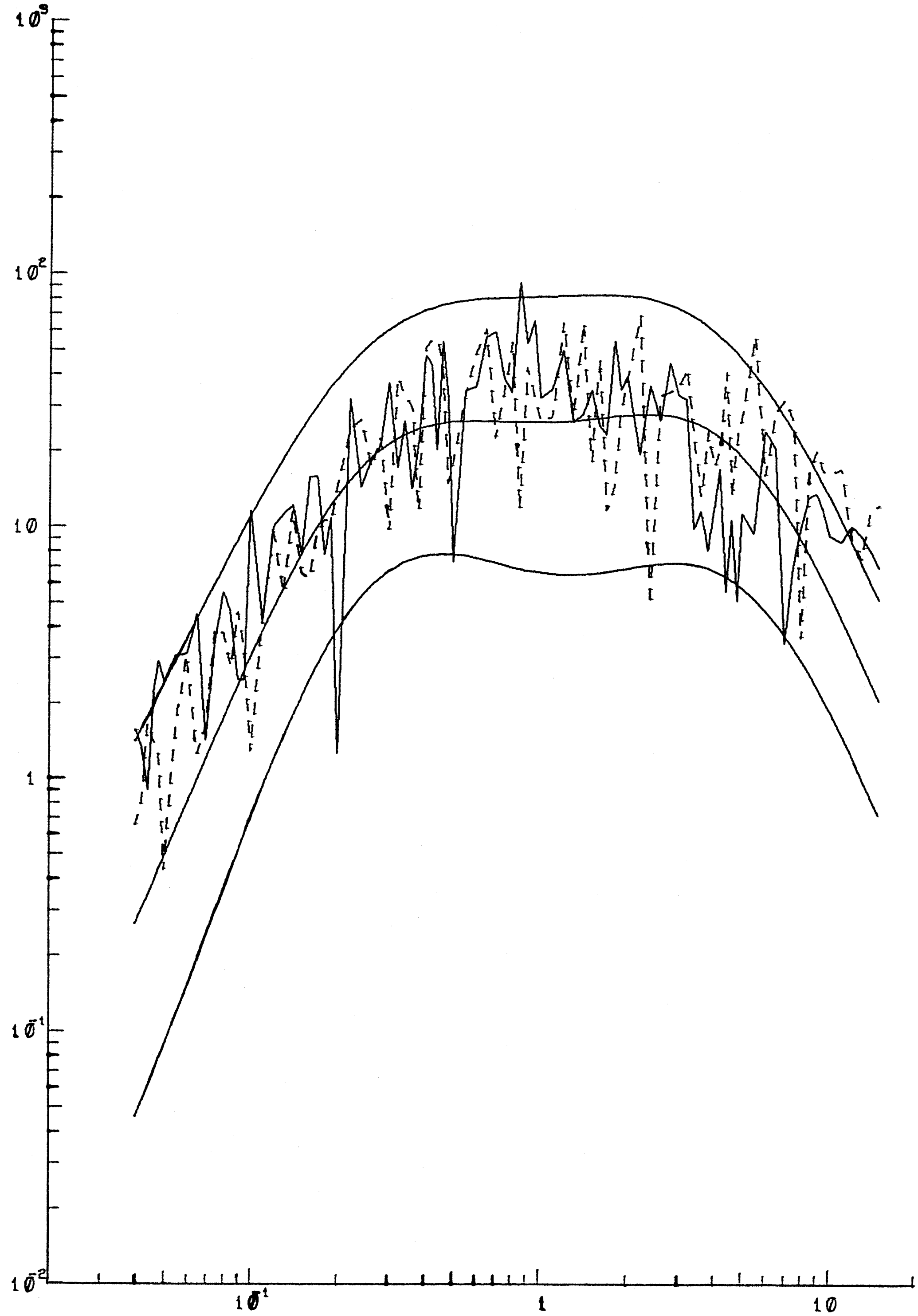

Figure III.3.5

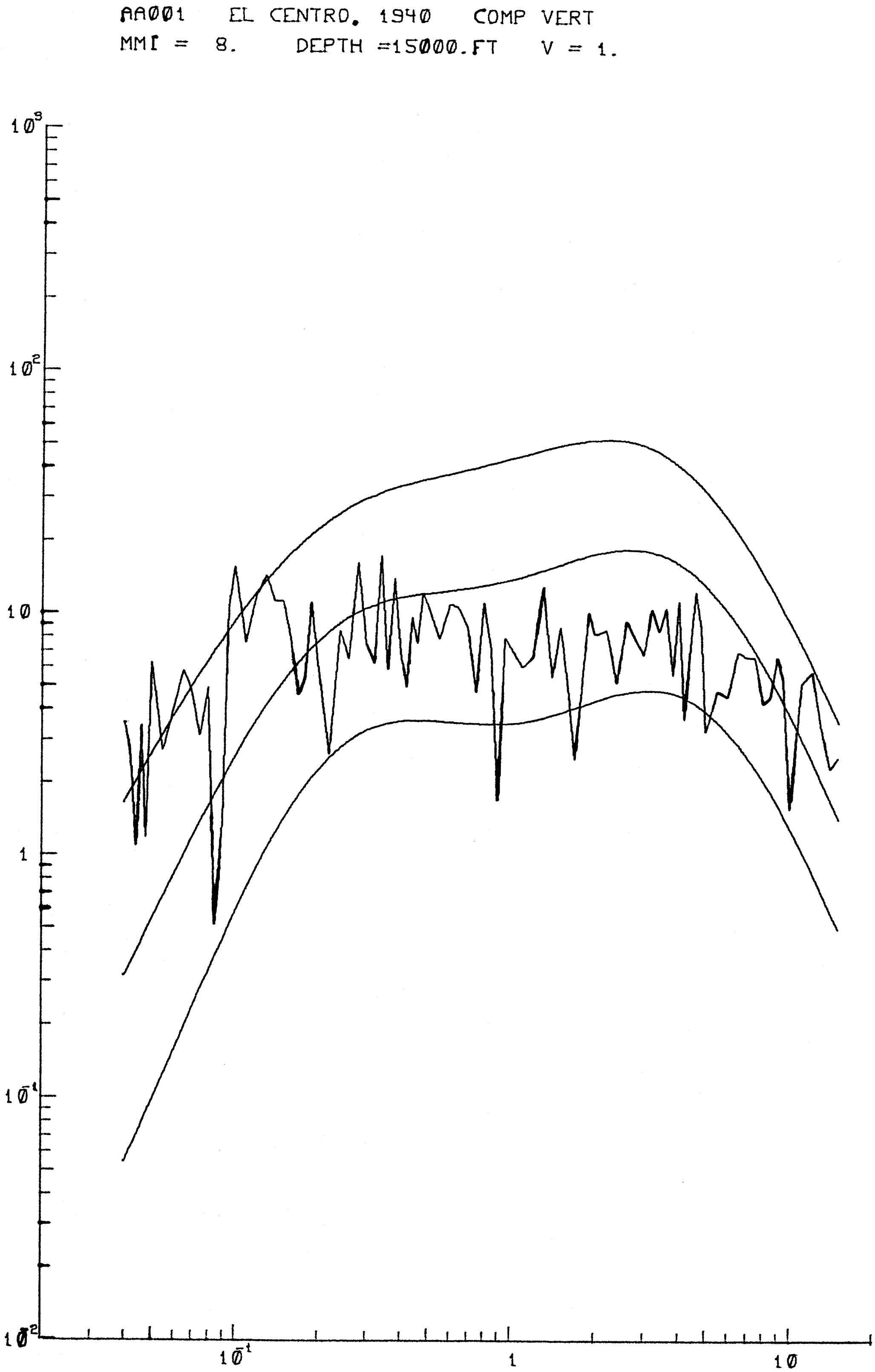

Figure III.3.6

the short period range of up to about 0.1 sec, beyond which the trend is reversed. It is also of interest to compare these figures with the corresponding figures (Figures I.6.1 and I.6.2) in Part I of this report dealing with the scaling of FS(T) in terms of M and Δ. It has been found there that the effect of the depth of sediments, h, beneath the recording station is important only from intermediate to long periods and is negligible at short periods. There, for the short periods, no trend reversal has been observed.

A comparison of the corresponding horizontal and vertical amplitudes in Figures III.3.1 and III.3.2 also shows that the vertical amplitudes are smaller than the horizontal amplitudes, except at short periods, a trend which is consistent with all previous analyses.

Figures III.3.3 and III.3.4 compare the amplitudes of Fourier spectra computed from accelerations recorded at Pacoima Dam during the San Fernando earthquake of 1971, with spectral amplitudes computed from equation (III.1.3) for p = 0.1, 0.5 and 0.9 with MMI = 10, h = 0 ft. and for the vertical and two horizontal components. The agreement between the observed and estimated amplitudes is good for all three components. Figures III.3.5 and III.3.6 compare the FS amplitudes computed from accelerations recorded during the Imperial Valley, California earthquake of 1940, in El Centro, with the estimated amplitudes using MMI = 8 and h = 15000 ft for both the vertical and horizontal components. The agreement is good for the two horizontal components and fair for the vertical component.

This completes the description of the preliminary model for scaling FS(T) in terms of MMI, h and v.

PART IV: SCALING OF FOURIER SPECTRA IN TERMS OF MMI, s and v

IV.1 THE SCALING RELATION

Part IV of this report continues the description of the preliminary empirical model for scaling Fourier amplitude spectra of strong ground motion in terms of Modified Mercalli Intensity (MMI) at the site and local geology. As in Part II of this report, this part of the analysis replaces the depth of sedimentary deposits h, employed as site characterization in the previous Part III, by the corresponding site parameter s = 0, 1 and 2. After modifying the scaling relation of Part III, equation (III.1.3), the scaling relation now takes the form

$$\log_{10} FS(T) = b_1(T)\hat{I}_{MM} + b_2(T)s + b_3(T)v + b_4(T) \quad , \qquad \text{(IV.1.1)}$$

with all parameters defined as before. $b_2(T)$ is now the coefficient associated with the site parameter s.

The scaling functions $b_1(T)$ through $b_4(T)$ are determined again through a regression analysis of the new database of 1314 components of spectral amplitudes, FS(T), at 91 discrete periods T ranging from 0.04 sec to 15.0 sec. As in the previous Part III of this report, the data are first screened for possible bias in the model. All procedures in data preparation and selection, and the steps of regression analysis employed here are identical to those in Part III of this report, and so their description will not be repeated here.

The coefficients at each period T resulting from linear regression have been denoted by $\hat{b}_1(T)$, $\hat{b}_2(T)$, $\hat{b}_3(T)$ and $\hat{b}_4(T)$ (equation (IV.1.1)), respectively. Much of the format of the description in the sections to follow will almost be identical to that in Part III of this work. The reader may refer to the corresponding sections of Part III for a more detailed description.

IV.2 THE REGRESSION COEFFICIENTS

Figure IV.2.1 shows the smoothed coefficients $\hat{b}_1(T)$ through $\hat{b}_4(T)$ (solid lines) together with the estimates of their 80%, 90% and 95% confidence intervals (dashed lines). Comparison of this figure with the corresponding Figure III.2.1 in the previous Part III of this report shows that the functions $\hat{b}_1(T)$, $\hat{b}_3(T)$ and $\hat{b}_4(T)$ as given respectively by the top and bottom two graphs are almost identical. These functions correspond to the same respective parameters, I_{MM}, v and 1 in the scaling relations and their similarity again demonstrates the stability of the two regression models used for scaling. The functions $\hat{b}_2(T)$ as given by the second graph from the top in both figures are opposite in sign. This again is consistent for the two models since $s = 2$ corresponds to $h = 0$ km (basement rock), while $s = 0$ corresponds to $h >> 0$ km (alluvium).

Figure IV.2.2 shows the plot of the residual levels corresponding to $p^*(\varepsilon,T) = 0.1, 0.2,\ldots,0.8, 0.9$ for $\log_{10}FS(T)$. Refer to the same Figure III.2.2 in Part III of this report for a complete description of each set of these curves.

It is again of interest to compare the two figures IV.2.2 and III.2.2. Since the two smooth surfaces $p^*(\varepsilon,T)$ represent the spread of the observed data about their corresponding models, which differ only in the characterization of local site geology, the resemblance of the two figures again shows that the uncertainties associated with the characterization of local geology in terms of site conditions $s = 0$, 1 and 2 are not much greater than those associated with the site characterization in terms of depth of sedimentary deposits.

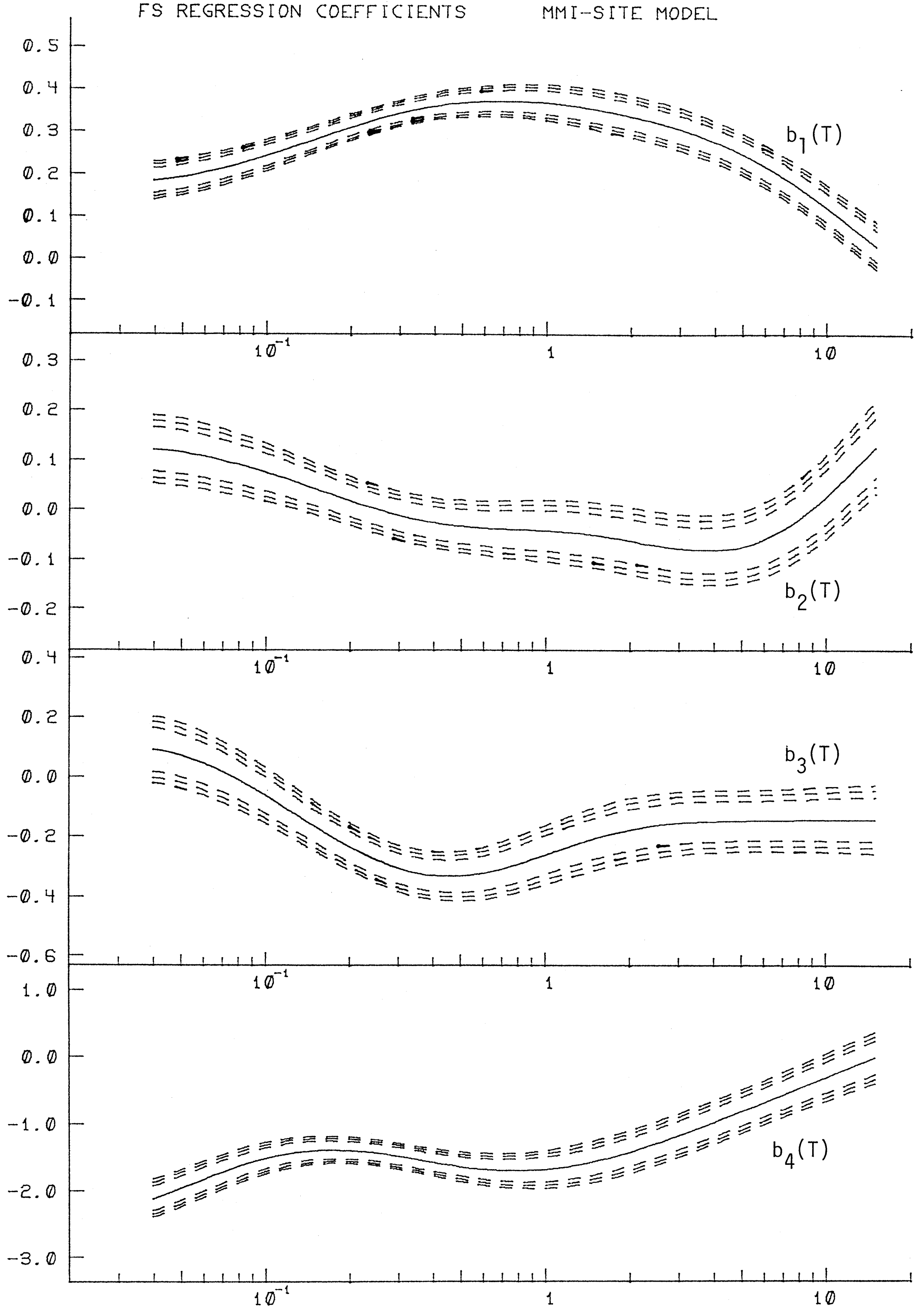
FS REGRESSION COEFFICIENTS MMI-SITE MODEL
b1(T)
b2(T)
b3(T)
b4(T)
0.5
0.4
0.3
0.2
0.1
0.0
-0.1
0.3
0.2
0.1
0.0
-0.1
-0.2
0.4
0.2
0.0
-0.2
-0.4
-0.6
1.0
0.0
-1.0
-2.0
-3.0
10⁻¹
1
10

Figure IV.2.1

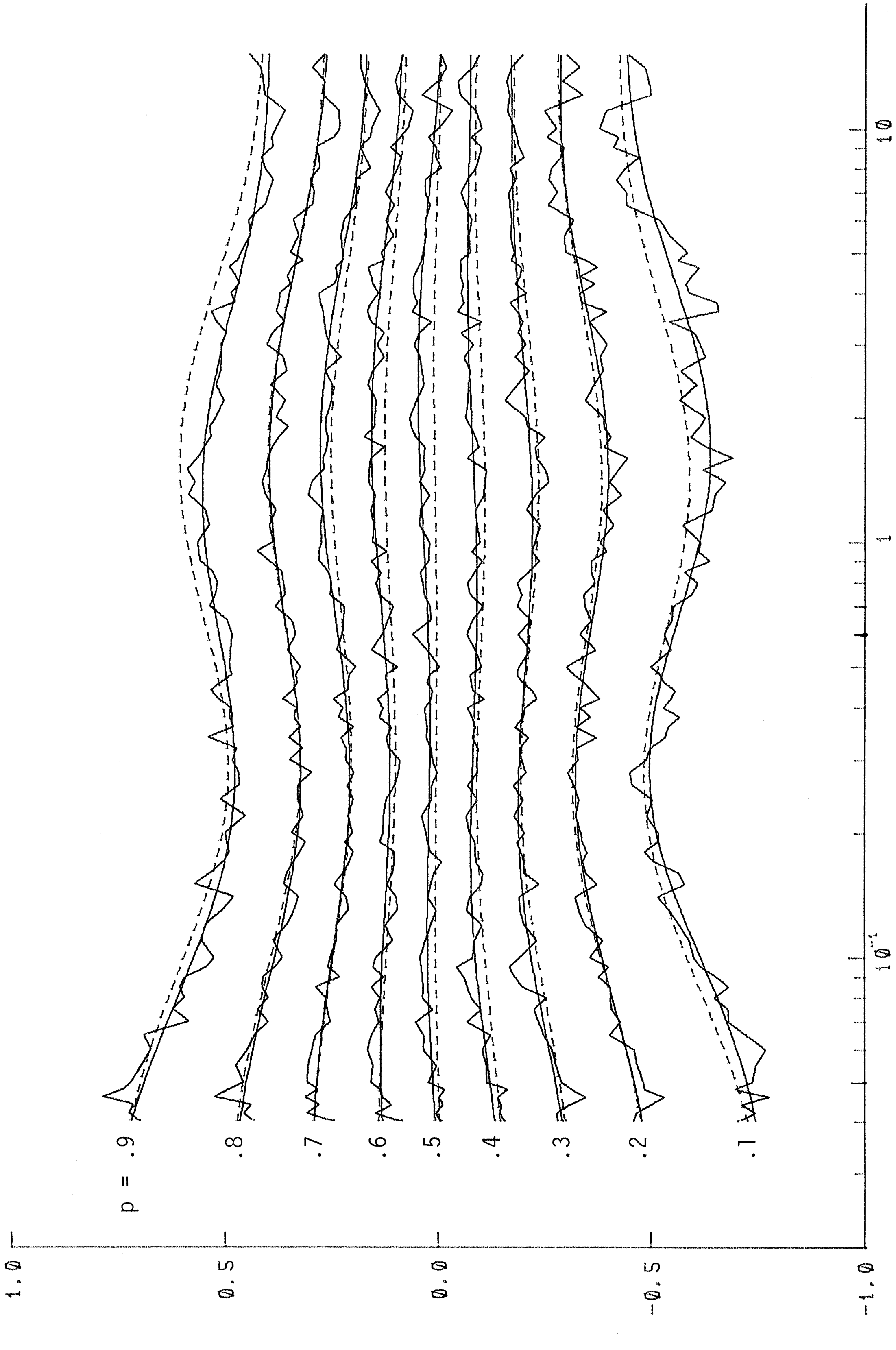

Figure IV.2.2

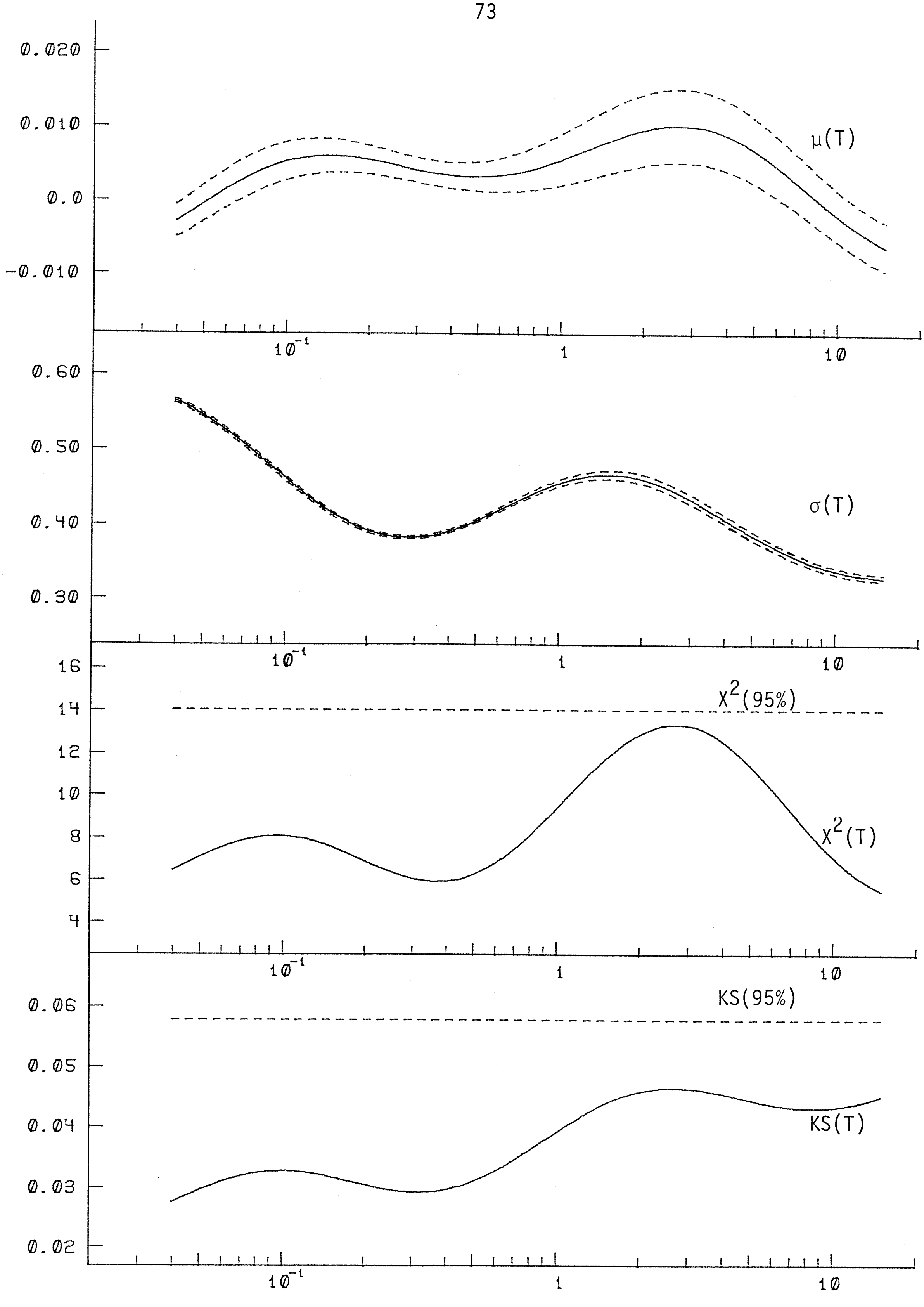
0.020
0.010
0.0
-0.010
μ(T)
0.60
0.50
0.40
0.30
σ(T)
16
14
12
10
8
6
4
χ2(95%)
χ2(T)
0.06
0.05
0.04
0.03
0.02
KS(95%)
KS(T)
10-1
1
10

Figure IV.2.3

TABLE IV.2.1

$$\log_{10} FS(T) = b_1(T) I_{MM} + b_2(T)s + b_3(T)v + b_4(T)$$

PERIOD, T(SEC)	.040	.065	.11	.19	.34	.50	.90	1.60	2.80	4.40	7.50	14.00
COEFFICIENTS:												
$b_1(T)$	.184	.209	.253	.306	.352	.368	.369	.347	.310	.263	.179	.045
$b_2(T)$	.121	.101	.065	.019	-.021	-.036	-.044	-.056	-.079	-.081	-.029	.109
$b_3(T)$	.091	.028	-.090	-.227	-.323	-.334	-.277	-.200	-.157	-.148	-.144	-.143
$b_4(T)$	-2.118	-1.774	-1.476	-1.397	-1.540	-1.659	-1.709	-1.542	-1.225	-.911	-.519	-.061
RESIDUES:												
p = .1	-.744	-.689	-.599	-.518	-.500	-.530	-.602	-.638	-.609	-.551	-.484	-.445
p = .2	-.478	-.433	-.375	-.332	-.326	-.345	-.384	-.399	-.372	-.333	-.297	-.287
p = .3	-.291	-.253	-.213	-.190	-.194	-.205	-.220	-.217	-.199	-.184	-.174	-.172
p = .4	-.133	-.107	-.084	-.077	-.083	-.089	-.090	-.082	-.072	-.068	-.071	-.075
p = .5	.008	.019	.024	.022	.019	.021	.031	.044	.048	.039	.020	-.003
p = .6	.131	.135	.128	.116	.113	.122	.142	.156	.151	.134	.108	.088
p = .7	.290	.273	.242	.213	.209	.224	.258	.277	.262	.232	.194	.169
p = .8	.465	.428	.375	.332	.326	.343	.380	.397	.378	.342	.298	.266
p = .9	.719	.647	.557	.490	.479	.501	.542	.551	.514	.466	.421	.400
RESIDUE STATISTICS:												
$\mu(T)$	-.003	.002	.006	.006	.004	.003	.005	.009	.010	.008	.002	-.006
$\sigma(T)$	.565	.516	.448	.394	.385	.405	.450	.467	.439	.397	.353	.329
$\chi^2(T)$	6.504	7.750	8.047	7.008	5.962	6.306	8.829	12.095	13.381	12.090	8.821	5.678
KS(T)	.028	.032	.033	.031	.029	.031	.038	.045	.047	.045	.043	.045

Figure IV.2.3 shows the plot of the statistical parameters employed in the description of the residuals, namely, $\hat{\mu}(T)$, $\hat{\sigma}(T)$, $X^2(T)$ and KS(T), from top to bottom. Comparison with the Figure III.2.3 in Part III again shows the degree of the resemblance of this model and that discussed in Part III.

Table IV.2.1 gives, for 12 periods between T = 0.04 sec and T = 14 sec, the four coefficients, $\hat{b}_1(T)$ through $\hat{b}_4(T)$, the nine residue levels corresponding to $p^*(\varepsilon,T) = 0.1$ through 0.9, the coefficients $\hat{\mu}(T)$ and $\hat{\sigma}(T)$ of the normal distribution and finally the $X^2(T)$ and KS(T) statistics.

IV.3 THE ESTIMATED FOURIER SPECTRA

Figures IV.3.1 and IV.3.2 present examples of the Fourier amplitude spectra, FS(T), computed from equation (IV.1.1) for $p(\varepsilon,T) = 0.5$, for MMI levels IV, VI, VIII, X and XII. Figure IV.3.1 is for horizontal motion ($v = 0$) while Figure IV.3.2 is for vertical motion ($v = 1$). The solid lines in both figures correspond to the site condition $s = 2$ while the dashed lines correspond to $s = 0$. The diagonal dashed lines again represent the empirical average Fourier amplitudes of digitization noise.

Comparison of these figures with the corresponding Figures III.3.1 and III.3.2 of Part III of this report again shows great similarity, and hence the similar conclusions can be drawn from these figures.

Figures IV.3.3 and IV.3.4 compare the amplitudes computed from the 1971 Pacoima Dam acceleration with those calculated for $p = 0.1$, 0.5 and 0.9, MMI = X and $s = 2$. Similarly, Figures IV.3.5 and IV.3.6 compare those computed from the 1940 El Centro acceleration with those calculated for MMI = VIII and $s = 0$. The agreement ranges from fair to good.

This completes the description of the Part IV of the scaling of FS(T) in terms of MMI, s and v.

ESTIMATED FOURIER AMPLITUDES SPECTRA - IN/SEC

S = 0.2 M.M.I. = 4,6,8,10,12

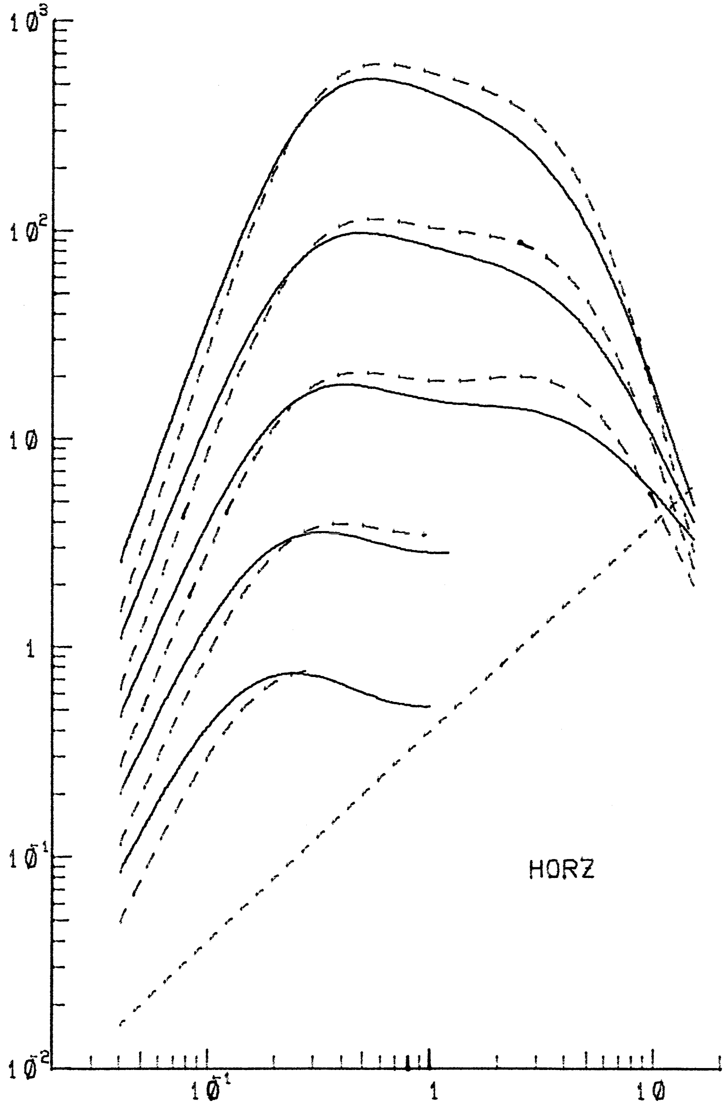

Figure IV.3.1

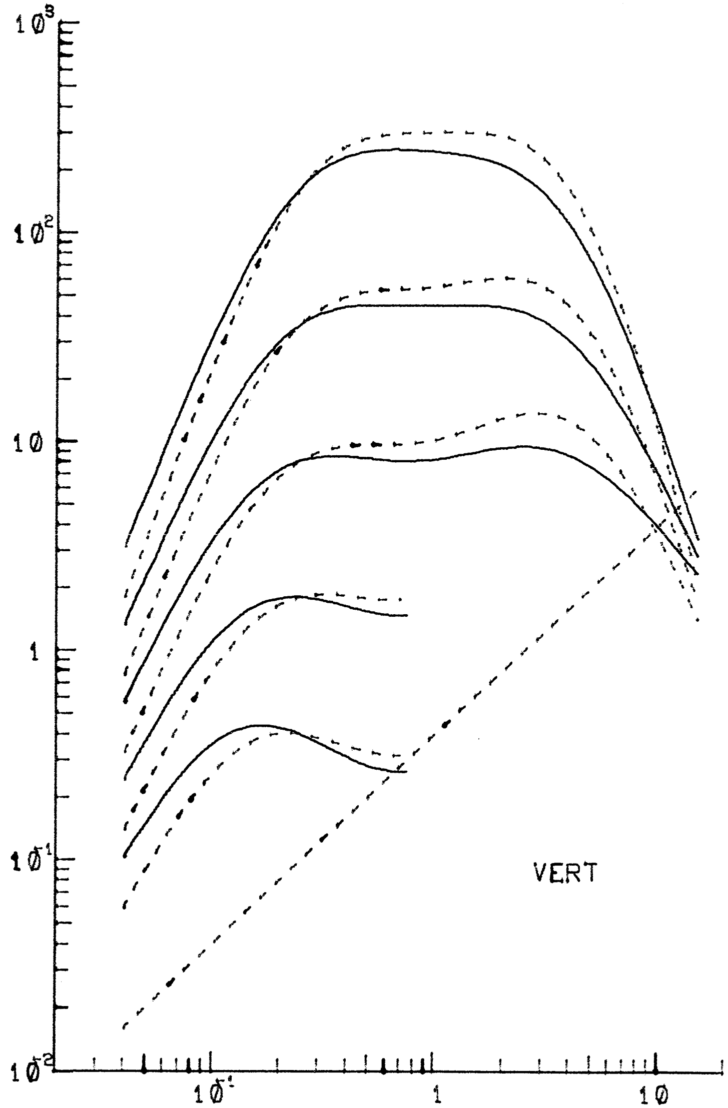

PERIOD - SEC

Figure IV.3.2

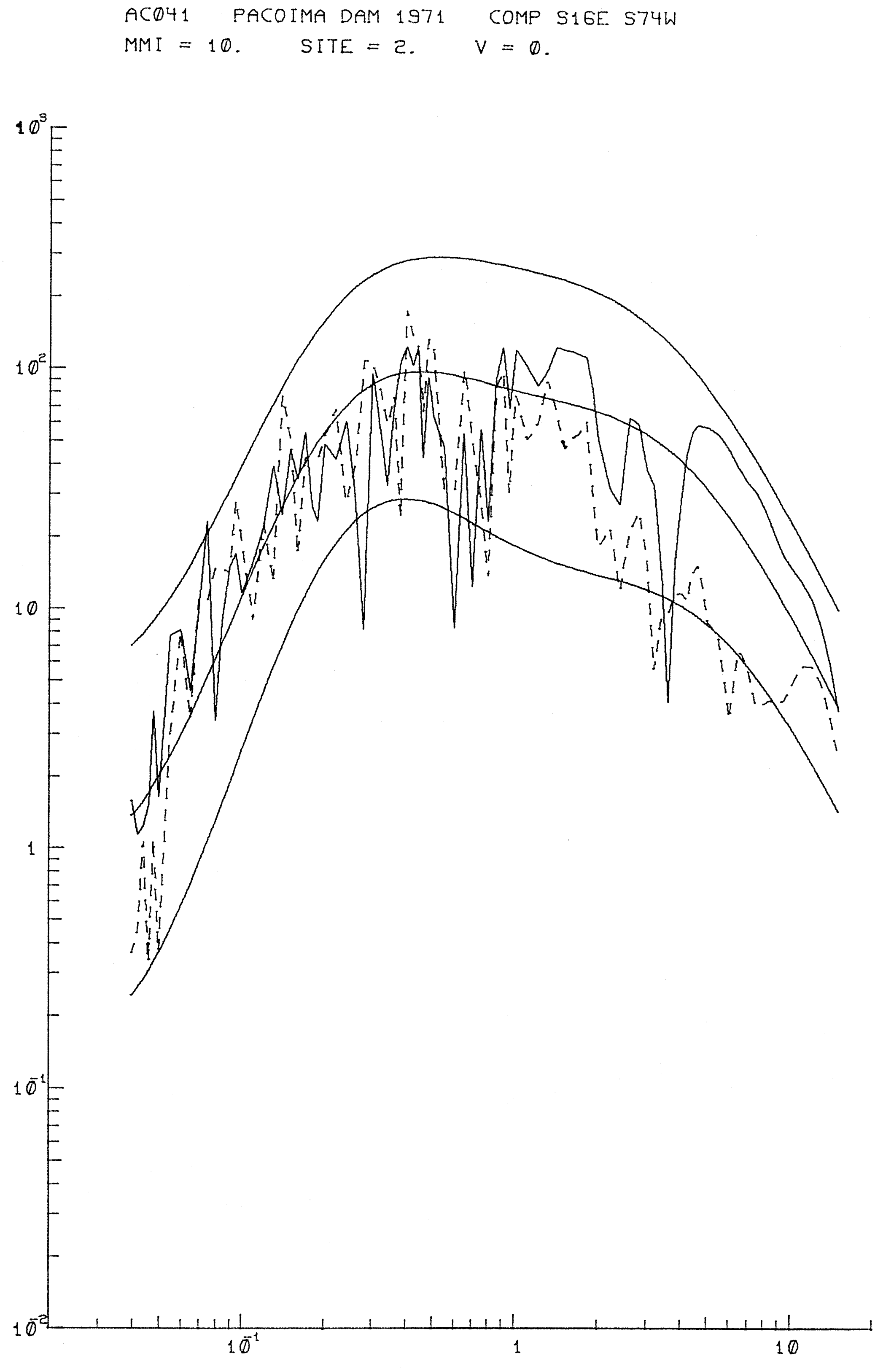
AC041 PACOIMA DAM 1971 COMP S16E S74W
MMI = 10. SITE = 2. V = 0.
10³
10²
10
1
10⁻¹
10⁻²
10⁻¹
1
10

Figure IV.3.3

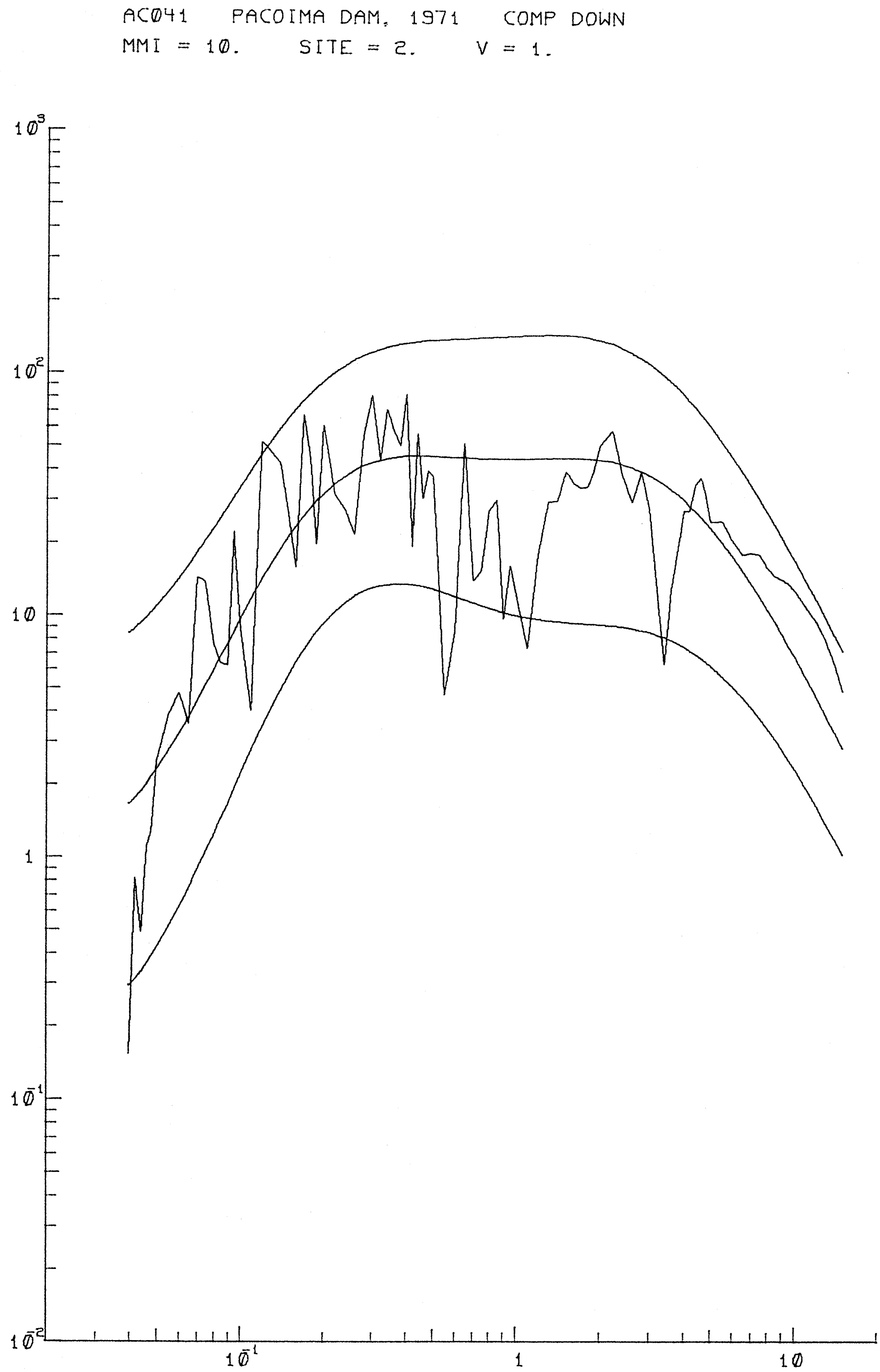
AC041 PACOIMA DAM, 1971 COMP DOWN
MMI = 10. SITE = 2. V = 1.
10^3
10^2
10
1
10^{-1}
10^{-2}
10^{-1}
1
10

Figure IV.3.4

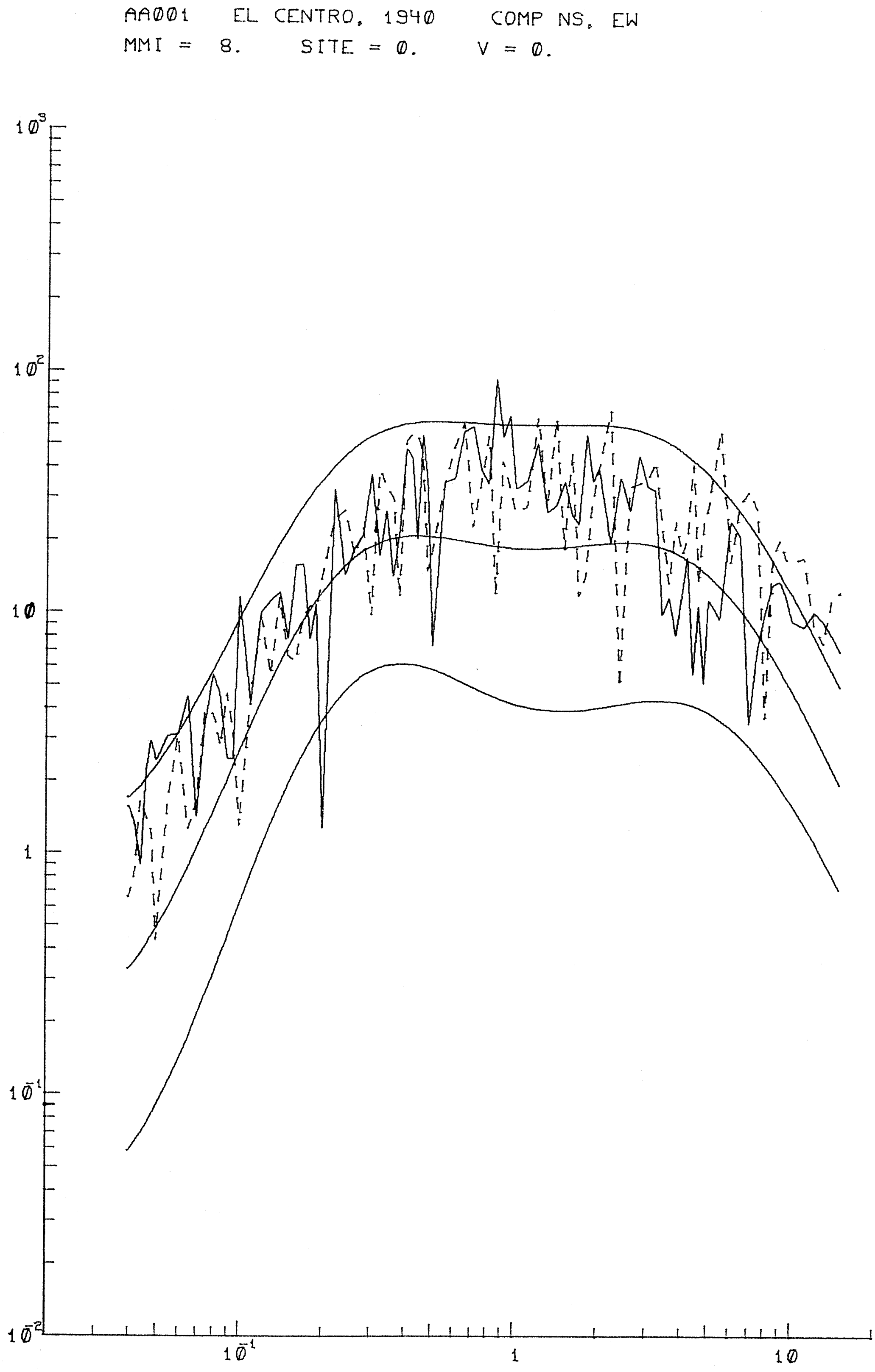
AA001 EL CENTRO, 1940 COMP NS, EW
MMI = 8. SITE = 0. V = 0.
10³
10²
10
1
10⁻¹
10⁻²
10⁻¹
1
10

Figure IV.3.5

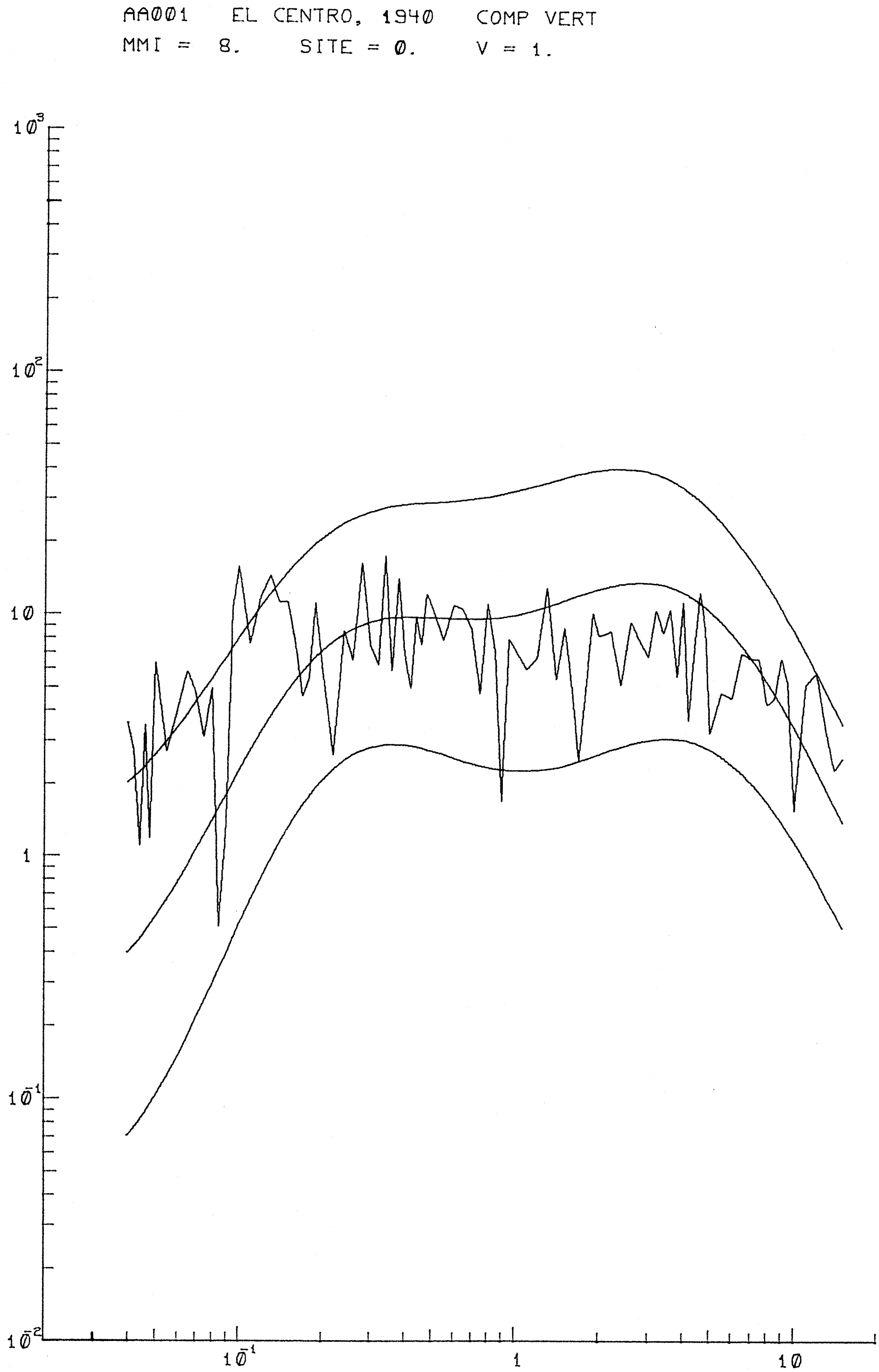
AA001 EL CENTRO, 1940 COMP VERT
MMI = 8. SITE = 0. V = 1.
10³
10²
10
1
10⁻¹
10⁻²
10⁻¹
1
10

Figure IV.3.6

CONCLUSIONS

The results of this study can be summarized as follows:

1. On the logarithmic scale the Fourier spectrum amplitudes grow linearly for small magnitudes ($M \lesssim 3$). This growth rate reduces for intermediate magnitudes and stops for $M \gtrsim 8$, in agreement with our earlier studies (Trifunac, 1976b).

2. For intermediate and long periods Fourier spectrum amplitudes recorded on alluvium are larger than those recorded on basement rock. At high frequencies, in contrast to our previous work (Trifunac, 1976b), $b_2(T)$ in Model I remains positive though not significantly different from zero. While this may be a consequence of the overall model differences and the fluctuations of the "constant" term $b_5(T)$, this suggests that our earlier discussions based on d(T) in Trifunac (1976b) being negative may have to be modified. In most of the earlier analyses we found $b_2(T)$, or its equivalent, to be negative for frequencies higher than about 5 Hz, but with small amplitudes which are not significantly different from zero. The overall shape of $b_2(T)$ function or its equivalent, however, has been very stable in present as well as in all earlier analyses.

3. The scaling function $b_3(T)$ in all four models which reflects the differences between horizontal and vertical spectral amplitudes is in excellent agreement with e(T) in Trifunac (1976b). Again for high frequencies the vertical spectral amplitudes tend to be equal to slightly larger than the horizontal amplitudes.

4. The distribution of Fourier spectrum amplitudes about the estimated model can be described adequately by the log-normal distribution function. Except for periods longer than about 10 sec, the quality of

this fit is excellent. For periods longer than 0.2 sec the standard deviation of this distribution function is about 0.35.

ACKNOWLEDGEMENTS

This work was supported in part by a contract from the U.S. Nuclear Regulatory Commission through SEEC and by grants from the National Science Foundation.

REFERENCES

Anderson, J. G. and M. D. Trifunac (1978) Uniform risk functionals for characterization of strong earthquake ground motion, Bull. Seism. Soc. Amer., 68, 205-218.

Gusev, A. A. (1983) Descriptive statistical model of earthquake source radiation and its application to an estimation of short-period strong motion, Geophys. J. R. Astr. Soc., 74, 787-808.

Kreyszig, E. (1972) Advanced Engineering Mathematics, J. Wiley & Sons, New York.

Lee, V. W. and M. D. Trifunac (1985) Attenuation of Modified Mercalli Intensity for small epicentral distance in California (in press).

Richter, C. F. (1958) Elementary Seismology, Freeman Co., San Francisco.

Trifunac, M. D. (1976a) Preliminary analysis of the peaks of strong earthquake ground motion - dependence of peaks on earthquake magnitude, epicentral distance, and the recording site conditions, Bull. Seism. Soc. Amer., 66, 189-219.

Trifunac, M. D. (1976b) Preliminary empirical model for scaling Fourier amplitude spectra of strong ground acceleration in terms of earthquake magnitude, source to station distance and recording site conditions, Bull. Seism. Soc. Amer., 66, 1345-1373.

Trifunac, M. D. and A. G. Brady (1975) On the correlation of peak accelerations of strong motion with earthquake magnitude, epicentral distance and site conditions, Proc. U. S. National Conf. on Earthquake Eng., Ann Arbor, Michigan, 43-52.

Trifunac, M. D. and J. G. Anderson (1977) Preliminary Empirical Models for Scaling Absolute Acceleration Spectra, Dept. of Civil Eng. Report No. 77-03, Univ. of Southern California, Los Angeles, California.

Trifunac, M. D. and J. G. Anderson (1978a) Preliminary Empirical Models for Scaling Pseudo Relative Velocity Spectra, Dept. of Civil Eng. Report No. 78-04, Univ. of Southern California, Los Angeles, California.

Trifunac, M. D. and J. G. Anderson (1978b) Preliminary Models for Scaling Relative Velocity Spectra, Dept. of Civil Eng. Report No. 78-05, Univ. of Southern California, Los Angeles, California.

Trifunac, M. D. and V. W. Lee (1978) Dependence of the Fourier Amplitude Spectra of Strong Motion Acceleration on the Depth of Sedimentary Deposits, Dept. of Civil Eng. Report No. 78-14, Univ. Southern California, Los Angeles, California.

Trifunac, M. D. and V. W. Lee (1985) Frequency dependent attenuation of strong earthquake ground motion (in press).

Trifunac, M. D. (1979) Preliminary empirical model for scaling Fourier amplitude spectra of strong motion acceleration in terms of Modified Mercalli Intensity and geologic site conditions, Int. J. Earthquake Eng. and Struct. Dyn., 7, 75-83.

Westermo, B. D. and M. D. Trifunac (1978) Correlations of the Frequency Dependent Duration of Strong Earthquake Ground Motion with the Magnitude, Epicentral Distance, and the Depth of Sediments at the Recording Site, Dept. of Civil Eng. Report No. CE 78-12, Univ. of Southern California, Los Angeles, California